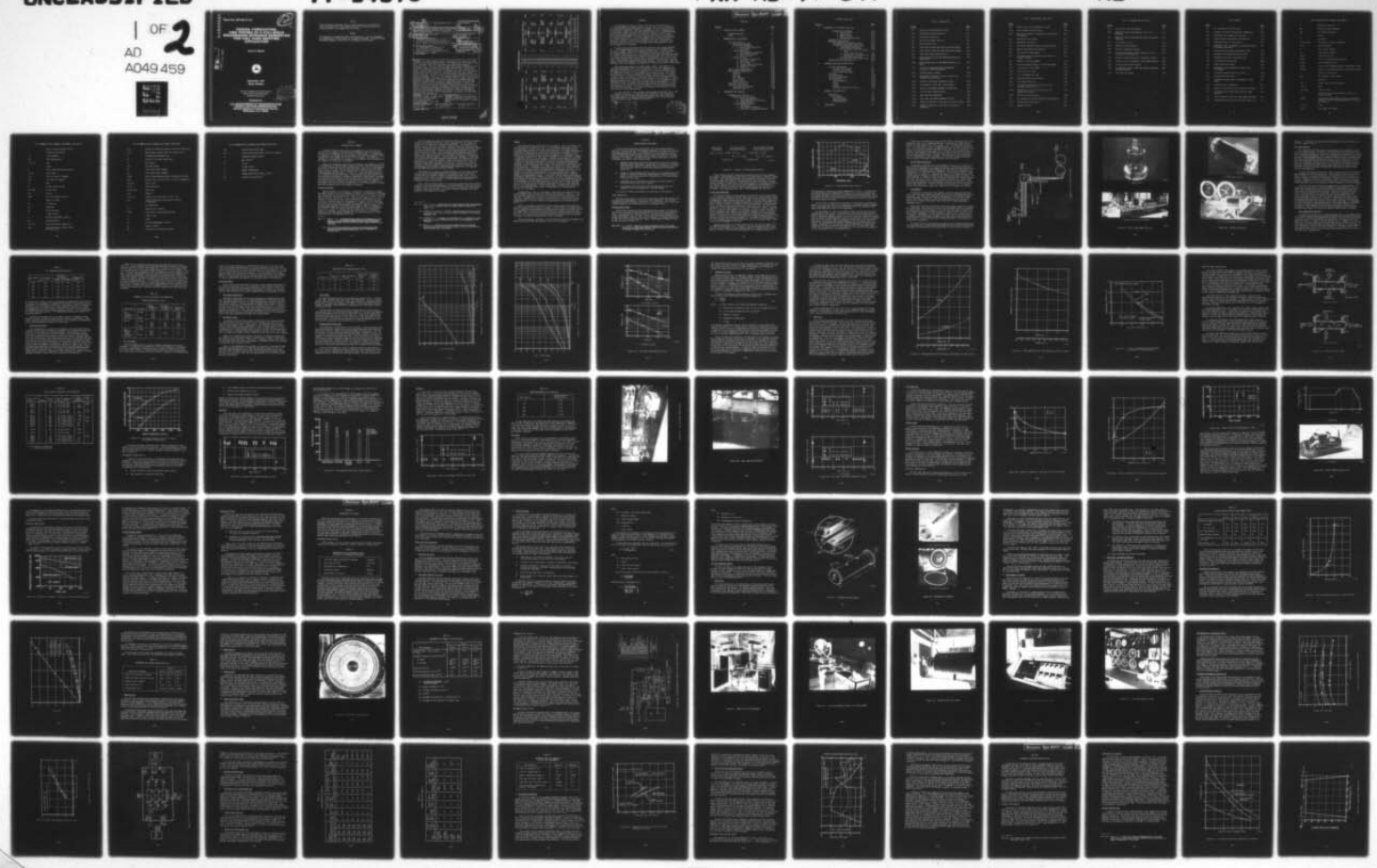
AD-A049 459 AIRESEARCH MFG CO OF CALIFORNIA TORRANCE F/G 1/3
DESIGN, FABRICATION, AND TESTING OF A FULL-SCALE BREADBOARD NIT--ETC(U)
SEP 77 S A MANATT DOT-FA75WA-3658
UNCLASSIFIED 77-14376 FAA-RD-77-147 NL



AD A049459

Report No. FAA-RD-77-147

DESIGN, FABRICATION, AND TESTING OF A FULL-SCALE BREADBOARD NITROGEN GENERATOR FOR FUEL TANK INERTING APPLICATION

Scott A. Manatt

AD No. ____ DDC FILE COPY



September 1977
FINAL REPORT

DDC
RECEIVED
FEB 1 1978
D

Document is available to the public through the
National Technical Information Service,
Springfield, Virginia 22151.

Prepared for

U.S. DEPARTMENT OF TRANSPORTATION
FEDERAL AVIATION ADMINISTRATION
Systems Research & Development Service
Washington, D.C. 20590

NOTICE

The United States Government does not endorse products or manufacturers. Trade or manufacturers' names appear herein solely because they are considered essential to the object of this report.

NOTICE

This document is disseminated under the sponsorship of the U.S. Department of Transportation in the interest of information exchange. The United States Government assumes no liability for its contents or use thereof.

Technical Report Documentation Page

1. Report No. FAA-RD-77-147	2. Government Accession No.
3. Recipient's Catalog No.	
4. Title and Subtitle: DESIGN, FABRICATION, AND TESTING OF A FULL-SCALE BREADBOARD NITROGEN GENERATOR FOR FUEL TANK INERTING APPLICATION	5. Report Date: Sep[illegible] 1977
	6. Performing Organization Code
7. Author(s): Scott A. Manatt	8. Performing Organization Report No. 77-14376
9. Performing Organization Name and Address: AiResearch Manufacturing Co. of Calif. A Division of The Garrett Corporation 2525 W. 190th St., Torrance, California 90509	10. Work Unit No. (TRAIS)
	11. Contract or Grant No. DOT-FA75WA-3658
12. Sponsoring Agency Name and Address: U.S. Department of Transportation Federal Aviation Administration Systems Research & Development Service Washington, D.C. 20590	13. Type of Report and Period Covered: Final Technical Report June 1975 – Sept 1977
	14. Sponsoring Agency Code: ARD-520

15. Supplementary Notes

16. Abstract

Aircraft fuel tank ullage may contain a mixture of fuel vapor in air that presents a fire and explosion hazard. This hazard can be eliminated if the air is replaced by an inert gas containing insufficient oxygen to allow ignition. Fuel tank inerting systems using onboard storage of liquid nitrogen to supply the inert gas have been demonstrated by the FAA and others and have been retrofitted into some U.S. Air Force transport aircraft. Tests by NAFEC and the Air Force have shown that fuel ullage oxygen concentration must be reduced to 9 percent or less to protect against ignition sources. The use of hollow fiber permeable membranes in an onboard inert gas generator (IGG) fuel tank inerting system has been shown to be a feasible alternative to systems using stored liquid nitrogen, which must be periodically replenished. A program to optimize the permeable membrane geometry; generate data required for system design; and to design, fabricate, and test full-scale breadboard permeable membrane air separation modules was conducted using the McDonnell-Douglas DC-9 aircraft as a design baseline. Results of membrane development, full-scale breadboard module design, and testing are reported; a preliminary design is presented for a hollow fiber permeable membrane IGG system for the DC-9; and ownership considerations for the airborne system design, including a life cycle cost analysis, are discussed.

17. Key Words	18. Distribution Statement
Membrane nitrogen inerting systems Fuel tank inerting systems Inert gas generators Fire protection in fuel tanks Aviation safety	Document is available to the public through the National Technical Information Service, Springfield, Virginia, 202151.

19. Security Classif. (of this report)	20. Security Classif. (of this page)	21. No. of Pages	22. Price
Unclassified	Unclassified	128	

Form DOT F 1700.7 (8-72)

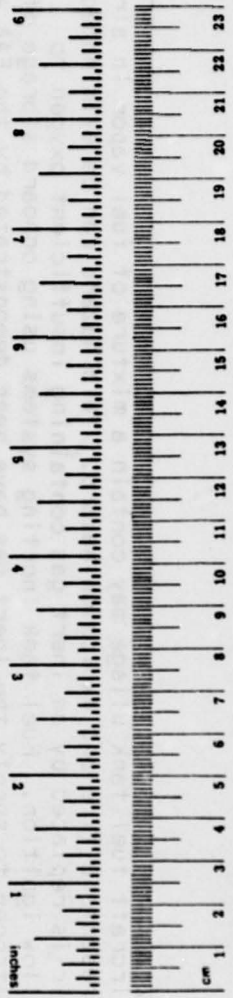
384343

METRIC CONVERSION FACTORS

Approximate Conversions to Metric Measures

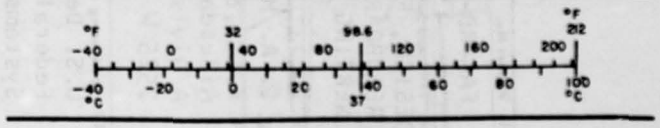
Symbol	When You Know	Multiply by	To Find	Symbol
		LENGTH		
in	inches	*2.5	centimeters	cm
ft	feet	30	centimeters	cm
yd	yards	0.9	meters	m
mi	miles	1.6	kilometers	km
		AREA		
in^2	square inches	6.5	square centimeters	cm^2
ft^2	square feet	0.09	square meters	m^2
yd^2	square yards	0.8	square meters	m^2
mi^2	square miles	2.6	square kilometers	km^2
	acres	0.4	hectares	ha
		MASS (weight)		
oz	ounces	28	grams	g
lb	pounds	0.45	kilograms	kg
	short tons (2000 lb)	0.9	tonnes	t
		VOLUME		
tsp	teaspoons	5	milliliters	ml
Tbsp	tablespoons	15	milliliters	ml
fl oz	fluid ounces	30	milliliters	ml
c	cups	0.24	liters	l
pt	pints	0.47	liters	l
qt	quarts	0.95	liters	l
gal	gallons	3.8	liters	l
ft^3	cubic feet	0.03	cubic meters	m^3
yd^3	cubic yards	0.76	cubic meters	m^3
		TEMPERATURE (exact)		
°F	Fahrenheit temperature	5/9 (after subtracting 32)	*Celsius* temperature	°C

*1 in = 2.54 (exactly). For other exact conversions and more detailed tables, see NBS Misc. Publ. 286, Units of Weights and Measures, Price $2.25, SD Catalog No. C13.10:286.



Approximate Conversions from Metric Measures

Symbol	When You Know	Multiply by	To Find	Symbol
		LENGTH		
mm	millimeters	0.04	inches	in
cm	centimeters	0.4	inches	in
m	meters	3.3	feet	ft
m	meters	1.1	yards	yd
km	kilometers	0.6	miles	mi
		AREA		
cm^2	square centimeters	0.16	square inches	in^2
m^2	square meters	1.2	square yards	yd^2
km^2	square kilometers	0.4	square miles	mi^2
ha	hectares (10,000 m^2)	2.5	acres	
		MASS (weight)		
g	grams	0.035	ounces	oz
kg	kilograms	2.2	pounds	lb
t	tonnes (1000 kg)	1.1	short tons	
		VOLUME		
ml	milliliters	0.03	fluid ounces	fl oz
l	liters	2.1	pints	pt
l	liters	1.06	quarts	qt
l	liters	0.26	gallons	gal
m^3	cubic meters	35	cubic feet	ft^3
m^3	cubic meters	1.3	cubic yards	yd^3
		TEMPERATURE (exact)		
°C	Celsius temperature	9/5 (then add 32)	Fahrenheit temperature	°F



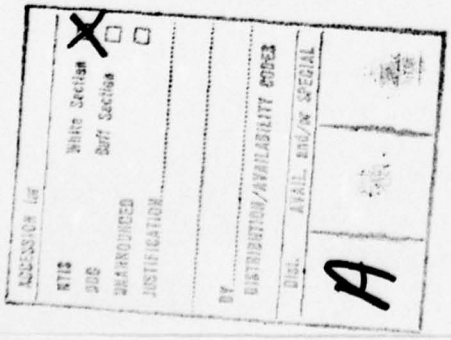
FOREWORD

The development program for design, fabrication, and testing of a full-scale breadboard nitrogen generator for fuel tank inerting application was conducted by AiResearch Manufacturing Company of California, a division of The Garrett Corporation, under the sponsorship of the U.S. Department of Transportation, Federal Aviation Administration Contract No. DOT-FA75WA-3658. The work was accomplished under the technical direction of the Aircraft Safety and Noise Abatement Division of the Aircraft Design Criteria Branch, Mr. Richard Kirsch, Chief. U.S. Navy Commander John J. Shea of the FAA was the contract technical coordinator throughout the period of performance. Additional technical direction was provided by Mr. Robert Clodfelter, Fire Protection Branch of the U.S. Air Force Aero Propulsion Laboratory, which was co-sponsor for the program.

The contractual performance period was from June 1975 through September 1977. The program manager and principal investigator for AiResearch was Mr. Scott A. Manatt, engineering department group leader in the Environmental and Energy Systems product line. Significant contributions were made by Mr. Joseph M. Ruder who directed the laboratory development phase and the design of the full-scale breadboard air separation module, by Mr. Dan S. Matulich who coordinated the design and construction of the breadboard test facility, and by Mr. Lucky Sawamura who performed system analysis. Contributions to the Dow Chemical subcontracted membrane fabrication elements of the program, under the direction of Dr. Earl Wagener, were made by Dr. Thomas Davis and Mr. Steven Styer.

The program was conducted in three phases. Phase I consisted of (1) laboratory development work to establish optimum hollow fiber membranes and generate sufficient data to permit the design of full-scale breadboard test air separation modules, and (2) preparation of an initial preliminary design projecting the results of the test phase to an airborne system. This phase concluded with an interim presentation of Phase I program results in August of 1976. Phase II provided the design and fabrication of the breadboard test modules and the facility required for their testing. During Phase III, the air separation modules were installed in the test facility and subjected to tests representative of full-scale airborne system operating requirements. At the conclusion of the final phase, the preliminary design was updated to include data available as a result of the test program. A life cycle cost-of-ownership study was conducted. This report is a summation and compilation of the results of all three program phases.

All work reported in this document was performed at AiResearch facilities in Torrance, California, with the exception of membrane fiber and module fabrication and some of the laboratory development, which was accomplished at the Dow Chemical, USA Western Research Laboratory facilities in Walnut Creek, California, under AiResearch subcontract.



DDC
RECEIVED
FEB 1 1978

Preceding Page BLANK - NOT FILMED

CONTENTS

Section		Page
1	INTRODUCTION AND SUMMARY	1-1
	Program Background	1-1
	Summary	1-3
2	MEMBRANE MODULE DEVELOPMENT	2-1
	Fiber Fabrication	2-1
	Methylpentene Polymer	2-1
	Hollow Fiber Membranes	2-2
	1. Hollow Fiber Fabrication	2-4
	2. Test Samples	2-4
	Fiber Optimization	2-8
	1. Spin Temperature Selection	2-8
	2. Quench and Draw Rate	2-9
	3. Wall Thickness	2-10
	Evaluation Tests	2-11
	1. Microscopic Examination	2-11
	2. Hydrostatic Tests	2-11
	3. Axial Creep	2-12
	4. Pressure Hoop Stress Tests	2-12
	5. Permeability Tests	2-16
	6. Fiber Life	2-17
	Operating Mode Investigation	2-20
	Environmental Compatibility	2-24
	Oxidation	2-25
	Humidity	2-27
	Fuel Vapor	2-28
	Fuel Immersion	2-32
	Thermal Shock	2-32
	Random Vibration	2-32
	Tube Sheet Construction	2-32
	Molecular Crosslinking	2-37
	Program Accomplishments	2-38
	Additional Effort	2-39
3	BREADBOARD TEST PROGRAM	3-1
	Breadboard Module Design	3-1
	Module Scaling Evaluations	3-2
	1. Spinning Evaluation	3-2
	2. Tube Sheet Bonding Evaluation	3-2
	3. Module Scale-up	3-3
	Initial Breadboard Module	3-5
	1. Fabrication	3-5
	2. Performance Evaluation	3-8
	3. Additional Intermediate Modules	3-9

CONTENTS (Continued)

Section		Page
3	BREADBOARD TEST PROGRAM (Continued)	
	Breadboard Test Modules	3-10
	1. Module SN R-2	3-13
	2. Module SN R-3	3-14
	3. Module SN R-4	3-14
	4. Module Acceptance Tests	3-14
	Laboratory Test Facility	3-17
	Breadboard Module Tests	3-17
	Single-Module Air Separation Tests	3-24
	Three-Module Breadboard System Tests	3-24
	1. Flow Balancing Calibration	3-24
	2. Steady-State Performance	3-28
	a. Structural Limit Performance Test	3-28
	b. Ullage Purge Flow Test	3-28
	c. Design Point Performance Test	3-28
	d. Performance Evaluation	3-31
	3. Mission Profile Performance Tests	3-33
	Breadboard Module Design Review	3-33
4	AIRBORNE SYSTEM PRELIMINARY DESIGN	4-1
	Aircraft Requirements	4-1
	Available Air Pressure	4-2
	Aircraft Descent Rate	4-2
	Inert Gas Delivery Rate	4-6
	ASM Design	4-6
	IGG System Design	4-15
	Inerting System Design	4-19
	System Operation	4-23
	Ground Operation	4-24
	Ascent	4-27
	Cruise	4-27
	Descent	4-27
	Redundant/Emergency Provisions	4-28
5	OWNERSHIP CONSIDERATIONS	5-1
	Reliability	5-1
	Life Cycle Cost	5-3
	Initial Costs	5-3
	Maintenance Costs	5-3
	Operating Costs	5-5
6	CONCLUSIONS	6-1

LIST OF ILLUSTRATIONS

Figure		Page
2-1	Synthesis of Methylpentene Polymer	2-2
2-2	Grade DX-810 Polymer Selection	2-3
2-3	Hollow Fiber Extrusion	2-5
2-4	Hollow Fiber Beaker Test Unit	2-6
2-5	Hollow Fiber PM Unit	2-7
2-6	Fiber Tensile Creep Test Data (Low Stress Range)	2-13
2-7	Fiber Tensile Creep Test Data (High Stress Range)	2-14
2-8	Fiber Hoop Creep Characteristics	2-15
2-9	Methylpentene Hollow Fiber Measured Permeability Coefficients	2-18
2-10	Methylpentene Hollow Fiber Measured Selectivity Ratio	2-19
2-11	Limiting Transmembrane Pressures Based on Structural Life Considerations	2-20
2-12	Pressure Operating Modes	2-22
2-13	Performance Characteristics for Internal and External Pressurization	2-24
2-14	Oxidation Test Beaker Permeability Data	2-25
2-15	Environmental Effect Test, Tensile Results	2-26
2-16	Humidity Test Beaker Permeability Test Data	2-27
2-17	Jet Fuel Vapor Exposure Setup	2-29
2-18	Vapor Saturation Bubblers	2-30
2-19	Fuel Vapor Test Beaker Permeability Data	2-31
2-20	Effect of Immersion in Jet Fuel on the Yield Stress	2-33
2-21	Effect of Immersion in Jet Fuel on the Elastic Elongation	2-34

LIST OF ILLUSTRATIONS (Continued)

Figure		Page
2-22	Thermal Shock Test PM Permeability Data	2-35
2-23	PM Unit Random Vibration Test	2-36
2-24	Resulting Increases in Strength for Crosslinked Polyethylene	2-37
3-1	Breadboard Module Design	3-6
3-2	Breadboard Test Module	3-7
3-3	Shell-Side Pressure Gradient vs Packing Factor	3-11
3-4	Radial Flow-Pressure Drop Results	3-12
3-5	Tube Sheet Following Repair	3-15
3-6	Inert Gas Generator Laboratory Test Facility Schematic Diagram	3-18
3-7	3000-cu ft Altitude Chamber	3-19
3-8	Inert Gas Generator Module in Altitude Chamber	3-20
3-9	Simulated Fuel Tank Volume	3-21
3-10	Facility Control Panel	3-22
3-11	Test Instrumentation Panel	3-23
3-12	Purge Optimization Test Results	3-25
3-13	Inert Gas Productivity	3-26
3-14	Air Separation Module Installation in the Laboratory Test Facility	3-27
3-15	Comparison of Analytical Predictions and Laboratory Test Data	3-32
3-16	Mission Profile Simulation	3-34
4-1	Air Pressure at Various Locations During Descent	4-3
4-2	Typical DC-9 Flight Profile	4-4
4-3	Descent Profiles	4-5

LIST OF ILLUSTRATIONS (Continued)

Figure		Page
4-4	Descent Inert Gas Requirements	4-7
4-5	Membrane Transfer Area Required, Life Limit Pressures	4-11
4-6	Membrane Transfer Area Required, Boosted Available Pressures	4-12
4-7	Life Pressure Limits	4-13
4-8	Design Point Requirements	4-14
4-9	Bleed Air Temperature Control	4-16
4-10	Air Separation Module (ASM) Pressure Limit as a Function of Inert Gas Flow	4-17
4-11	Bleed Air Boost and Purge Air Temperature Control	4-18
4-12	Airborne Inert Gas Generator (IGG) System Schematic	4-20
4-13	Inerting System Block Diagram	4-21
4-14	Air Separation Module (ASM) Performance Projection and Mode Crossover	4-25
4-15	Fuel Tank Vent System	4-26

LIST OF TABLES

Table		Page
2-1	Spin Temperature Selection Data	2-9
2-2	Permeability Data at Selected Spin Temperature	2-10
2-3	Hydrostatic Dye Leakage and Burst Tests	2-12
2-4	Typical Results, Operating Life Comparison	2-23
2-5	Temperature-Humidity Test Results	2-28
3-1	Breadboard Inert Gas Generator System Design Point Performance Requirement	3-1
3-2	Design Evaluation Module Data Summary Sheet	3-10
3-3	Breadboard Test Module Fabrication Data	3-13
3-4	Breadboard Test Module Evaluation Data	3-16
3-5	Flow Balancing Calibration	3-29
3-6	Steady-State Test Results	3-30
3-7	Breadboard Inert Gas Generator Design Point Performance	3-31
4-1	Estimated System Weights and Airflows	4-22
4-2	Estimated Scaling Factors	4-23
5-1	Estimated Component Mean Time Between Failures (MTBF)	5-2
5-2	Maintenance Cost Assumptions	5-4
5-3	Summary of Maintenance Cost of Ownership Elements	5-5
5-4	Estimated Energies Used During Typical System Operation	5-6
5-5	Typical Penalty Factors for Power Usage and Weight	5-7
5-6	System Operating Costs in Dollars per Flight Hour	5-7

LIST OF ABBREVIATIONS, ACRONYMS, AND SYMBOLS

A	membrane surface area
AGE	aerospace ground equipment
ASM	air separation module
C	Celsius
cm	centimeter
cm Hg, CM Hg	centimeters of mercury (pressure)
cu cm	cubic centimeter
D_i	fiber inside diameter
D_o	fiber outside diameter
dM/dt	inert gas flow rate
dP/dt	rate of ullage gas pressure charge
dV/dt	fuel consumption rate
DX-810	grade of methylpentene polymer, manufacturer's code
DX-845	grade of methylpentene polymer, manufacturer's code
E	externally pressurized
ECS	environmental control system
F	Fahrenheit
FAA	Federal Aviation Administration
ft, FT	feet
fpm, FPM	feet per minute
g	acceleration due to gravitational force at the earth's surface
G^2/HZ	acceleration power spectral density, acceleration squared divided by frequency bandwidth (in cycles per second)
hr, HR	hour
HSID	high speed idle descent

i	subscript used to denote i^{th} gas
I	internally pressurized
ID	inside diameter
IGG	inert gas generator
in., IN.	inch
L	length
$\dot{L}$	fiber linear fabrication velocity
lb, LB	pound (mass)
L/D	ratio of length to diameter
LRID	long range idle descent
M	mass
$\dot{M}$	polymer extrusion rate
min, MIN	minute (time)
min.	minimum
MTBF	mean time between failures
n	number of fibers
N_2	nitrogen gas
O_2	oxygen gas
OD	outside diameter
P	ullage pressure
p	pressure measurement location
PM	prototype module
psi, PSI	pounds (force) per square inch
psia	absolute pressure, pounds (force) per square inch

psid	differential pressure, pounds (force) per square inch
psig	gage pressure, pounds (force) per square inch
$\dot{Q}$	transmembrane permeation rate
Q_F	volumetric flow rate along fibers
R	gas constant
rms	root mean square
R_1	fiber bundle inner diameter
R_2	fiber bundle outer diameter
RT-20	grade of methylpentene polymer, manufacturer's code
SCFM	standard cubic feet per minute (0°C and 1 atmosphere)
sec, SEC	second (time)
sq cm	square centimeter
sq ft, SQ FT	square feet
STD	standard
std cu cm	standard cubic centimeter (cu cm at STP)
STP	standard temperature and pressure (0°C and 1 atmosphere)
T	gas temperature
th	membrane wall thickness
TPX®	trade name for methylpentene polymer
V	ullage volume
wt	weight
W	flow rate measurement location
ΔL	change in length
ΔP	transmission differential pressure

ΔP_l	pressure drop along fibers
ΔP_r	pressure drop along radial direction of module
Θ	temperature sense location
μ	gas viscosity
μm	micron
ρ	polymer density
°	degree (temperature)
%	oxygen concentration sense location
TP	permeability coefficient

SECTION 1

INTRODUCTION AND SUMMARY

A potential hazard exists due to the susceptibility of aircraft fuel tanks and vent systems to overpressure and subsequent explosion induced by the ignition of flammable fuel air mixtures in these zones. The combination of atmospheric environment and turbine engine fuel properties used for current transport aircraft exposes the aircraft to this danger. The program is addressed to an evaluation of the feasibility of onboard inert gas generation as a method of eliminating this exposure.

Despite the outstanding safety record achieved by the commercial airlines in the operation of turbine powered transport aircraft, data collected by FAA and others indicate that aircraft explosions due to ignition of the flammable mixture within the fuel tanks and vent systems of commercial aircraft have caused extensive damage, loss of equipment, and injury and death of the aircraft passengers and crew (Refs. 1-1 and 1-2). Following data evaluation by an FAA-Industry Advisory Committee, it was concluded that fuel system fires and explosions were primarily caused or aggravated by electrostatic discharge during refueling, penetration of the fuel tank by hot engine parts resulting from engine failure, lightning striking the aircraft skin, and crashes. In some impact-survivable crashes, the resultant fires spread or caused wing explosions, prohibiting aircraft evacuation prior to the occurrence of intense heat and the generation of toxic combustion products.

PROGRAM BACKGROUND

Numerous methods for eliminating or substantially reducing this hazard have been explored with varying degrees of success. The technique with perhaps the widest potential application to transport aircraft is to provide a nonflammable ullage and vent mixture that will not allow ignition to occur. Since a system to control the mixture in the ullage and vent spaces has little or no latitude in adjusting the fuel vapor concentration, such systems have been principally directed toward the replacement of ullage air with an inert gas. While both carbon dioxide and nitrogen gas have been successfully utilized as the inert gas, logistics and economics have tended to favor nitrogen gas. Systems demonstrated for aircraft use have tended to store the nitrogen gas as a liquid. Since this concept requires the delivery of a considerable quantity of nitrogen, its storage has been found to be at a considerable expense of weight and volume, together with an associated need for regular ground supply of the expendable inert gas.

Ref. 1-1: Horeff, T. G., A Crashworthiness Analysis with Emphasis on Fire Hazard: U.S. and Selected Foreign Turbine Aircraft Accidents 1964-1974, Federal Aviation Administration, Report FAA-RD-75-156, July 1976.

1-2: U.S. Air Carrier Accidents Involving Fire 1965 through 1974 and Factors Affecting the Statistics, Report NTSB-AAS-77-1, February 1977.

While nitrogen fuel tank inerting offers perhaps the optimum performance solution for explosion prevention in the ullage and fuel vent spaces, the storage of inert gas entails considerable penalties. These penalties of weight, volume, logistics of resupply, additional vehicles required during aircraft turn-around, operating costs, cryogenic equipment related maintenance training, and operational flexibility constraints are undesirable from the operator's point of view. Studies conducted under government sponsorship, both military and civilian, have concluded that complete elimination of oxygen is not required to maintain a nonflammable mixture for turbine fuel and potential ignition sources. These studies vary somewhat in the evaluation of the minimum allowable oxygen concentration, but generally fall into a range of 10 to 12 percent oxygen by volume required for ignition at the most severe fuel vapor concentrations (Refs. 1-3 through 1-5). Thus, a system to remove about 50 percent of the oxygen in air could be utilized in place of liquid nitrogen storage vessels as a source of inert gas. For the purposes of this program, a maximum oxygen concentration of 9 percent has been established as the limiting criterion.

The feasibility of onboard nitrogen generation for fuel tank inerting using hollow fiber permeable membranes as a means of the enrichment of nitrogen from air has been successfully demonstrated (Ref. 1-6). At the conclusion of this effort in 1974, the system operating principle had been demonstrated and initial estimates of system penalties extrapolated to commercial transport application.

Due to the encouraging results of the previous program and the continuing interest in the study and development of alternate means of fuel tank inerting protection within the FAA and military services, this more ambitious program to design, fabricate, and test a full-scale nitrogen breadboard inert gas generator (IGG) system was initiated.

Ref. 1-3: Zinn, Jr. S.V., Inerted Fuel Tank Oxygen Concentration Requirements, Federal Aviation Administration, Interim Report FAA-RD-71-42, August 1971.

1-4: Steward, P.B., and E.S. Starkman, Inerting Conditions for Aircraft Fuel Tanks, WADC Technical Report 55-418, University of California, September 1955.

1-5: Zabetakis, M. G., Flammability Characteristics of Combustible Gases and Vapors, Bureau of Mines Bulletin 627, U.S. Department of the Interior.

1-6: Manatt, S.A., Feasibility Study and Demonstration of Nitrogen Generation For Fuel Tank Inerting, Federal Aviation Administration Report FAA-RD-74-112, June 1974.

SUMMARY

The program has been organized into three phases. The first phase of the program consisted of two parts. Part 1, the laboratory development effort, was undertaken to develop the hollow fiber fabrication techniques required to produce membrane material of consistent properties, to evaluate manufacturing techniques, to develop the optimum fiber configuration and geometry, and to establish sufficient design data to permit the design of a large-scale unit. Program activity during the laboratory development part of the Phase I program is reported in Section 2 of this report. Laboratory development of the fibers included tests of hollow fiber permeability and structural properties and confirmation of tube-side pressurization as the most favorable operating mode. In addition, the effects of exposure to various environmental extremes were evaluated, including humidity, fuel vapors, fuel immersion, thermal shock, and random vibration. Investigation of a means of improving the fiber properties by increasing their life and/or decreasing their weight was initiated. This evaluation of polymer crosslinking showed that the necessary condition for the success of this technique has been met. Part 2 of program Phase I was to establish a preliminary system design for a representative small transport category turbine-powered aircraft. A preliminary system design established for the McDonnell Douglas DC-9 commercial transport was used to establish hardware design guidelines necessary to fabricate and test full-scale breadboard air separation modules. As the program continued, the preliminary design was updated to incorporate additional data available at the conclusion of some long-term tests initiated during the laboratory development effort and tests conducted with the full-scale modules. A preliminary design, updated after the conclusion of the breadboard test program, is presented for a 270-lb system in Section 4 of this report.

Program Phases II and III, the design, fabrication, and test of the full-scale breadboard inert gas generator modules, are reported in Section 3. Fabrication steps leading to the final three test modules and the design of the test facility established to permit the simulation of flight profiles are discussed. Results of the successful test program and a discussion of recommended changes to future air separation module designs also are provided in Section 3.

Section 5 provides an evaluation of the system ownership considerations, using the baseline DC-9 aircraft as a model. In this section, the quantifiable costs of ownership are presented and non-quantifiable system attributes, such as its independence of the constraints associated with regular ground servicing, are noted. The life cycle cost analysis of Section 5 presents data for evaluation of initial costs and for the maintainance and operating costs an operator can expect to encounter throughout the life of the system.

Section 6 provides a discussion of the principal program accomplishments and general conclusions that were drawn as a result of the program.

Preceding Page Blank - Filmed

SECTION 2

MEMBRANE MODULE DEVELOPMENT

The previous FAA-sponsored program (Ref. 2-1)* had established the feasibility of using hollow fiber permeable membranes to produce inert gas for use aboard transport aircraft. The purpose of the initial phase of the full-scale breadboard system program was to define an optimum membrane fiber and establish sufficient fiber and module data to permit the design of full-scale breadboard test modules. The laboratory test program established to achieve these goals consisted of the following steps:

- Manufacturing process conditions were varied to obtain hollow fiber membrane samples made under a large number of conditions. Screening tests were then conducted to evaluate the fiber characteristics and select the best fiber for further performance and environmental evaluation.
- As part of the performance testing, fibers in small modules were subjected to internal and external pressurization. Results were compared to confirm the superiority of operation with internal pressurization of the fibers.
- Experiments were then conducted to determine the best method of incorporating the fibers into a module.
- Envrionmental tests were performed to determine the effect of expected aircraft environments on fiber performance.

The results of these investigations are described in this section.

FIBER FABRICATION

The most crucial effort in the initial laboratory development phase of the program was the development of the hollow fibers themselves. The following discussion considers the basic raw material, its fabrication into a useful gas transfer membrane, and the optimization of the membrane fibers.

Methylpentene Polymer

The previous program had identified methylpentene polymer as a superior material for use as the hollow fiber membrane for fuel tank inerting applications. The raw material, TPX®, currently is synthesized from propylene by Mitsui Petrochemical, Ltd. of Japan. Mitsui took over the manufacture of the polymer from Imperial Chemical Industries of England, the polymer manufacturer at the time of the previous program. Steps in the chemical synthesis of the polymer are shown in Figure 2-1.

*Ref. 2-1: S. A. Manatt, Feasibility Study and Demonstration of Nitrogen Generation for Fuel Tank Inerting, Federal Aviation Administration Final Report FAA-RD-74-112, June 1974.

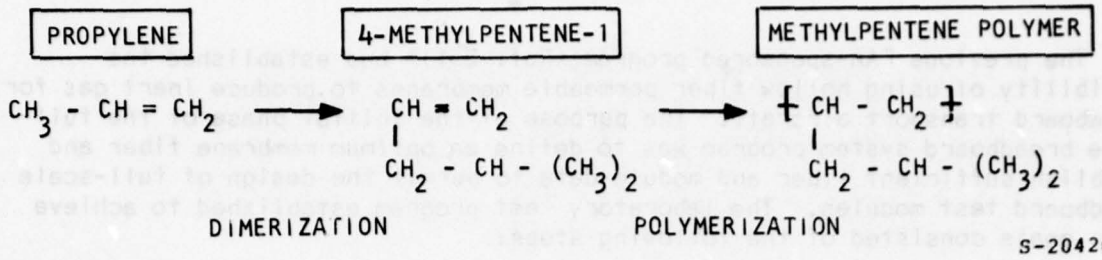


Figure 2-1. Synthesis of Methylpentene Polymer

Three different polymer grades were evaluated during the early stages of the program. These grades are identified by the manufacturer as DX-810, DX-845, and RT-20. Fibers were manufactured from the polymer, and step pressure tests (discussed below under Pressure Hoop Stress Tests) were conducted. Typical results are shown in Figure 2-2. Grade DX-810 exhibited the highest strength (lowest increase in normalized flow following exposure to high-pressure stress). This factor, together with the low extrusion temperature and low density of grade DX-810, led to its selection as the grade evaluated during the rest of the phase I test program and used later in the breadboard test modules.

Hollow Fiber Membranes

Although the property of gas permeation through thin films of solid materials has long been recognized and data show that certain gases permeate through a given material more readily than do other gases, actual practical applications of membranes to separate gases have been limited. With few notable exceptions, gas enrichment by the use of permeable membrane has remained a laboratory curiosity. Perhaps the major limitation on practical application of membrane separation has been the problems encountered in scaling up small laboratory test apparatus to sizes large enough to provide useful separation rates. The permeability of even the most permeable of materials is quite low when evaluated in terms of apparatus requirements for even modest separation rates. To achieve useful separation rates, large surface areas of extremely thin membrane must be used. Historically, this has been approached by manifolding flat membrane sheets to achieve the required surface area in a compact package geometry. This presents two significant design problems: (1) flat sheets of a thin material will not withstand much pressure differential, and (2) a suitable means to manifold alternate passages is required.

Numerous approaches to increase the structural load bearing capability of the membranes have been tried. In general, the favored approach usually has been to provide strength by using a matrix material: either a porous backing plate or a fabric, which has been impregnated with the membrane polymer to

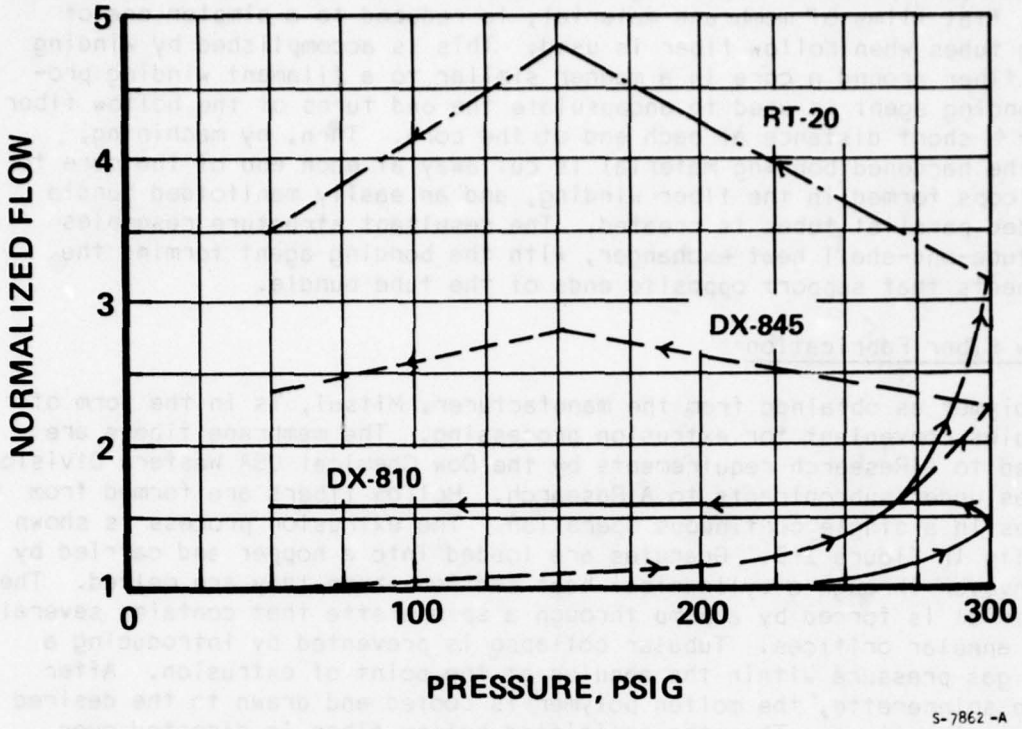


Figure 2-2. Grade DX-810 Polymer Selection

form many small, flat-plate surfaces between fabric fibers. In either case, alternate plates must be separated sufficiently to allow the required flow. While these techniques significantly increase the load bearing capabilites of the membrane surface, they tend to greatly increase the weight and the volume required to contain the required active surface area and further complicate the manifolding difficulties.

The difficulty in manifolding the sheets to interconnect alternate passages lies in the fact that not all edges may be connected; adjacent passages must be separately manifolded to form alternate high- and low-pressure passages, each separated by the thin-film membrane.

The development of small hollow membrane fibers has provided a practical breakthrough in the solution of the structural difficulties associated with membrane separation systems. Since hollow fibers form their own pressure vessels, no additional membrane backing material or structural support is required. With the proper polymeric material selection and design to limit the resultant hoop stress (or buckling load) to acceptable levels, the hollow fibers will withstand a high-pressure gas stream introduced into (or around) the hollow fibers. The selection of a relatively high-strength material enables self-supporting tube wall thickness to be relatively thin for small tube sizes. In addition, the absence of the requirement for a structural backing material allows the package size to be reasonably small.

The difficult problem of joining alternate plates, experienced when using large-area, flat films of membrane material, is reduced to a simpler one of manifolding tubes when hollow fiber is used. This is accomplished by winding the hollow fiber around a core in a manner similar to a filament winding process. A bonding agent is used to encapsulate the end turns of the hollow fiber winding for a short distance at each end of the core. Then, by machining, enough of the hardened bonding material is cut away at each end of the core to sever the loops formed in the fiber winding, and an easily manifolded bundle of open-ended parallel tubes is created. The resultant structure resembles that of a tube-and-shell heat exchanger, with the bonding agent forming the two tube sheets that support opposite ends of the tube bundle.

1. Hollow Fiber Fabrication

The polymer as obtained from the manufacturer, Mitsui, is in the form of small granules convenient for extrusion processing. The membrane fibers are manufactured to AiResearch requirements by the Dow Chemical USA Western Division Laboratories under subcontracts to AiResearch. Hollow fibers are formed from the granules in a single continuous operation. The extrusion process is shown schematically in Figure 2-3. Granules are loaded into a hopper and carried by a screw conveyor through a cylindrical heat section where they are melted. The molten material is forced by a pump through a spinnerette that contains several very small annular orifices. Tubular collapse is prevented by introducing a controlled gas pressure within the annulus at the point of extrusion. After leaving the spinnerette, the molten polymer is cooled and drawn to the desired hollow fiber dimensions. Then the solidified hollow fiber is directed over takeup reels and wound on a spool for later use in the assembly of a module.

2. Test Samples

In addition to individual fiber samples, test units were fabricated for use in evaluating performance and properties of fibers processed under various conditions. For tests that required a large number of test modules, "beaker units" were made. These units consisted of 800 fibers, 10 cm long (active length), manifolded inside of a small polycarbonate container as shown in Figure 2-4a. (Figure 2-4b shows 17 test units of this type undergoing an acceptance test.)

Where tests required a significant statistical sample, small-scale modules were fabricated. These test units, called prototype modules (PM's), consisted of 192,000 fibers of approximately 6.5 in. active length; each of these small-scale modules provided an equivalent length of fiber of almost 20 miles. The PM units were packaged in a clear plexiglas cylinder 9.25 in. long by 3.20 in. in diameter. The assembly of the module into test fixtures that manifolded the exposed ends of the fibers allowed visual inspection of the fibers during certain tests. Figure 2-5 shows one of the PM units and its installation in a hydrostatic test setup.

During the course of the program, the need to build intermediate-size modules was identified. These modules (designated SN 3) were used to develop module assembly techniques before fabricating the full-size modules discussed in

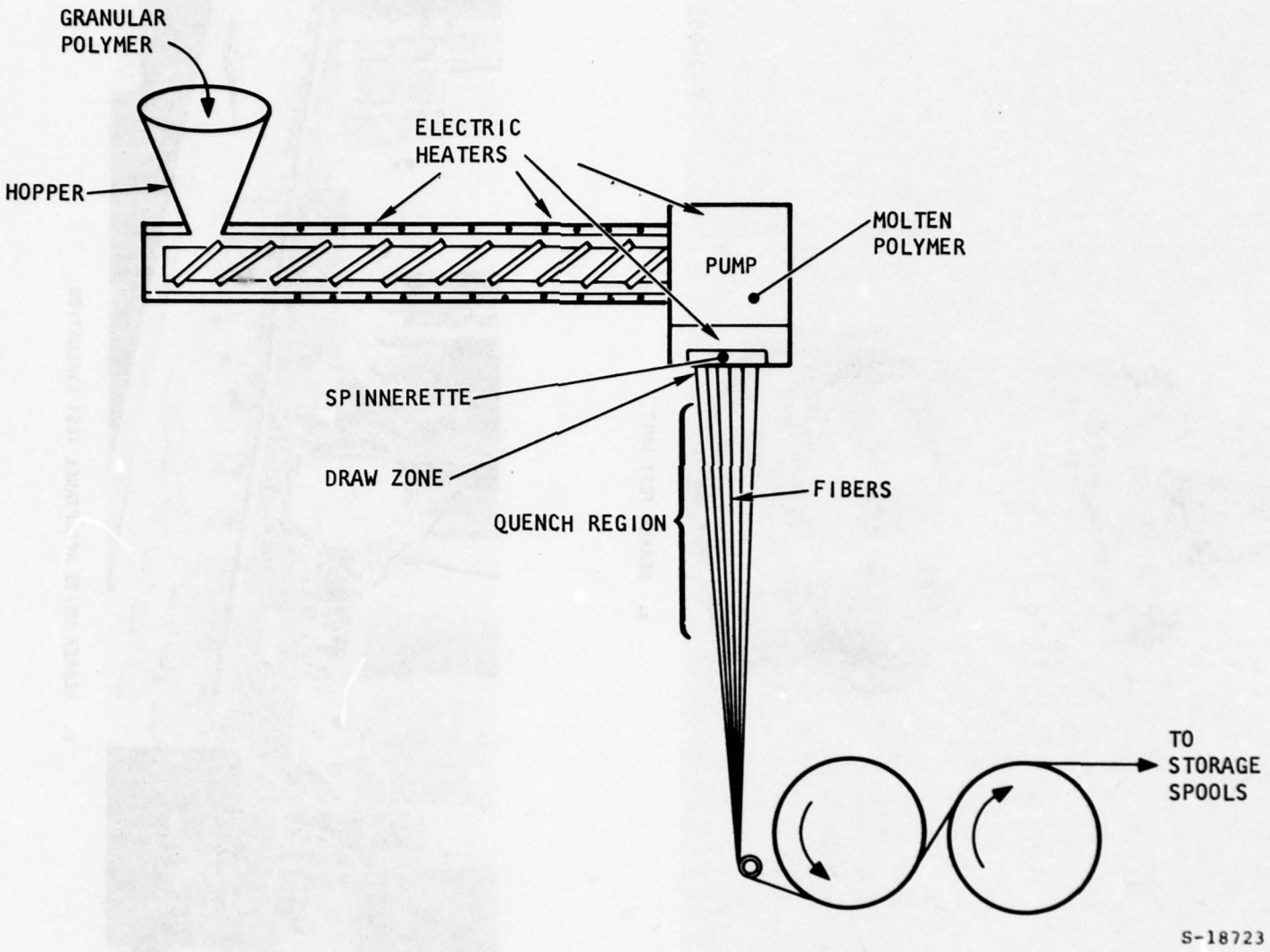
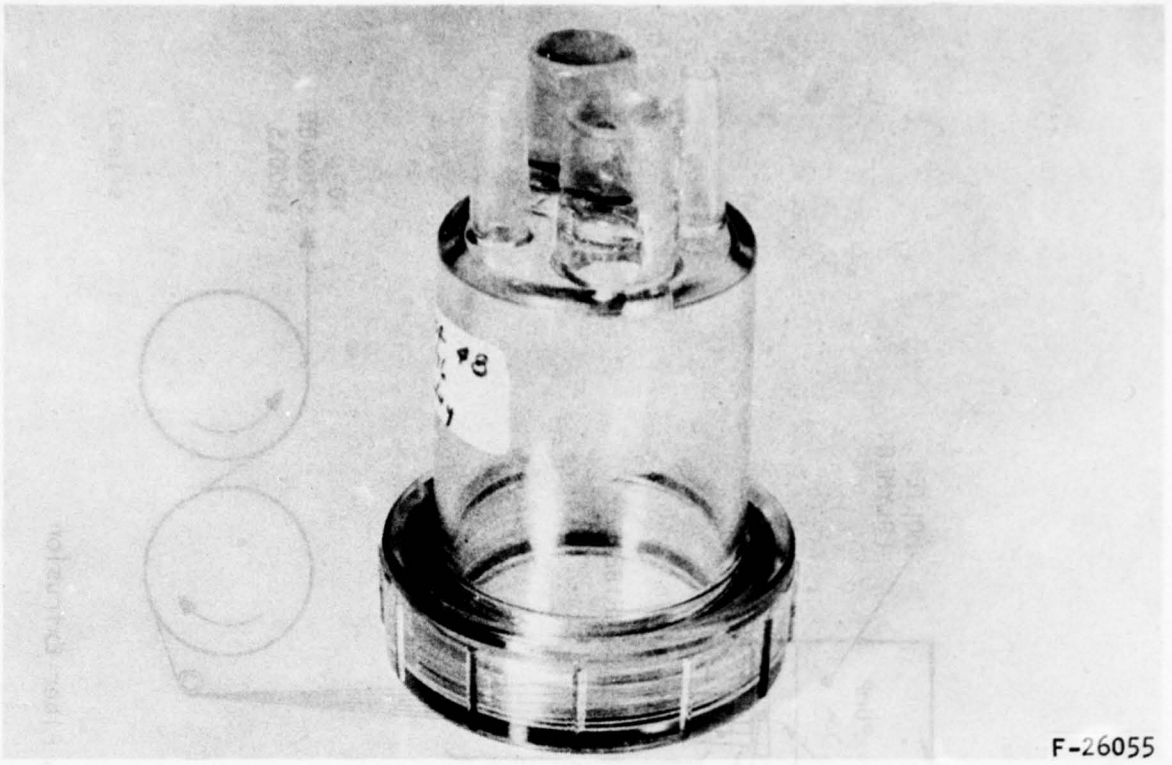
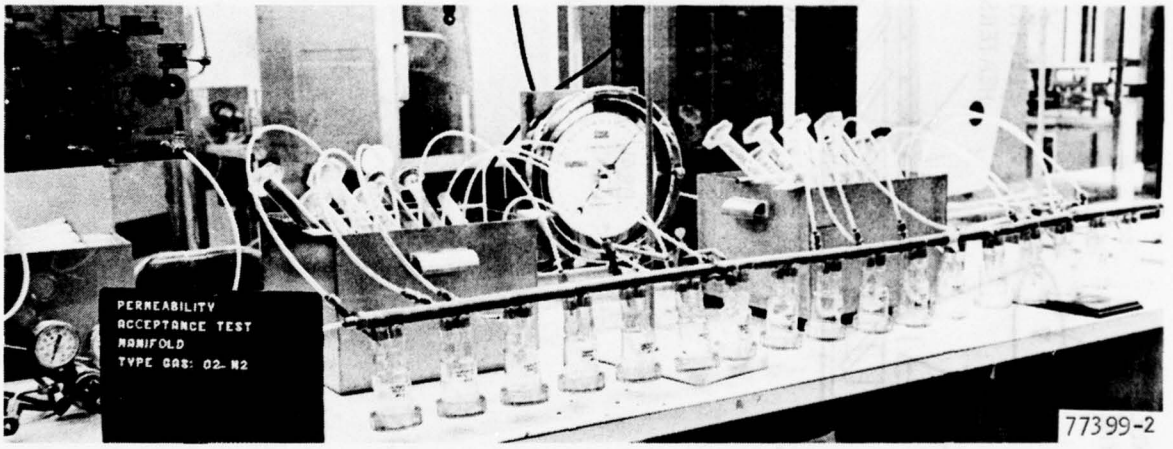


Figure 2-3. Hollow Fiber Extrusion



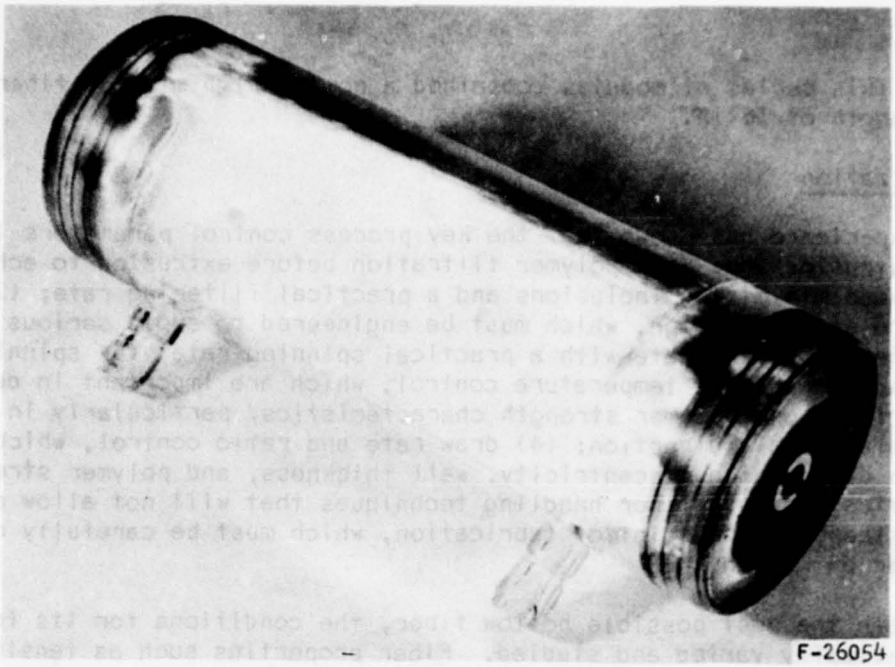
a. BEAKER TEST UNIT



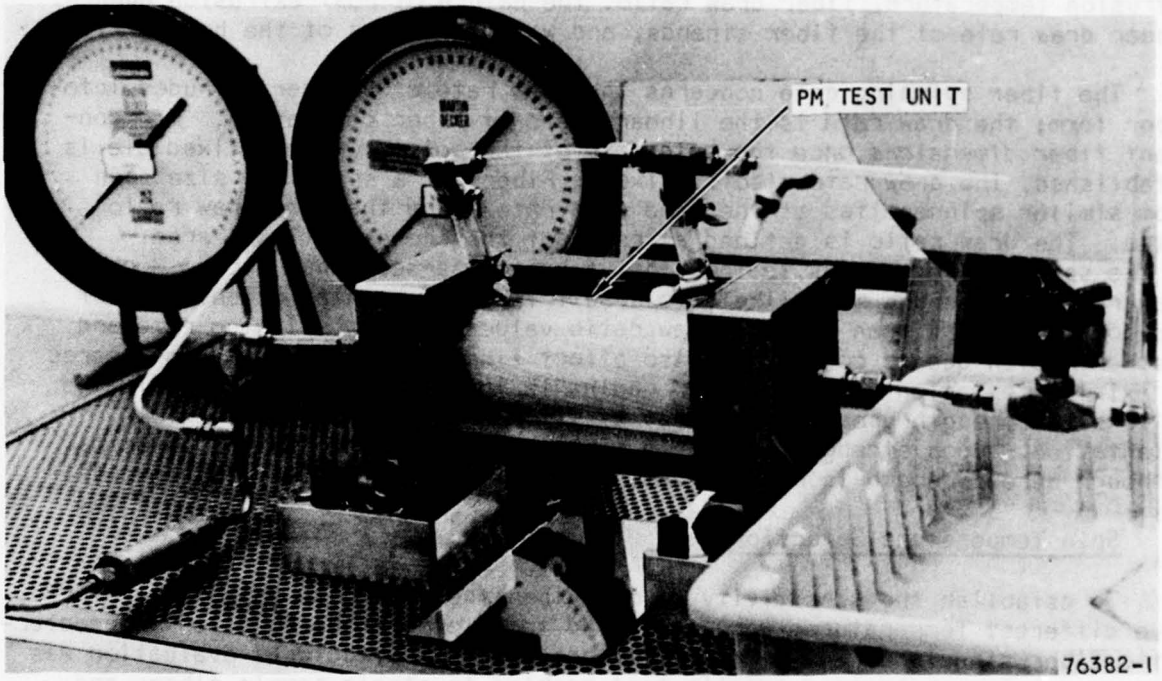
b. BEAKER UNITS ACCEPTANCE TEST EVALUATION

F-26056

Figure 2-4. Hollow Fiber Beaker Test Unit



a. PROTOTYPE MODULE (PM) UNIT



b. PM UNIT IN HYDROSTATIC TEST EVALUATION F-26053

Figure 2-5. Hollow Fiber PM Unit

Section 4. This series of modules contained a nominal 1.5 million fibers with an active length of 36 in.

Fiber Optimization

Past experience has shown that the key process control parameters in hollow fiber extrusion are: (1) polymer filtration before extrusion to achieve a balance between minimizing inclusions and a practical filtering rate; (2) extrusion pressure and die design, which must be engineered to avoid serious entrance and exit effects commensurate with a practical spinning rate; (3) spinning temperatures and quench-zone temperature control, which are important in determining concentricity and polymer strength characteristics, particularly in the hoop (circumferential) direction; (4) draw rate and ratio control, which also are vital in determining concentricity, wall thickness, and polymer strength characteristics; and (5) fiber handling techniques that will not allow any additional stress to the point of fabrication, which must be carefully controlled after extrusion.

To obtain the best possible hollow fiber, the conditions for its formation were systematically varied and studied. Fiber properties such as tensile and hoop strengths, single gas permeability, and separation factor (permeability ratio of oxygen to nitrogen) were measured for the various fiber spinning conditions. Parameters that were investigated included the fiber spinning rate, extrusion temperature, fiber draw ratio, the nature of post-extrusion quench, linear draw rate of the fiber strands, and wall thickness of the hollow fibers.

The fiber spinning rate concerns the mass rate of polymer extruded into fiber form; the draw rate is the linear speed of fiber generation. For constant fiber dimensions once the spin rate of the polymer from a fixed die is established, the draw rate also is fixed. Fibers of a specified size spun from similar spinnerettes at the same spin rate share the same draw ratio value. The draw ratio is defined as ratio of the cross-sectional area of the spinnerette annulus to the final fiber cross-sectional area. Higher draw ratio values are more likely to result in greater axial orientation of the polymer chains than are low draw ratio values. Fiber spinning rate and post-extrusion quench conditions also affect fiber morphology. A high degree of axial orientation of the polymer chains in the fibers should be indicated by tensile strength greater than that of similar material without axial orientation. Hoop strength in such a fiber also shows orientation effects, although here strength is reduced over material without axial orientation.

1. Spin Temperature Selection

To establish the sensitivity of methylpentene fibers to spin temperatures, five different temperatures were evaluated to determine the resultant characteristic fiber structural and permeability properties. Structural evaluation was performed using an Instrom tensile test machine to strain sample fibers and determine yield and ultimate strength characteristics. Permeability was evaluated using leak-free, 800-loop-cell beaker samples pressurized to 50 psig. All spin temperature screening tests were conducted at laboratory ambient temperature and pressure; results are shown in Table 2-1. The data indicate that methylpentene fiber tensile yield strength and permeability exhibit little sensitivity to spin temperatures.

TABLE 2-1

SPIN TEMPERATURE SELECTION DATA

Spin Temp, °F	Yield Stress, psi x 10^{-3}	Permeability, cu cm/min		Separation Factor
		Oxygen	Nitrogen	
595	5.59	5.74	1.58	3.63
600	4.99	5.12	1.15	4.45
605	5.51	6.07	1.41	4.30
610	5.32	4.88	1.15	4.24
620	5.78	6.25	1.41	4.43

Spin conditions, listed in order of increasing test temperature, show variation in structural and permeability properties that can easily be accounted for by consideration of the geometric uncertainty; no definitive trend is established, indicating little or no sensitivity to spin temperature variation. At each spin temperature, the yield stress in Table 2-1 is the mean of eight samples. The standard deviation for all samples was about ±560 psi. The ultimate stress for these fibers was 12,800 psi. All samples were strained at a rate of 25 percent per minute.

The 605°F spin temperature was selected as optimum. Permeability and separation factor are very high, and the yield stress is satisfactory. Some higher values were obtained at 620°F; however, this extremely high temperature could cause manufacturing reproducibility problems.

2. Quench and Draw Rate

With the selection of a 605°F spin temperature, the two remaining manufacturing process control parameters to evaluate are the quench and draw rates. Originally it was planned to vary one parameter, conduct permeability and stress tests, select the best condition, and then vary the other parameter. After the first parameter was varied, it was also planned to fabricate small-scale test modules using the selected manufacturing control parameter condition. As a result of additional small-scale module fabrication experience, which provided confidence in module fabrication, it was decided to decrease the number of small-scale test modules fabricated and increase the number of specific manufacturing control parameters investigated. Rather than fabricating fibers at two draw rates, selecting a draw rate, and then varying quench rate, it was decided to fabricate fibers at four different draw rates and three different quench rates for each draw rate. This gives a larger matrix from which to choose the optimum fiber. Accordingly, fibers were spun for these 12 different manufacturing control conditions at the selected spin temperature.

Results for 12 different quench and draw rate combinations are shown in Table 2-2. Quench and draw rate effects were generally as expected: low quench and draw rates yield better fiber properties. In Table 2-2, the higher permeability rates shown for the higher quench rates are due to fiber leakage. This is confirmed by the low separation factor (permeability ratio of oxygen to nitrogen). Pressure tests conducted at this time indicated that the allowable fiber hoop stress was considerably lower than the yield stress shown in Table 2-2. Yield stress values in Table 2-2 were obtained from tensile tests in which the fibers are loaded in the axial direction, i.e., the same direction in which they are drawn during manufacture. This indicated that a biaxial yield stress distribution existed in the fiber. To allow the polymer to return to a more random orientation, the quench rate was further reduced after drawing by heating the quench zone. The result was that the allowable stresses in the radial and axial directions were made nearly identical, and the allowable fiber hoop stress was increased.

TABLE 2-2

PERMEABILITY DATA AT SELECTED SPIN TEMPERATURE

(800-FIBER-LOOP CELL, 21°C)

Quench Rate	Draw Rate	Oxygen Permeability, cu cm/min	Nitrogen Permeability, cu cm/min	Separation Factor
Low (Natural convection cooling)	A (High)	5.51	1.23	4.48
	B	5.97	1.31	4.56
	C	5.79	1.29	4.49
	D (Low)	6.09	1.30	4.68
Medium	A (High)	-	-	-
	B	29.0	26.1	1.11
	C	28.3	26.0	1.09
	D (Low)	26.2	24.9	1.05
High (Maximum forced convection cooling)	A (High)	-	-	-
	B	141.2	-	-
	C	66.1	65.3	1.01
	D (Low)	45.0	-	-

3. Wall Thickness

Since the permeation rate is almost inversely proportional to the wall thickness, it is desirable to fabricate a hollow fiber membrane of minimum wall thickness, commensurate with applied stress, in order to maximize inert flow for a given size of module. Limitations on minimum fiber sizes are associated with the manufacturing process and with structural limitations of the pressurized

fiber. With present technology, a manufacturing lower limit of 7 microns was found for the methylpentene polymer. This was the smallest fiber that could be made consistently for the draw rates required from the spinnerette. In later tests, it was found that this size of fiber also closely approaches the minimum wall thickness from a structural standpoint. Thus, an optimum hollow fiber membrane size of 50 microns ID by 64 microns OD was selected for the breadboard system. (If the polymer can be spun and then crosslinked, a potential exists for further weight and size reduction as discussed later in this section).

Evaluation Tests

Various tests were established to evaluate the performance characteristics of the hollow fiber test units for the purpose of fiber optimization and the generation of the materials properties data required for design. Three basic types of tests were performed. These included quality control tests used during the fiber fabrication, structural properties tests, and permeability tests.

1. Microscopic Examination

Microscopic examination of the fibers was used as a standard quality control check during manufacturing. Periodic examination of the fiber cross section was made to ensure that all 16 fibers being extruded from the spinnerette were uniform, that the internal and external diameter were concentric and of satisfactory dimensions, and that the wall thickness was uniform. In evaluating hoop stress failure modes, beaker units were pressurized with a liquid dye solution to structural failure. The failure areas indicated by the dye were examined microscopically. This evaluation assisted in solving the early biaxial stress distribution problem, which resulted in modification to the relaxation zone in the fiber manufacturing process, as discussed above.

2. Hydrostatic Tests

To determine the short-term pressure limitations of the fibers, hydrostatic leak and burst tests were conducted using the small-scale PM test units (the test setup was as shown in Figure 2-5b). Although the fibers are fabricated to handle gaseous flows, measurement of fiber leakage is best conducted using a fluid to which the polymer exhibits little or no permeability. Since the permeability of methylpentene polymer to water is orders of magnitude below that for oxygen or nitrogen, water was selected as the test fluid. The injection of a blue dye provided a visual indication of the location of fiber leakage.

Based on an incompressible laminar-flow model, the measured leakage rate was converted to an equivalent number of broken fibers. Results of the analysis using this model are shown in Table 2-3. These data, taken at 69°F (20.6°C) indicate that most of the fibers are capable of withstanding very high pressures for relatively short periods of time.

Later, it was determined that long-term failure due to creep was the more important design consideration. Rather than hydrostatic tests, primary life test data were obtained by using a lower constant gas pressure over a long period of time. By monitoring the total rate (permeation and leakage) through the wall as a function of time, the life characteristics of the unit could be accurately determined.

TABLE 2-3

HYDROSTATIC DYE LEAKAGE AND BURST TESTS

Module No.	Wall ID, microns	Wall Thickness, microns	Max. Press Tested, psig	Percent Unbroken Fibers
3	50	10	400	98.2
13	50	10	210	97.5
12	50	6	147	94.7

3. Axial Creep

No creep data were available for extruded methylpentene fiber. To obtain initial data, long-term axial creep tests were conducted on individual methylpentene fibers (50 by 70 microns). Tests were conducted by suspending a known weight from a single fiber attached to a frame. Fiber length was periodically checked to determine creep deformation; these tests were conducted at ambient conditions of 70°F.

The data shown in Figures 2-6 and 2-7 indicate that the fibers tend to creep even at relatively low tensile stress levels (for the test fiber geometry, one gram represents an initial axial stress of 755 psi or an equivalent hoop stress resulting from 185 psig internal pressure). These data indicated that long-term creep characteristics of the fiber are of prime importance in fiber module design. This indicated the necessity of long-term pressure hoop tests to establish the pressure life characteristics of the fiber.

4. Pressure Hoop Stress Tests

To evaluate the life characteristic of the fibers, long-term pressure hoop tests were conducted. Beaker units containing 800 fibers were fabricated and maintained at various constant pressure and temperature conditions. The flow rate of gas from the low-pressure side was monitored. Characteristically, for a relatively long period of time the flow would remain constant, and would correspond to the predicted permeant gas flow. Later, the rate would increase, indicating a fiber was starting to leak due to a hoop stress failure associated with long-term creep. Apparent permeation (the sum of permeation and leakage) rate was plotted as a function of time. The time until onset of failure is defined as the point of intersection of the slopes of the measured transmembrane flow curves established before and after the increase indicating leakage.

Results of the beaker unit tests to determine the hoop creep characteristics of the 50- by 70-micron and 50- by 64-micron fibers are shown in Figure 2-8, views a and b, respectively. Data points with arrows indicate that no leakage occurred at the time the test was concluded. The data indicate that

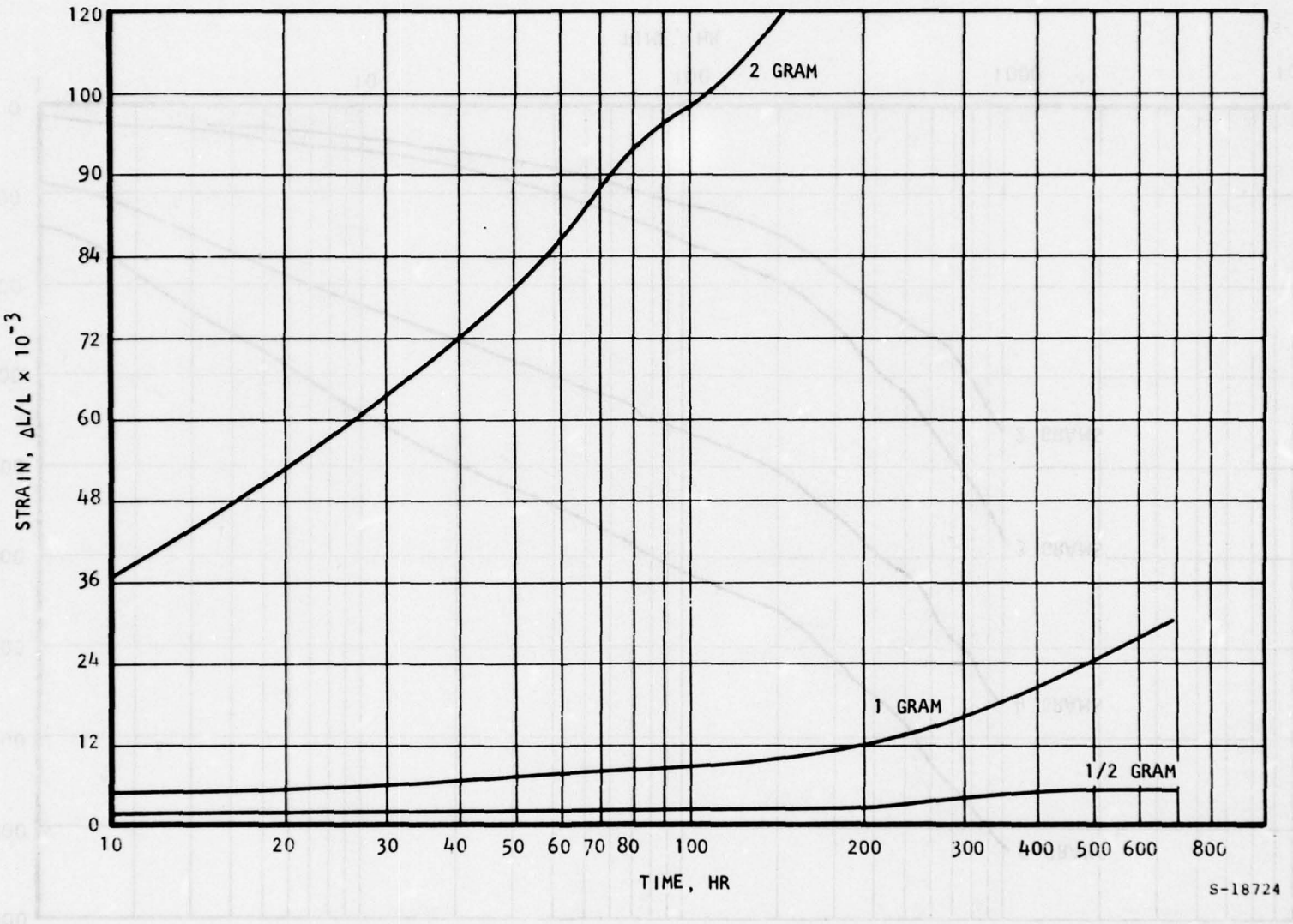


Figure 2-6. Fiber Tensile Creep Test Data (Low Stress Range)

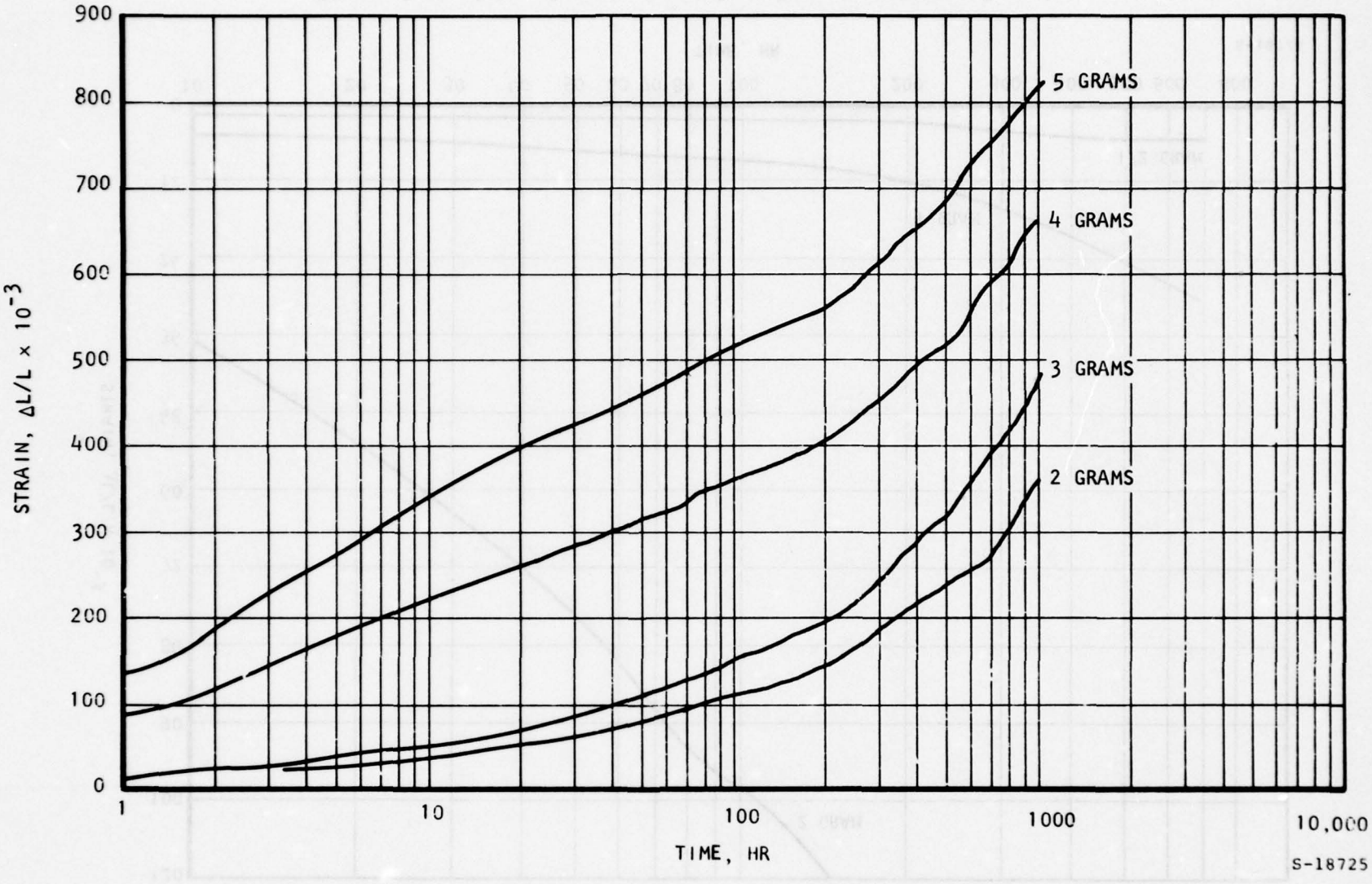
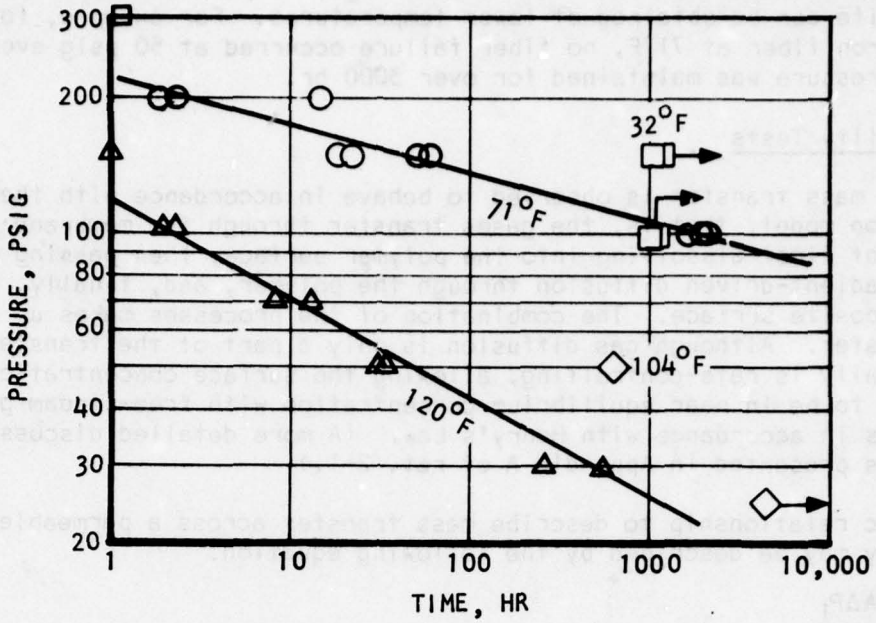
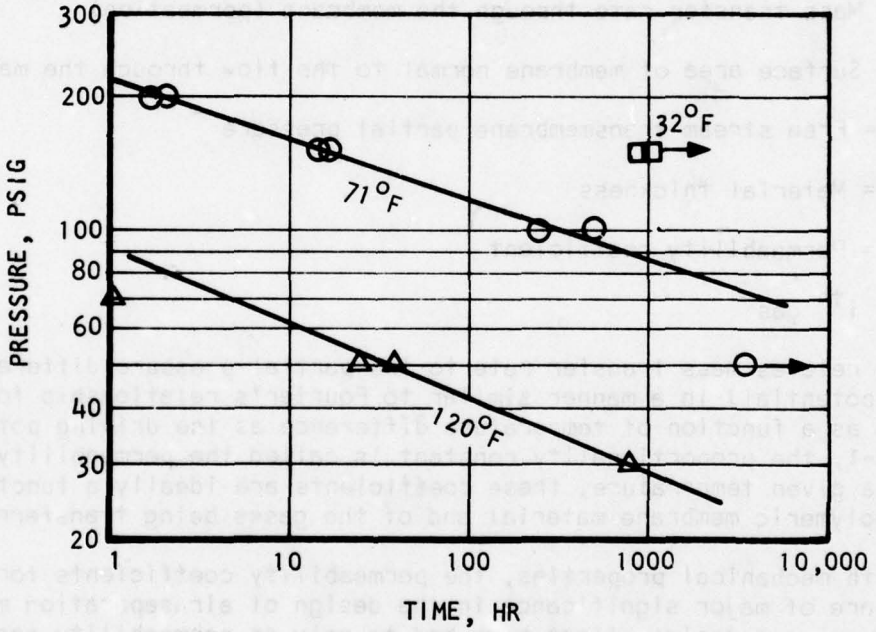


Figure 2-7. Fiber Tensile Creep Test Data (High Stress Range)



a. 10 MICRON WALL THICKNESS



S-10308-A

b. 7 MICRON WALL THICKNESS

Figure 2-8. Fiber Hoop Creep Characteristics

the creep characteristics of the fiber are strongly temperature dependent, and much longer life can be obtained at lower temperatures. For example, for the 50- by 64-micron fiber at 71°F, no fiber failure occurred at 50 psig even though this pressure was maintained for over 3000 hr.

5. Permeability Tests

Membrane mass transfer is observed to behave in accordance with the activated diffusion model, that is, the gases transfer through the membrane walls by a process of first dissolving into the polymer surface, then passing by concentration-gradient-driven diffusion through the polymer, and, finally, evolving at the opposite surface. The combination of the processes makes up permeable gas transfer. Although gas diffusion is only a part of the transfer mechanism, it usually is rate-controlling, allowing the surface concentration of dissolved gas to be in near equilibrium concentration with free-stream gas partial pressures in accordance with Henry's Law. (A more detailed discussion of this theory is presented in Appendix A of ref. 2-1.)

The basic relationship to describe mass transfer across a permeable membrane boundary may be described by the following equation.

$$\dot{Q}_i = \frac{TP_i A \Delta P_i}{th} \qquad (2\text{-}1)$$

where: $\dot{Q}$ = Mass transfer rate through the membrane (permeation)

A = Surface area of membrane normal to the flow through the material

ΔP = Free stream transmembrane partial pressure

th = Material thickness

TP = Permeability coefficient

$i = i^{th}$ gas

This equation relates mass transfer rate to the partial pressure difference (the driving potential) in a manner similar to Fourier's relationship for heat transfer rate as a function of temperature difference as the driving potential. In Equation 2-1, the proportionality constant is called the permeability coefficient. At a given temperature, these coefficients are ideally a function only of the polymeric membrane material and of the gases being transferred.

Along with mechanical properties, the permeability coefficients for oxygen and nitrogen are of major significance in the design of air separation modules. Previous analysis and design effort have had to rely on permeability coefficient data published by the manufacturer of the polymer with little laboratory verification. Uncertainties existed in the use of these data due to questions of applicability to the polymer following extrusions and re-crystalization in the hollow fiber spinning process. In addition, module optimization for aircraft system application requires an understanding of the variation in these key design parameters as functions of temperature; these data were unavailable at the outset of the program.

To establish these data, leak-free samples were fabricated and subjected to single-gas permeability tests. The test procedure consisted of elimination of all but the individual test gas from the test units to enable simple, reliable measurement of transmembrane partial pressure differences. One side of the membrane was then established at a selected pressure and the resultant flow rate was measured on the opposite, ambient-pressure side. Since this method cannot distinguish between permeant gas and leakage flows, beaker units were used to reduce the statistical leakage possibility to a minimum.

These important tests were concentrated during the first phase of the program; however, testing continued throughout the program. It is considered that reliable values of permeability coefficients for oxygen and nitrogen have been established for the polymeric fibers developed during the Phase I fiber optimization effort. Data were taken throughout the potential normal operating temperature range of interest with more intensive study in expected selection range of 50° to 85°F. Current data indicate the methylpentene hollow fiber permeability coefficients of oxygen and nitrogen to be 18.70×10^{-10} and 4.36×10^{-10} (cu cm/sec at STP)(cm)/(sq cm)(cm Hg) respectively at 77°F (25°C). Data for the range of 0° to 50°C are shown in Figure 2-9. Data outside of the range of principal interest have been plotted by assuming that the coefficients fit theoretical Arrhenius relationships. Data within the range of principal interest fit these relationships quite satisfactorily; data outside this range also compare reasonably well, allowing the use of equations to relate permeability coefficients to temperature.

Since the membrane selectivity ratio (i.e., ratio of oxygen to nitrogen permeability coefficients) is significant for air separation modules, current values for this parameter also have been established as a function of temperature. These data are shown in Figure 2-10.

6. Fiber Life

Axial creep and pressure-hoop stress test data indicate the principal failure mode of the methylpentene fiber is currently long-term plastic deformation, which results in leakage. Although the necessary initial work to substantially reduce or eliminate this failure mode has proved successful (see the discussion on molecular crosslinking later in this section), this creep behavior of methylpentene currently is the life-limiting parameter. Using the pressure-hoop stress test data discussed previously, analysis has been conducted to determine the time to the onset of leakage as a function of operating temperature. Figure 2-11 shows the results of this analysis for time to onset of leakage of 1000 and 3000 hr throughout the expected range of design operating temperature. The life limits shown by the curves of Figure 2-11 are for accumulated time at the full transmembrane pressure shown on the ordinate. Since system design for a flight mission only requires the application of full design pressure for a fraction of the operating time, system design can extend the life of membrane fibers by limiting application of full pressure throughout the major part of the operating time with inert gas concentration well within design requirements. As can be seen by reference to Figure 2-11, a reduction of only about 5 psi in transmembrane pressure differential can be expected to triple fiber life; in flight system designs, considerably greater operating pressure reductions are possible, thereby extending the operating life of the membranes to several times the values shown in Figure 2-11.

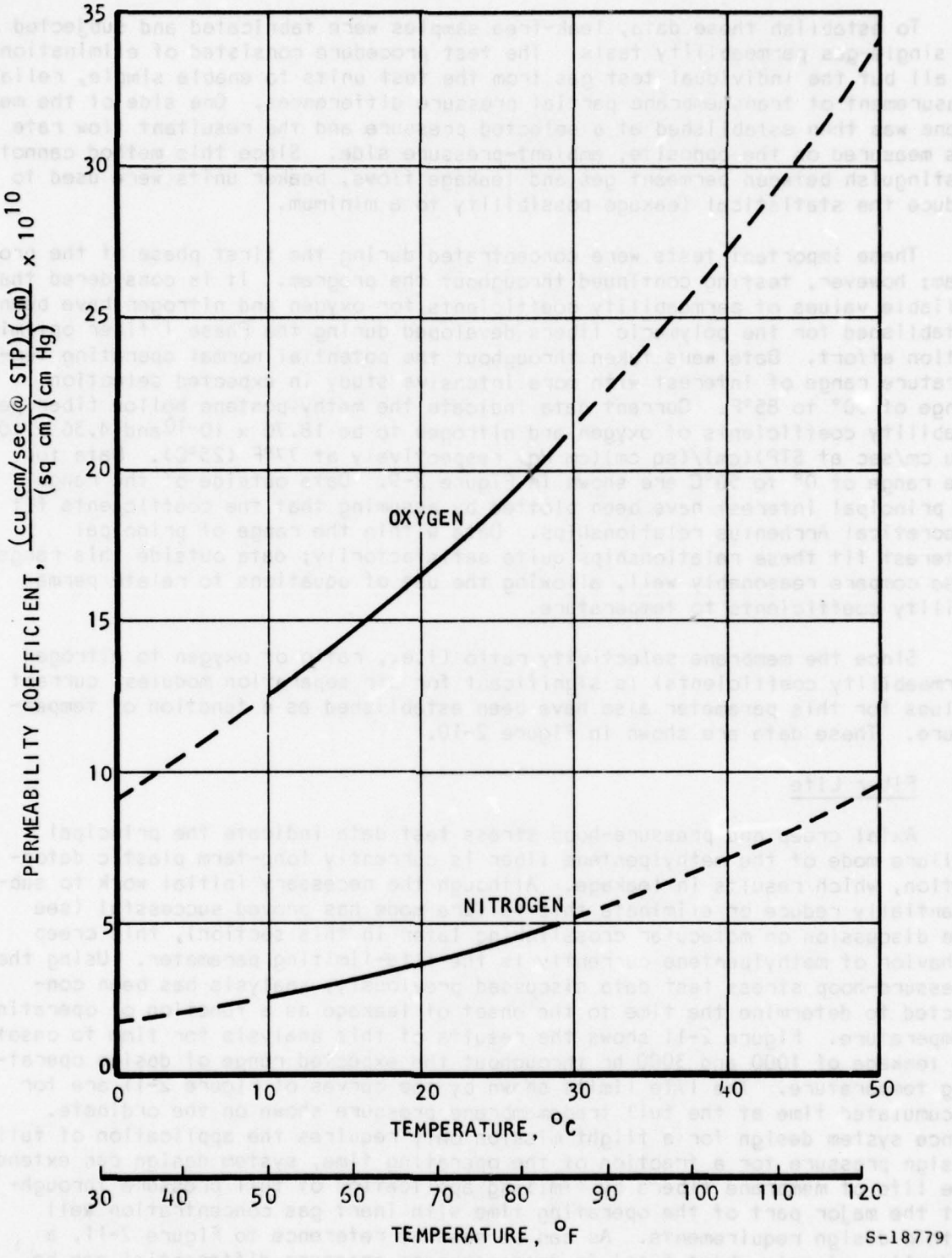


Figure 2-9. Methylpentene Hollow Fiber Measured Permeability Coefficients

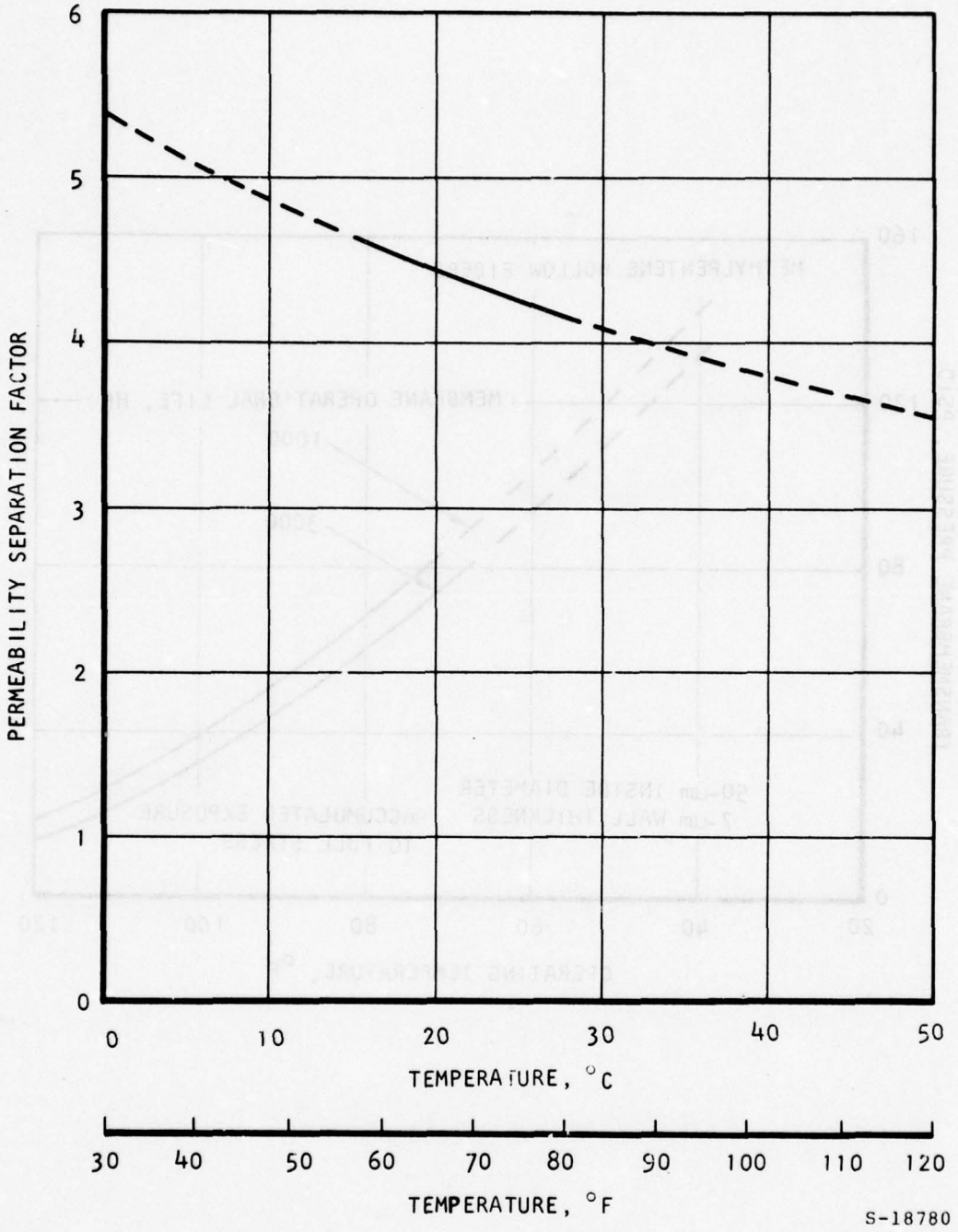


Figure 2-10. Methylpentene Hollow Fiber Measured Selectivity Ratio

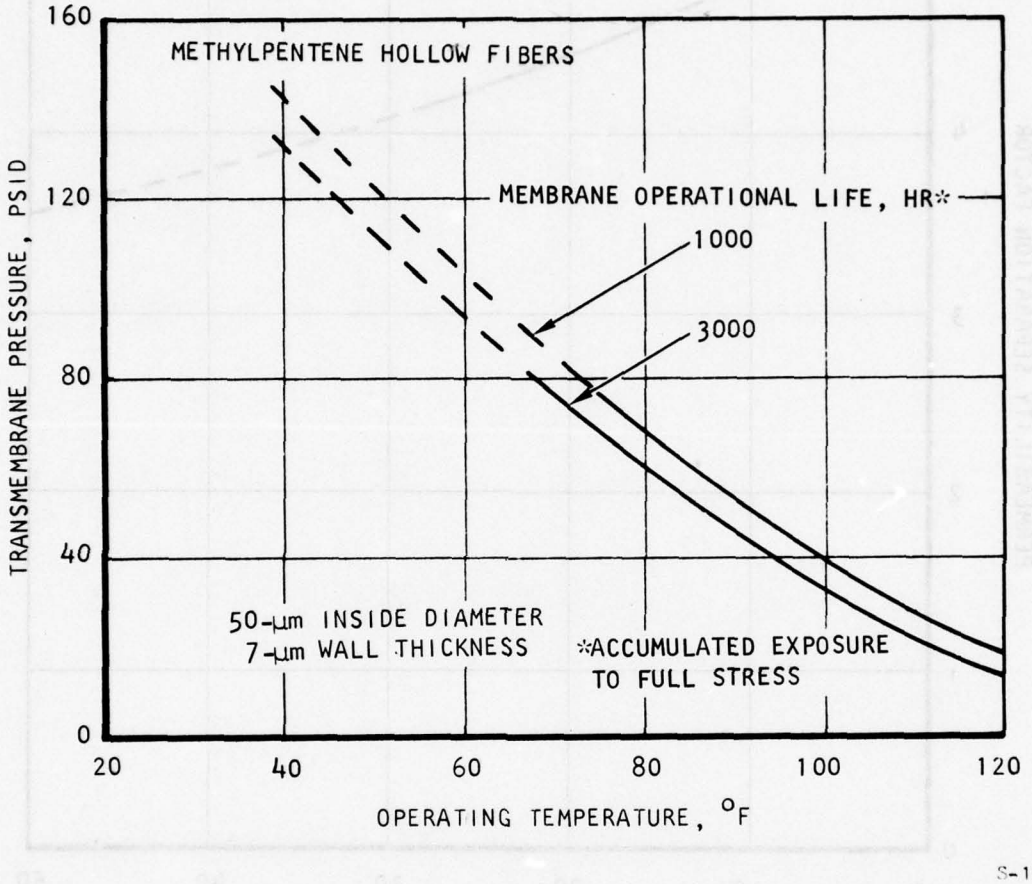


Figure 2-11. Limiting Transmembrane Pressures Based on Structural Life Considerations

OPERATING MODE INVESTIGATION

Due to the long-term creep behavior of the methylpentene fibers, investigations indicated that the attainment of adequate operating life requires the fibers be subjected to stress levels (pressures) considerably below yield or ultimate values. Pressurization of the fibers in past studies has considered the high pressure to be within the fiber bore and the low-pressure side to be external to the fiber. Due to the pressure of the creep failure mode, consideration was given to operating the devices with the high-pressure side external to the fibers and the low-pressure side within the fiber, resulting in compressive hoop loading. Investigations were conducted to determine if fibers would be able to sustain this stress loading more easily than in the internally pressurized mode. Schematic representation of air separation module (ASM) operation with internal and external pressurization is shown in Figure 2-12. The high-pressure product is the nitrogen enriched stream (inert gas) and the low-pressure product is the oxygen enriched stream (permeant gas).

Continuous testing of fiber samples with external pressurization under conditions similar to the previously discussed internally pressurized pressure hoop stress tests was conducted. It became evident that the fibers could survive longer for the same pressure and temperature conditions with external pressure. Table 2-4 shows typical failure time data for cells subjected to both operating modes.

At the same temperature, units operated with external pressurization could withstand approximately twice the pressure of those with internal pressurization for similar lengths of time. It was clear that, mechanically speaking, the externally pressurized mode of operation was superior to internal high pressurization for the hollow fibers; questions remained regarding the permeant gas pressure loss and mass transfer efficiency of the external mode of operation.

Air separation performance data were measured for a small-scale PM unit to evaluate these factors. Under 50-psig internal and external test conditions, inert gas flow and oxygen concentration were measured and compared. Results are shown in Figure 2-13. Much larger inert gas flows for the same inert gas oxygen composition are seen for the internal pressure mode than for the external mode; the external pressure mode inert gas flow at 9 percent oxygen content was only 29 percent of the internal pressure results.

Although higher operating pressures are possible using externally pressurized fibers, the loss in efficiency due to distribution difficulties of the high pressure gas in the externally pressurized mode more than negates this gain. In larger externally pressurized modules, additional decrease in flow capacity can be expected due to low-pressure permeant gas pressure losses inside of the fibers, reducing available gas transfer driving potential.

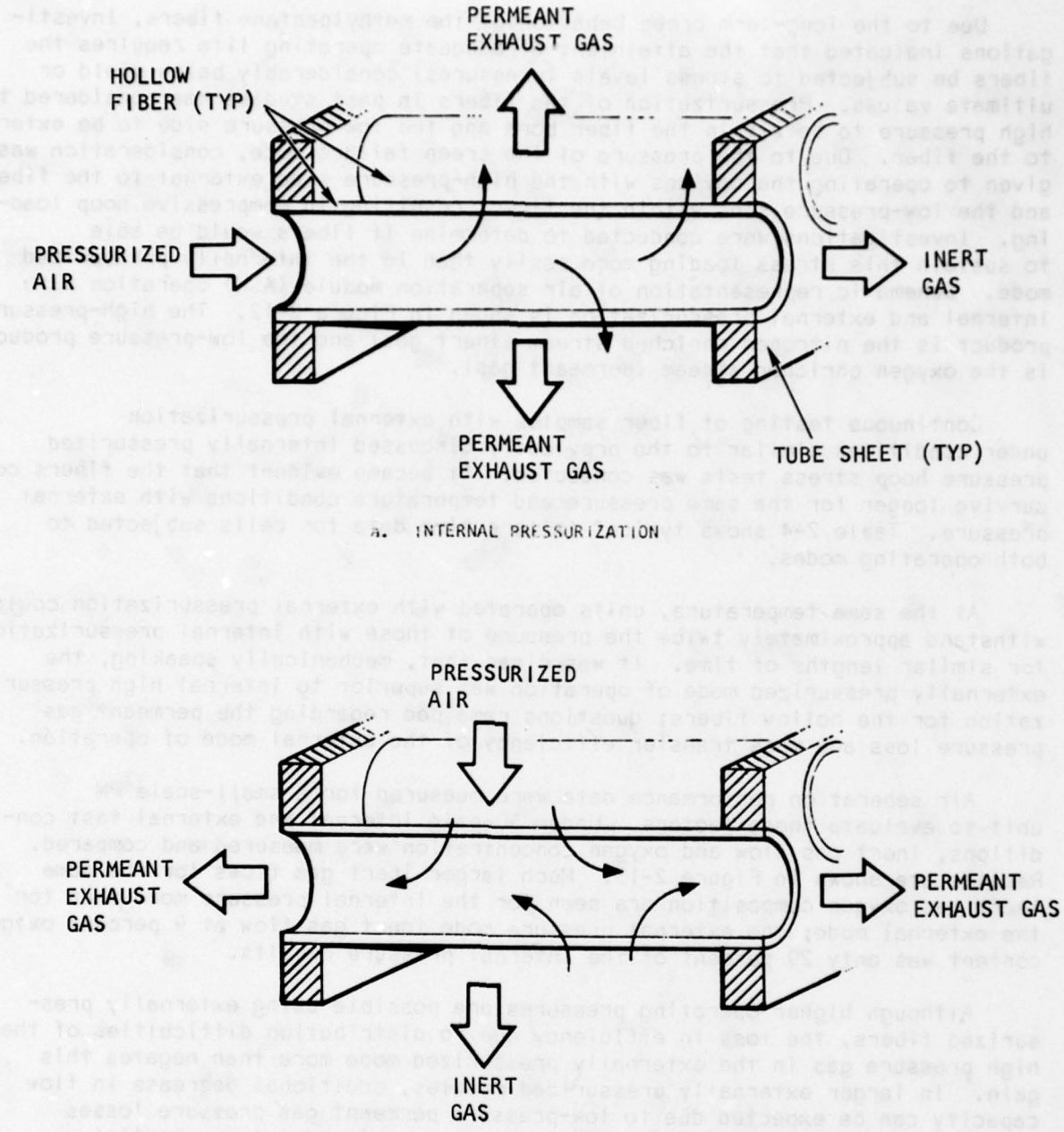


Figure 2-12. Pressure Operating Modes

TABLE 2-4

TYPICAL RESULTS, OPERATING LIFE COMPARISON

Fiber ID/OD, microns	Mode*	Pressure, Psig	Test Gas	Temperature, °C (°F)	Time Leakage Noted, hr	Test Time, hr
50/70	E	50	N_2	40 (104)	-	>3450
50/70	E	100	O_2	40 (104)	~600	-
50/70	E	150	O_2	40 (104)	~450	-
50/70	I	25	N_2	40 (104)	-	>3000
50/70	I	50	N_2	40 (104)	~625	-
50/70	I	100	O_2	22.4 (72.3)	~1800	-
50/70	I	100	O_2	22.4 (72.3)	-	>1270
50/70	I	100	O_2	22.4 (72.3)	~1225	-
50/70	I	100	O_2	22.4 (72.3)	-	>700
50/70	I	150	O_2	22.4 (72.3)	~20	-
50/70	I	150	O_2	22.4 (72.3)	~50	-
50/70	I	200	O_2	22.4 (72.3)	<15	-
50/64	E	100	O_2	40 (104)	~460	-
50/64	I	50	O_2	40 (104)	~360	-
50/64	I	50	N_2	22.4 (72.3)	-	>1635
50/64	I	100	O_2	22.4 (72.3)	~60	-
50/64	I	100	O_2	22.4 (72.3)	<12	-
50/64	I	150	O_2	22.4 (72.3)	<15	-

* E = Externally pressurized
I = Internally pressurized

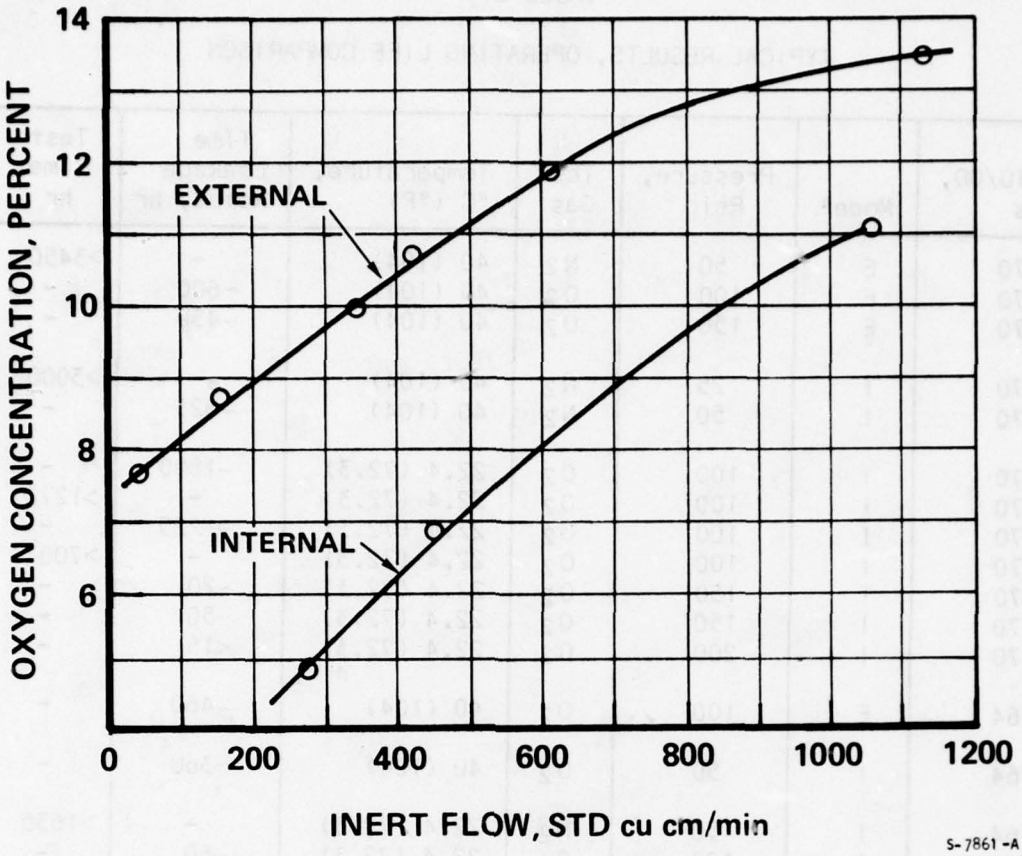


Figure 2-13. Performance Characteristics for Internal and External Pressurization

It has been concluded, therefore, that internally pressurized fibers remain the more favorable mode of operation. Future improvements in increasing structural capacity (see discussion on crosslinking) and subsequent tube wall thickness reductions will further increase the attractiveness of this mode of operation.

ENVIRONMENTAL COMPATIBILITY

In addition to the optimization of the permeable membrane fibers and generation of sufficient data to permit the design of the breadboard modules, the Phase I laboratory development effort was directed at evaluating the suitability of the methylpentene fibers to withstand aircraft environments. Environmental conditions representing off-design extremes were selected. Included were the following tests:

- Polymer oxidation--highly concentrated oxygen exposure
- High humidity--to saturation conditions

- Fuel exposure--both liquid fuels and saturated vapor environments.
- Thermal Shock--temperature cycling
- Dynamic environment--random vibration

Except for polymer swelling and reduction in yield strength during liquid fuel immersion, test results indicate acceptable performance following exposure to environmental extremes. Direct exposure of the polymeric fibers to the aircraft liquid fuel must be prevented for safety considerations in any event; system design requirements must include means to prevent backflow from the fuel tanks into the inert gas generator (IGG) system.

Oxidation

Since the fibers can be expected to be continuously exposed to oxygen, a test was conducted to evaluate changes in fiber structure or permeability as a result of prolonged exposure to excessive oxygen concentration. The procedure required that initial nitrogen and oxygen permeability data be established prior to concentrated oxygen exposure. For this test, two beaker units were used. Following establishment of initial permeability results, the beaker test units were subjected to 500 continuous hours of oxygen gas exposure. This was accomplished by displacing all air from the shell side of the beaker units with oxygen gas and internally pressurizing the fibers with oxygen to 20 psig at laboratory ambient temperature (70° to 75°F). Oxygen permeability was monitored at various times throughout the 500-hr test period. At the conclusion of this period, permeability of the units to nitrogen was again checked. The permeability data shown in Figure 2-14 indicate no significant change in

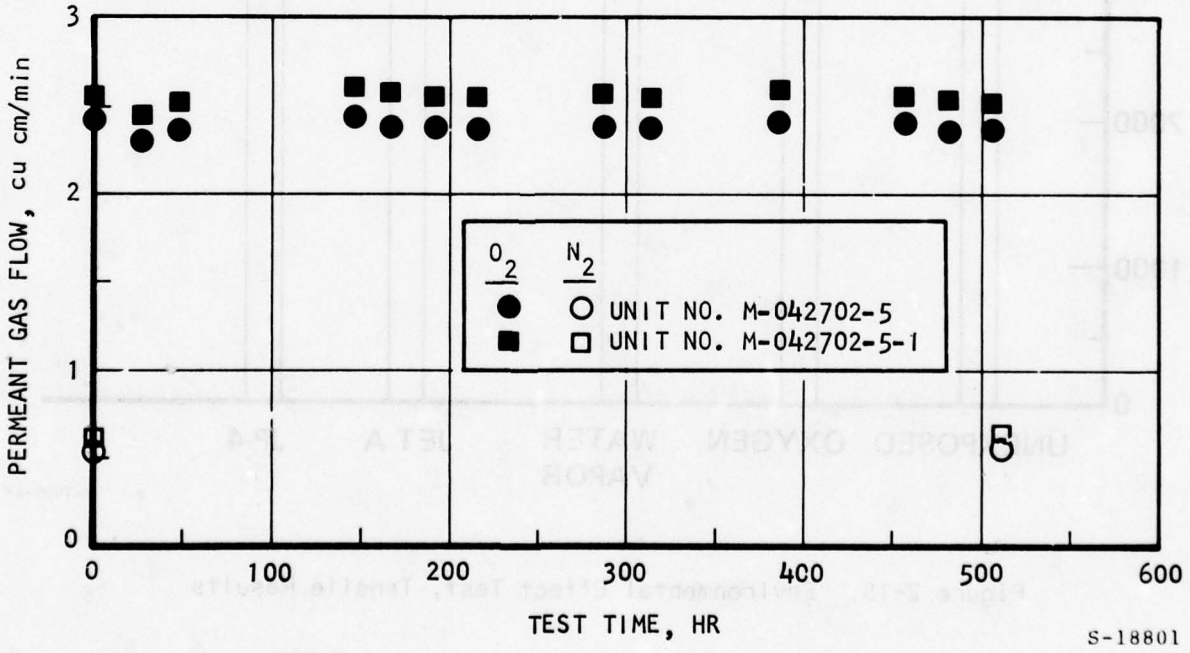


Figure 2-14. Oxidation Test Beaker Permeability Data

methylpentene permeability to either oxygen or nitrogen as a result of the 500-hr test period.

At the conclusion of the permeability test program, fibers were removed from the two beaker units and subjected to Instron tensile tests to determine whether any significant shift in structural properties, as determined by changes in yield strength, had occurred. Data were compared with Instrom yield data taken on fiber samples from the same fiber spool before the test units were fabricated. This comparison, along with tensile test data following exposure to water vapor and fuel-vapor-saturated air, is shown in Figure 2-15. As can be seen from the test result range, an apparent slight decrease in yield stress resulted for all tests. Since current design considers the long-term creep failure mode, and since the restriction to operating life limits (Figure 2-11) results in operation at a small fraction of the yield stress, this apparent decrease is not considered significant.

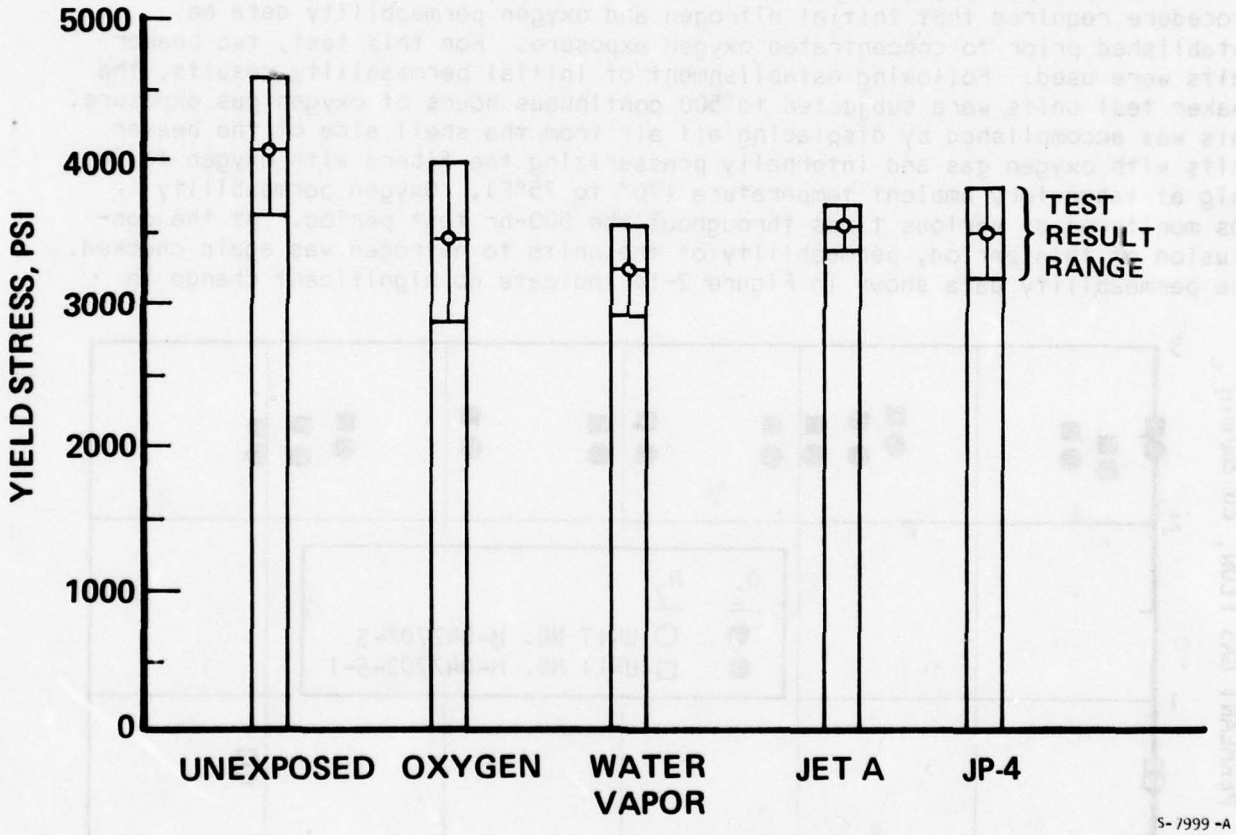


Figure 2-15. Environmental Effect Test, Tensile Results

Humidity

A test similar to the oxidation test was conducted using two other beaker test units. Following initial permeability tests for both oxygen and nitrogen, the modules were exposed to nitrogen gas saturated with water vapor by first bubbling the gas through a container of water using a frittered glass tube to dispense the gas in the water. The gas, at 20 psig, was passed through both the tube and the shell sides of the beaker unit for the 500-hr test period. During the exposure, the through-flow was periodically stopped and permeant gas flow was measured to check for shifts in nitrogen permeation as a result of polymer swelling or any other effect of high humidity. At the conclusion of the 500-hr test period, oxygen permeability was again measured as a final check against the initial values. These data, shown in Figure 2-16, show no degredation in permeability as a result of exposure to humidity. Post-test fiber yield tensile data, shown in Figure 2-15, also indicate no significant degredation of performance.

Due to the possibility of degraded behavior at combined high humidity and temperature, a second evaluation to determine any high-temperature effects was conducted. A beaker unit was placed in a test chamber and exposed to 100-percent relative humidity at 65°C (149°F). The unit was unpressurized while under test; at intervals the unit was removed from the environmental chamber, allowed to equilibrate at room temperature, and permeability was measured with oxygen at a pressure of 50 psig. Readings were taken until the flow stabilized. The data are shown in Table 2-5.

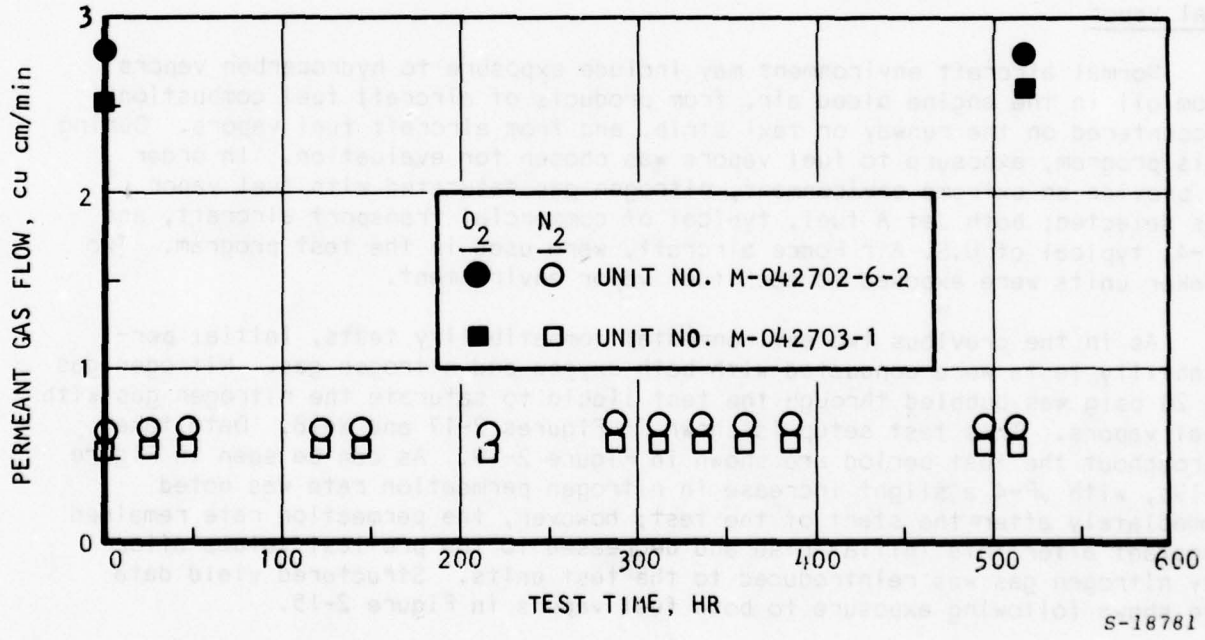


Figure 2-16. Humidity Test Beaker Permeability Test Data

TABLE 2-5

TEMPERATURE-HUMIDITY TEST RESULTS

Test Time, hr	Oxygen Permeation, cu-cm/min-psig
0	0.107
150	0.135
620	0.139
860	0.138
1310	(0.144)

The last data point, at 54 days, was taken before the flow stabilized; shortly after the data point was taken the unit was inadvertently damaged. Flow variation after the initial data point is relatively small. The initial rise after 150 hr might have been due to a microscopic flaw in one of the fibers that caused some leakage. The flow is quite stable for the remainder of the test, indicating no significant effect on permeability due to the environmental exposure.

Fuel Vapor

Normal aircraft environment may include exposure to hydrocarbon vapors from oil in the engine bleed air, from products of aircraft fuel combustion encountered on the runway or taxi strip, and from aircraft fuel vapors. During this program, exposure to fuel vapors was chosen for evaluation. In order to provide an extreme environment, nitrogen gas saturated with fuel vapor was selected; both Jet A fuel, typical of commercial transport aircraft, and JP-4, typical of U.S. Air Force aircraft, were used in the test program. Two beaker units were exposed to each fuel vapor environment.

As in the previous two environmental compatibility tests, initial permeability tests were conducted with both oxygen and nitrogen gas. Nitrogen gas at 20 psig was bubbled through the test liquid to saturate the nitrogen gas with fuel vapors. This test setup is shown in Figures 2-17 and 2-18. Data taken throughout the test period are shown in Figure 2-19. As can be seen in Figure 2-19b, with JP-4 a slight increase in nitrogen permeation rate was noted immediately after the start of the test; however, the permeation rate remained constant after this initial rise and decreased to the pre-test values after dry nitrogen gas was reintroduced to the test units. Structured yield data are shown following exposure to both fuel vapors in Figure 2-15.

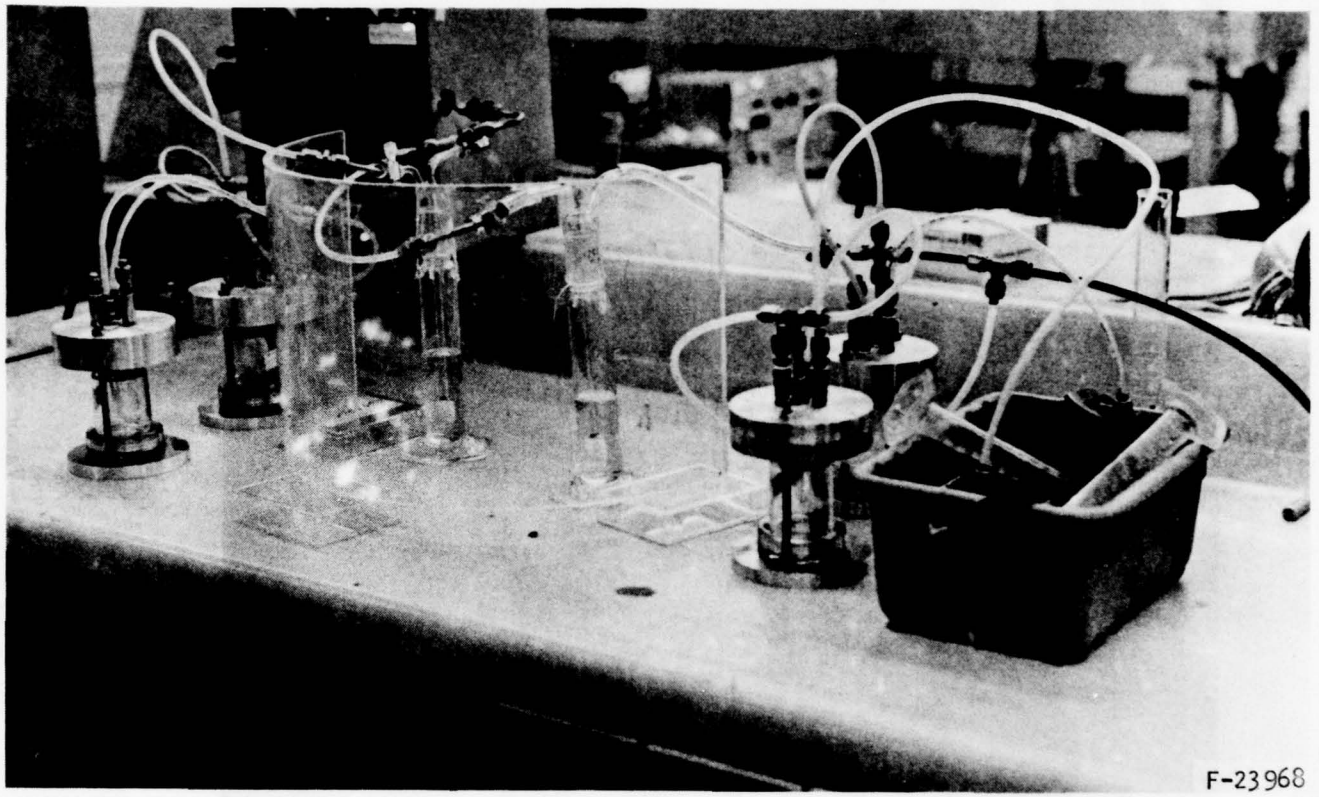


Figure 2-17. Jet Fuel Vapor Exposure Setup

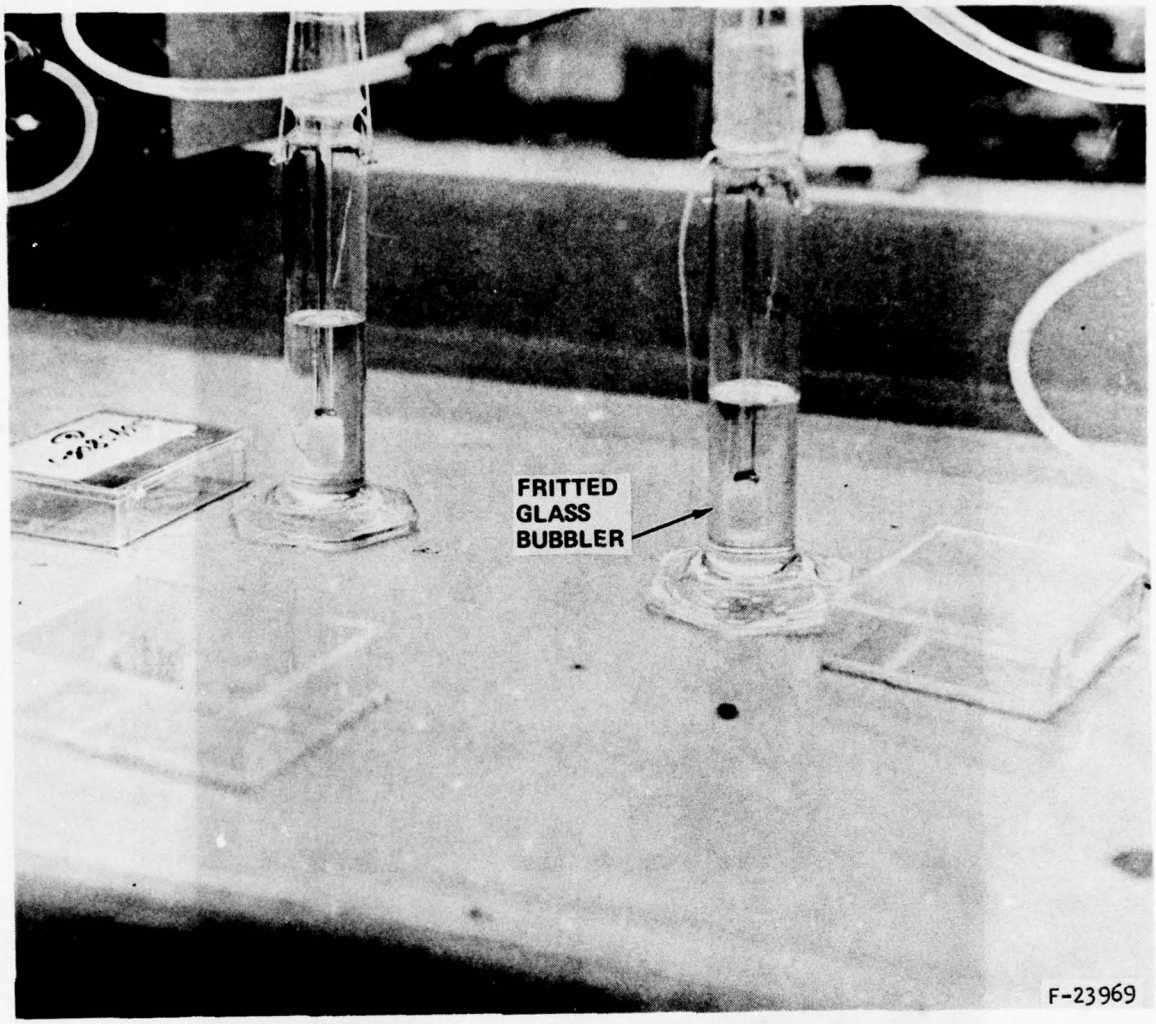
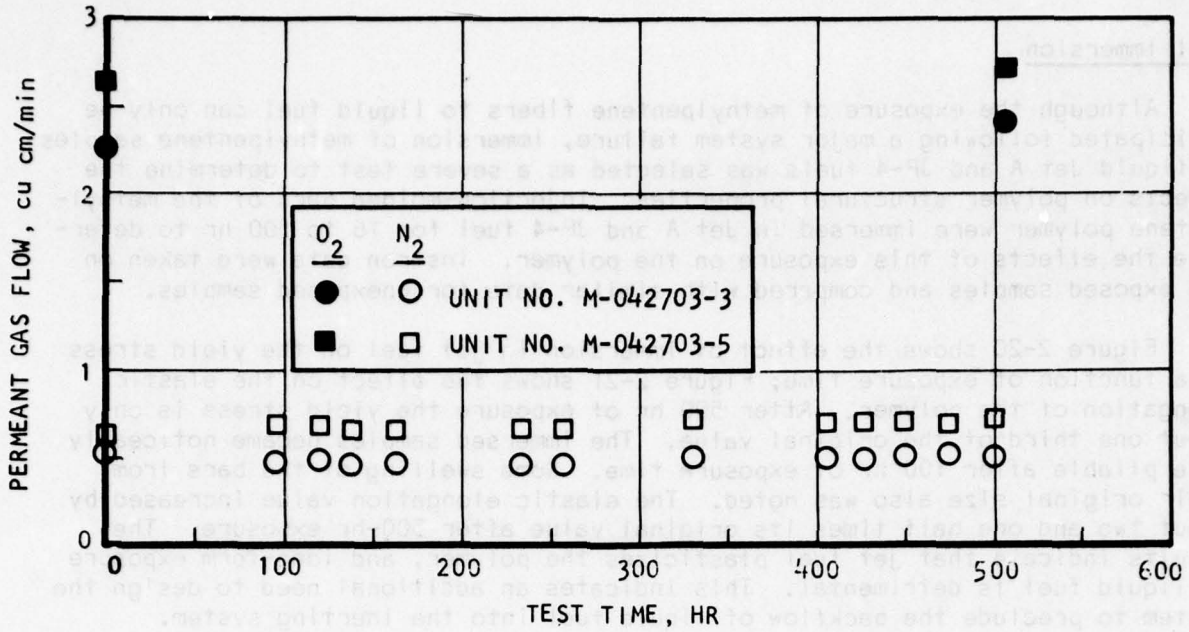
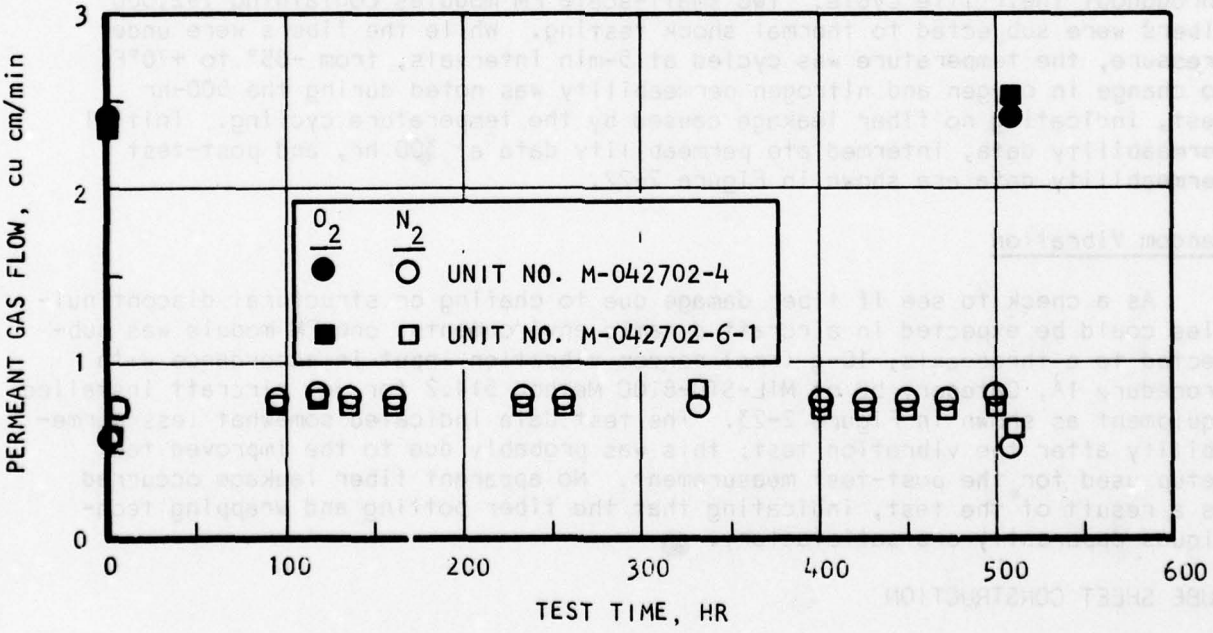


Figure 2-18. Vapor Saturation Bubblers



a. JET A FUEL VAPOR



b. JP-4 FUEL VAPOR

S-18782

Figure 2-19. Fuel Vapor Test Beaker Permeability Data

Fuel Immersion

Although the exposure of methylpentene fibers to liquid fuel can only be anticipated following a major system failure, immersion of methylpentene samples in liquid Jet A and JP-4 fuels was selected as a severe test to determine the effects on polymer structural properties. Injection-molded bars of the methylpentene polymer were immersed in Jet A and JP-4 fuel for 16 to 500 hr to determine the effects of this exposure on the polymer. Instron data were taken on the exposed samples and compared with similar data for unexposed samples.

Figure 2-20 shows the effect of immersion in jet fuel on the yield stress as a function of exposure time; Figure 2-21 shows the effect on the elastic elongation of the polymer. After 500 hr of exposure the yield stress is only about one third of the original value. The immersed samples became noticeably more pliable after 100 hr of exposure time. Some swelling of the bars from their original size also was noted. The elastic elongation value increased by about two and one half times its original value after 500-hr exposure. The results indicate that jet fuel plasticizes the polymer, and long-term exposure to liquid fuel is detrimental. This indicates an additional need to design the system to preclude the backflow of liquid fuel into the inerting system.

Thermal Shock

Although inerting system design will include means to stabilize and control the temperature of the membrane air separation modules (i.e., gas temperatures) to optimum conditions, temperature may be expected to "soak" to off-design values during periods of non-operation. Accordingly, the hollow fiber membranes must withstand temperature cycling during transient conditions throughout their life cycle. Two small-scale PM modules containing 192,000 fibers were subjected to thermal shock testing. While the fibers were under pressure, the temperature was cycled at 5-min intervals, from -65° to +70°F. No change in oxygen and nitrogen permeability was noted during the 500-hr test, indicating no fiber leakage caused by the temperature cycling. Initial permeability data, intermediate permeability data at 300 hr, and post-test permeability data are shown in Figure 2-22.

Random Vibration

As a check to see if fiber damage due to chafing or structural discontinuities could be expected in aircraft dynamic environments, one PM module was subjected to a three-axis, 10-g (rms) random vibration input in accordance with Procedure 1A, Category b2 of MIL-STD-810C Method 514.2 for jet aircraft installed equipment as shown in Figure 2-23. The test data indicated somewhat less permeability after the vibration test; this was probably due to the improved test setup used for the post-test measurement. No apparent fiber leakage occurred as a result of the test, indicating that the fiber potting and wrapping techniques apparently are satisfactory.

TUBE SHEET CONSTRUCTION

The tube sheet fabrication technique and materials to be utilized for the later full-scale modules is typical of construction used by Dow in other

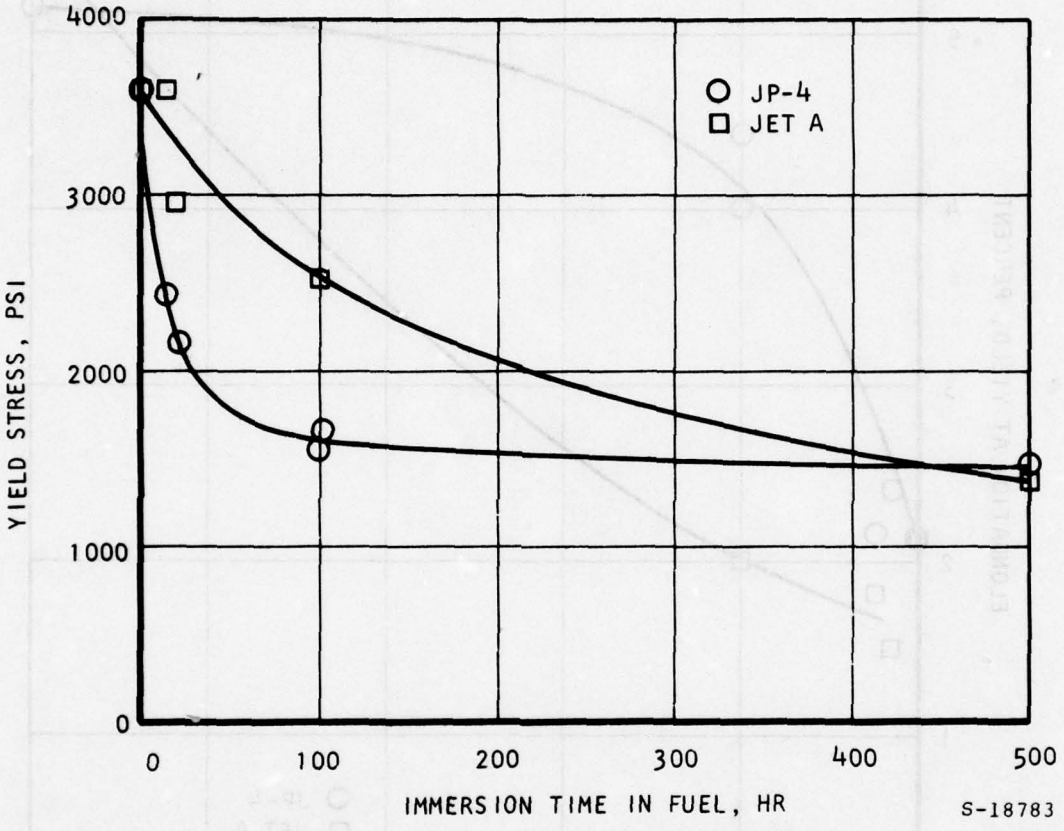


Figure 2-20. Effect of Immersion in Jet Fuel on the Yield Stress

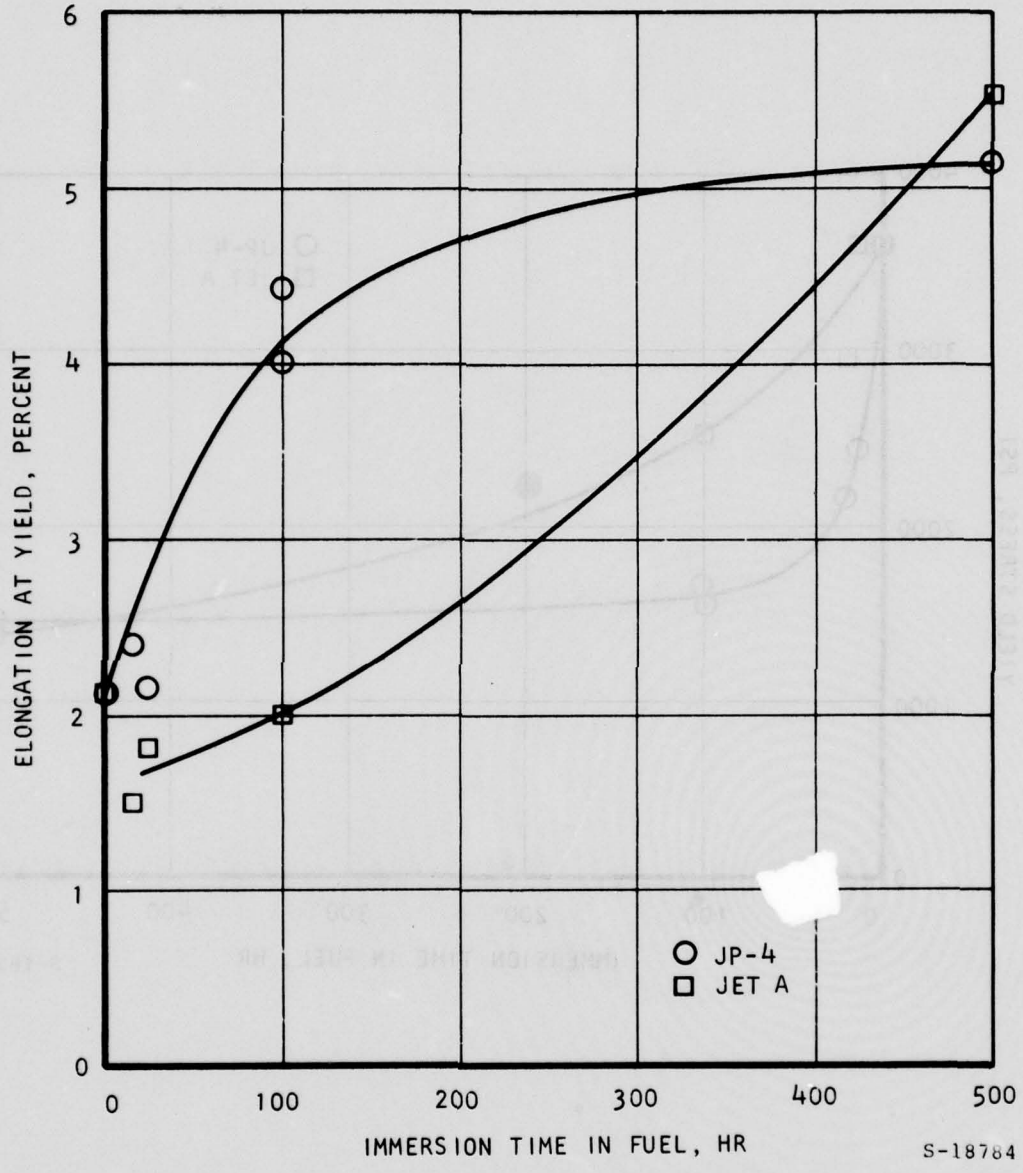
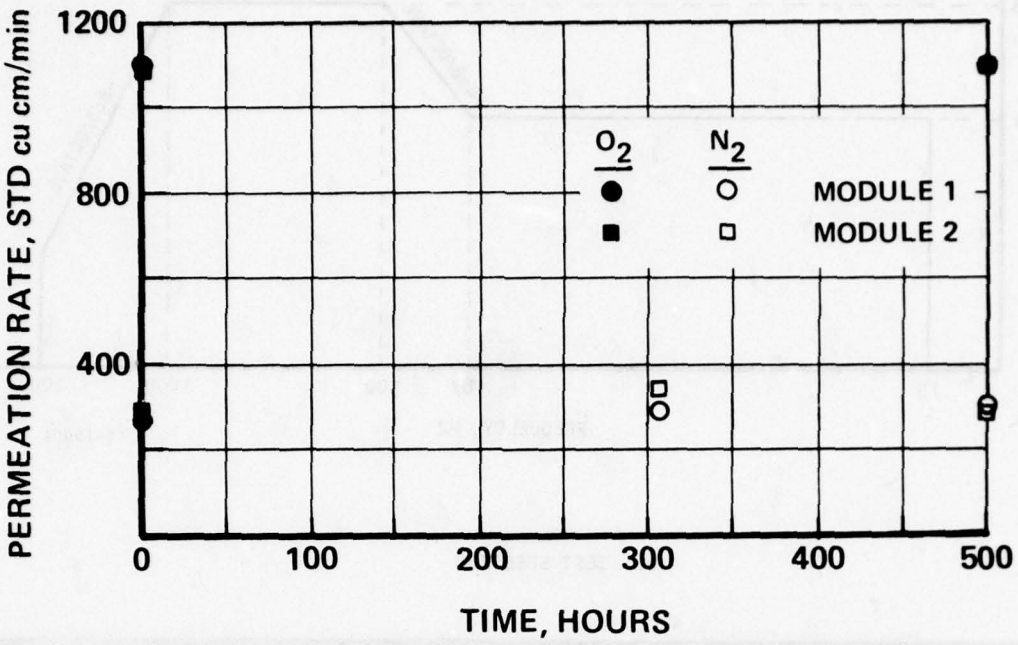


Figure 2-21. Effect of Immersion in Jet Fuel on the Elastic Elongation

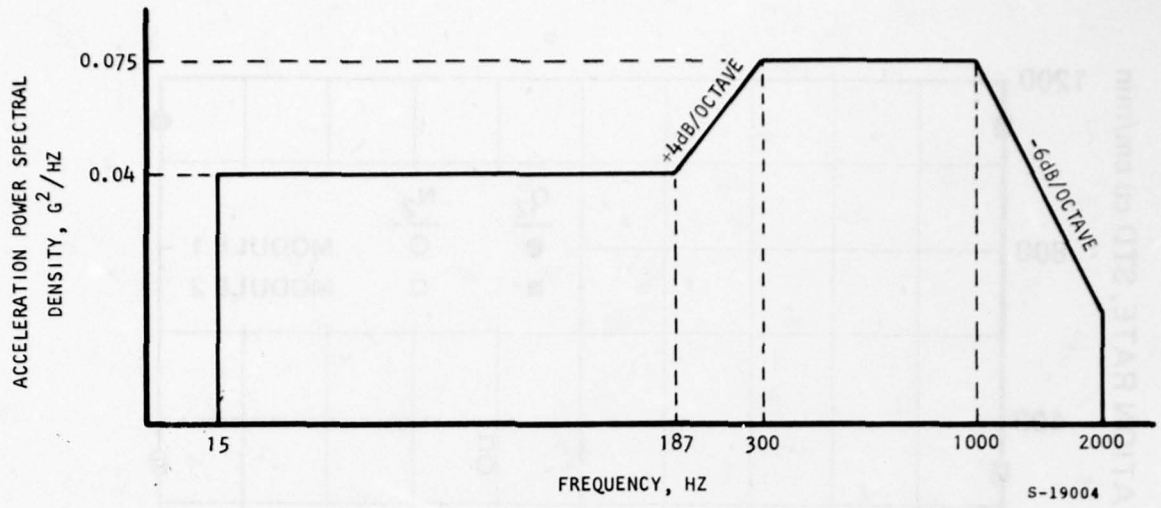


S-18792

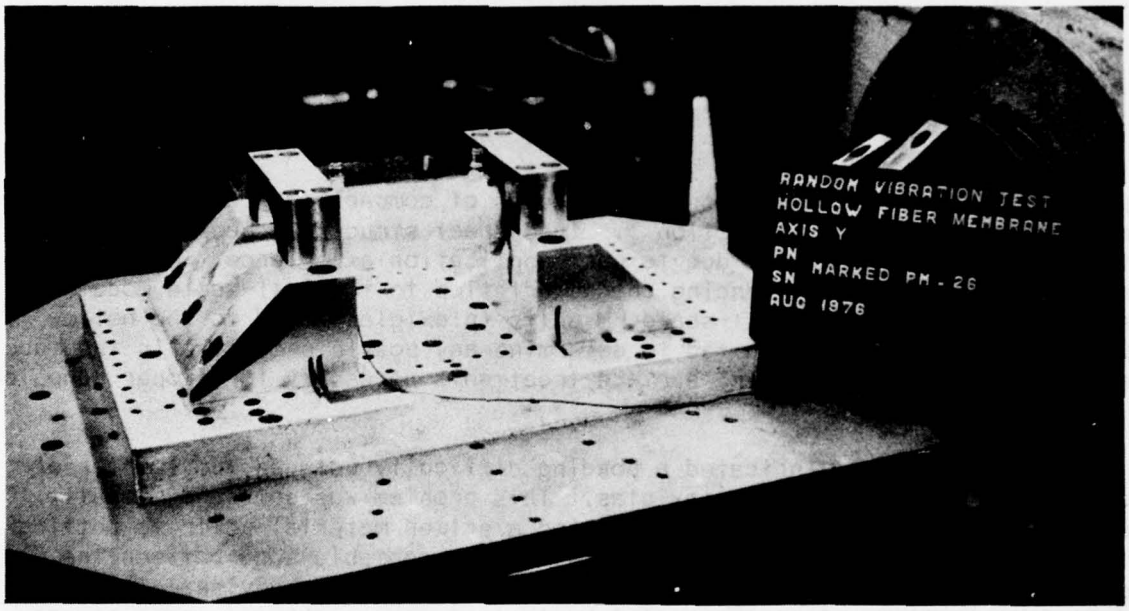
Figure 2-22. Thermal Shock Test PM Permeability Data

applications, such as reverse osmosis modules of comparable size to the breadboard modules discussed in Section 3. Tube sheet structural properties were not expected to be a problem due to past application experience. Laboratory tests of tube sheet epoxy bonding characteristics to the full-scale module case (aluminum), to the small-scale PM units (plexiglas), and to the hollow fibers themselves were evaluated to determine any possible changes in the tube sheet material or to determine surface treatments necessary for proper adhesion at interface locations.

Preliminary tests indicated a bonding difficulty between the tube sheet epoxy and the PM test module plexiglas. This problem was solved by locally roughening the plexiglas surface and using a primer material prior to potting with epoxy. This solution seems to produce an acceptable bond between the epoxy tube sheet and the plexiglas envelope as determined by visual inspection and Instron testing. As a check of tube-to-tube sheet adhesion under severe thermal shock, an additional test of the module was conducted. This check consisted of chilling the module to -63°F at a 2°F/min rate to simulate cold soak during a nonoperating period. Following a 2-hr cold soak at the -63°F temperature, the test chamber doors were opened and ambient-temperature gaseous nitrogen at 50 psig and 1.0 to 1.5 lb/min was introduced into the tube side of the unit and allowed to flow until the exit gas temperature was again stabilized at ambient temperature (about 30 min). No visual damage was apparent; pre- and post-leakage tests yielded identical results, indicating no failure as a result of the cold soak check.



a. TEST SPECTRUM



b. TEST SETUP F-26058

Figure 2-23. PM Unit Random Vibration Test

An evaluation of the bonding characteristics to the aluminum case of the larger breadboard modules indicated a similar need to achieve a good structural bond. A chromic acid etch pretreatment on the aluminum surfaces was used to aid in establishing a satisfactory tube sheet-to-aluminum shell bond.

No difficulties were encountered in bonding the epoxy tube sheet to the methylpentene fiber.

MOLECULAR CROSSLINKING

Crosslinking of the polymeric molecules that make up the walls of the methylpentene hollow fiber permeable membranes used in the modules offers a potential method of improving the inert gas productivity per unit weight and size of the fuel tank inerting system. Interconnecting the polymeric chains in the membrane by a crosslink would be expected to increase the creep resistance and hoop strength of the fibers so they can be operated at higher pressure or temperatures, or operated under the conditions presently used but with a thinner wall. Any of these alternatives would result in an increase in fiber permeability per unit weight of fiber and an increase in inert gas productivity per unit weight of module, and/or an increase in useful life.

An example of the improvement achieved for polyethylene tubes is shown in Figure 2-24. This dramatic increase in operating stress also may be obtainable for methylpentene. For example, Figure 2-24 shows that uncrosslinked

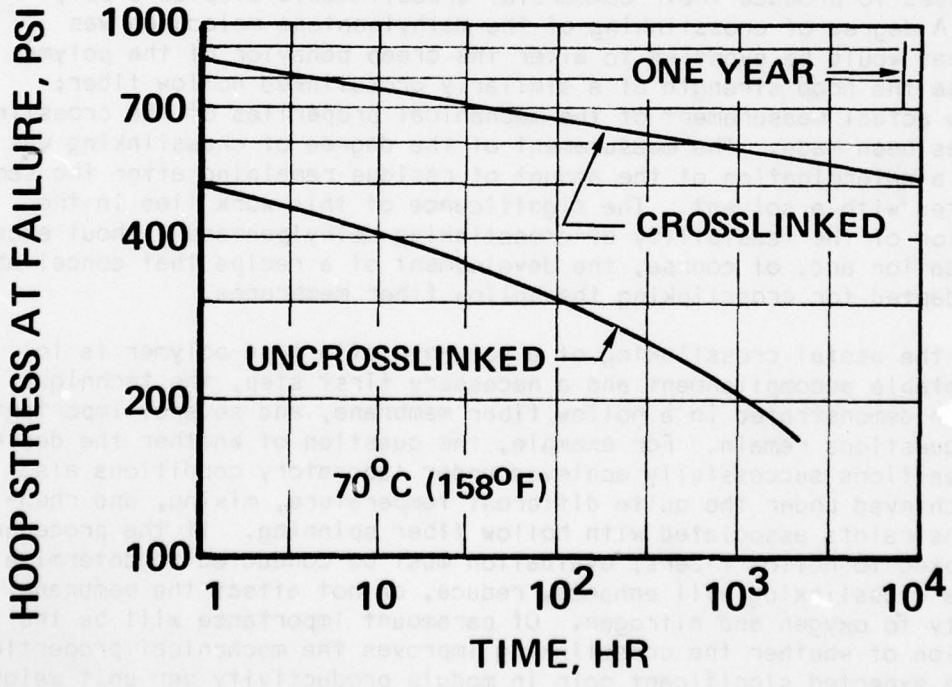


Figure 2-24. Resulting Increases in Strength for Crosslinked Polyethylene

polyethylene hoop stresses of about 200 psi will result in failure at about one thousand hours; the crosslinked polyethylene will have virtually unlimited stress life when subjected to a 200-psi hoop stress. Alternatively, the crosslinked polyethylene could be expected to fail at the 1000-hr period if subjected to a hoop stress increased to near 600 psi. Increased allowable stress for a similar life offers the possibility of reducing wall thicknesses by a factor of three with operation at the same pressures for the crosslinked polymer. Since the weight of the methylpentene air separation modules varies approximately as the square of the wall thickness and since the modules are the predominant contributors to system weight, the potential for system improvement is very significant. A successfully crosslinked methylpentene fiber of reduced wall thickness could be expected to substantially reduce system weight and at the same time extend membrane life.

Program Accomplishments

Although the methylpentene material in the hollow fiber membranes is an example of a polymeric class in which chemical crosslinking has been largely unsuccessful because of competing degradation reactions, recent development of a new crosslinking technique revived the possibility of crosslinking methylpentene. Dow Corning chemists were able to demonstrate crosslinking of methylpentene polymer during work done under subcontracts of this program.

As a result of work undertaken, the Dow Corning technical staff successfully crosslinked samples of methylpentene by a modification of the silane chemistry used to produce their commercial crosslinkable Sioplas E polyethylene. A degree of crosslinking of the methylpentene molecules was attained that would be expected to alter the creep behavior of the polymer and increase the hoop strength of a similarly crosslinked hollow fiber; however, no actual measurement of the mechanical properties of the crosslinked material has been made. The measurement of the degree of crosslinking was based upon a determination of the amount of residue remaining after the sample was extracted with a solvent. The significance of this work lies in the demonstration of the feasibility of crosslinking methylpentene without excessive degradation and, of course, the development of a recipe that conceivably might be adapted for crosslinking the hollow fiber membranes.

While the useful crosslinking of a poly-α-olefin type polymer is in itself a notable accomplishment and a necessary first step, the technique has not been demonstrated in a hollow fiber membrane, and several important technical questions remain. For example, the question of whether the desired chemical reactions successfully achieved under laboratory conditions also could be achieved under the quite different temperature, mixing, and rheological constraints associated with hollow fiber spinning. If the procedure can be adapted to hollow fibers, evaluation must be conducted to determine whether the crosslinking will enhance, reduce, or not affect the membrane permeability to oxygen and nitrogen. Of paramount importance will be the determination of whether the crosslinking improves the mechanical properties so that the expected significant gain in module productivity per unit weight, volume or life can be realized.

Additional Effort

Determining these data and adapting the crosslinking technique from a laboratory demonstration to a practical gain in efficiency for the fuel tank inerting modules are development problems that should be undertaken to fully exploit the potential of hollow fiber permeable membrane fuel tank inerting systems. The basic objectives of the crosslinking development remain the same; however, the scope and method of approach have become considerably refined as a result of the accomplishments discussed above. The tasks remaining in the development of a crosslinked methylpentene hollow fiber fall into two categories:

(a) Adaptation of the crosslinking procedure for methylpentene to hollow fiber membrane production

(b) Evaluation of the merit of the crosslinked membranes and determination of the best method to exploit the advantages of the crosslinked membrane in the fuel tank inerting system

Clearly, the first step, transfer of the crosslinking to the hollow fiber technology, is the critical one and the remaining work that involves development of new technology. After the successful completion of the first step, the second step should be a series of measurements and engineering analysis.

The adaptation of methylpentene crosslinking to the hollow fibers is a new technology, and disparities between the requirements of the Dow Corning crosslinking procedure and those of hollow fiber production are apparent. The technical approach recommended for Step (a) will be of an explanatory nature with the objective of either producing crosslinked methylpentene fibers within a few weeks or, in the worst case, knowing the technical problems are of a longer term nature. Initially, attempts to produce crosslinked fibers by the most simple and direct incorporation of the Dow Corning procedure in hollow fiber production will be made. In the event this is unsuccessful (difficulties can be expected because of the nature of the chemistry and the temperatures required for fiber spinning), several equipment and technique modifications, which at this point appear to be plausible solutions, should be tested.

If Step (a) is successful or partially successful in producing crosslinked methylpentene fibers, Step (b) can be initiated to determine the effect of the crosslinking upon the permeability of the membrane and the temperature-stress operating envelope by the use of small laboratory test cells. By partially successful, the situation is envisioned where samples of crosslinked fibers are produced, but the production is inconsistent and unsuited for module manufacture or preparation of a sequence of samples. The purpose of the small unit tests is to define, or at least provide an indication of, the benefits being gained from the crosslinking and to define the most favorable crosslinking conditions.

Preceding Page BLANK - FILMED

SECTION 3

BREADBOARD TEST PROGRAM

After the requirements were established for the airborne system during the initial preliminary design effort conducted at the conclusion of Phase I, the detail design and fabrication of air separation modules for a full-scale breadboard inert gas generation system were undertaken in Phase II. Breadboard tests to demonstrate system performance at the design point and during simulated mission profiles were completed during the third program phase. The design, fabrication, and testing of the breadboard IGG modules and the test facility established for the test program are discussed in this section. Also included is the module development program used to scale up from the 192,000-fiber PM modules, discussed in the previous section, to the full-scale modules, each containing over eight million fibers.

BREADBOARD MODULE DESIGN

From the Phase I initial airborne system preliminary design, the system design point (discussed in Section 4), shown in Table 3-1, was selected.

TABLE 3-1

BREADBOARD INERT GAS GENERATOR SYSTEM
DESIGN POINT PERFORMANCE REQUIREMENT

Inert gas oxygen concentration (maximum)	9 percent
Inert gas flow rate	2.33 lb/min
Conditioned air temperature	75°F
Pressure altitude	15,000 ft
Conditioned air pressure	74 psia

Although evaluations of subsequent laboratory development data indicated additional membrane surface area requirements, available data were evaluated to select a minimum membrane surface area requirement of 29,000 sq ft. Design tradeoffs indicate that overall module weight can be reduced, for a given surface area of fiber, by making the tube bundle as small as possible and obtaining the required area by increasing the length (high L/D ratio). Increased length, however, causes an increased tube-side pressure drop, reducing the permeation pressure differential and resulting in additional flow area required. Performance computer simulations indicated that the optimum length for the fiber active area (between the epoxy tube sheets) was approximately 36 in. Several configurations were evaluated, including a single large-diameter unit, multiple units of smaller diameter, and a single smaller unit with multiple separate insertable modules.

The selected design utilized two identical modules to provide the surface area required for the inert gas flow rates based on then available test data and the requirements of Table 3-1. A two-unit approach was selected to reduce the development risk associated with fabricating a single large unit and to gain additional experience in winding the tube bundle and fabricating the tube sheets. A design was developed that indicated each unit would contain a minimum of 8.25 million fibers, with an active flow length of 36 in. The tube sheets were to be bonded to the aluminum case and flat end plates were to be used to complete the fiber manifold. These would be attached to the case with flanges containing oversize bolt holes. The oversize holes would allow for proper alignment and sealing of the end plate to the purge tube. Outside diameter of the case was designed to be 11.7 in.; overall length was 42.4 in. to the face of the end plates.

Since the design of breadboard modules represented an increase in the number of fibers of a factor of over 40 and a surface area increase of a factor of about 250, a careful analysis of the problems of module fabrication scale-up was first undertaken.

Module Scaling Evaluations

Scale-up evaluations included increases to fiber spin rate capability, tube-sheet bonding evaluations, and most importantly, an intermediate sized module for direct evaluation of scale-up to gain confidence in the ability to fabricate the larger full-scale modules for the requirements of Table 3-1.

1. Spinning Evaluation

Spinning parameters were established for fabricating the fibers to be used in the breadboard modules. Using the baseline 16-fiber spinning head (spinnerette), the linear fiber rate was doubled and the other pertinent parameters (draw ratio and quench rate) were held at the baseline values used earlier in the development program. Tests showed that there was no change in permeability or hoop strength. Additional beaker units made from the higher spin rate fibers were placed on long-term, constant-pressure operation at room temperature and 100 psig. Performance consistent with the results of the previous development effort indicated the production of acceptable fiber.

2. Tube Sheet Bonding Evaluation

To obtain additional data on the epoxy tube sheet strength, three small (192,000-fiber) PM units were modified by removing part of the center section from the case wall. On pressurization, all the compressive load is then taken up by the small center purge tube. The units were tested to 600 psig, the maximum pressure of the test assembly. No epoxy failure occurred, although for most units the center core (purge tube) buckled due to the applied load at about 200 psig. For the 600-psig condition, the force on the tube sheet is 4825 lb and the shear stress on the bond is 2340 psi. Since the bond did not fail at this shear stress, the actual failure point would be higher. For the design of the breadboard module, epoxy shear stress is approximately 76 psi and bonding was not expected to be a problem. The tube sheet material and technique developed during Phase I was judged to be adequate and was selected for the breadboard system design.

3. Module Scale-Up

At the outset of the program, the minimum packaging factor design goal was 40 percent. (Packing factor is defined as the cross-sectional area of the tubes, based on their outside diameter, divided by the cross-sectional area of the tube bundle at the tube sheet face.) For the small prototype modules used in Phase I of the program, the mean packing factor value was 47.8 percent with a standard deviation of 5.5 percent. Based on the experience with these small units, it was decided to use a Dynel overwrap on the tube bundle and increase the design goal to a packing factor of 50 percent for the breadboard test modules.

Due to the large surface area scale-up from the PM size units to the breadboard test modules, the fabrication of an intermediate size module, designated as an SN 3 unit, containing approximately 3000 sq ft of membrane surface area, was selected to further evaluate module assembly techniques before the fabrication of the breadboard modules. The unit was fabricated with a 4.5-in.-dia tube bundle containing 1.7 million fibers with an active fiber length of 36 in.; the packing factor determined after fabrication was an unexpected 56 percent.

During fabrication of the SN 3-1 unit, the Dynel bundle overwrap was extended through the tube sheet face. Some leakage was found in the area of the Dynel overwrap, which is also the area used to epoxy the tube sheet to the case. These leaks were sealed and performance tests were conducted. The intermediate SN 3-1 module verified that:

- There were no fiber handling problems in scaling up from the 192,000-fiber module to the 1.7-million fiber module.
- A packing factor considerably in excess of 50 percent is achievable.
- The basic procedure for bonding the tube sheet to the case is satisfactory; however, the Dynel overwrap should not be extended through the tube sheet.
- Fiber-to-tube sheet bond is satisfactory.
- Bundle wrapping on a straight (rather than bias) winding machine is satisfactory.

In addition, the SN 3-1 module was used to develop a general procedure to determine the average dimension of the fiber, independent of measurements made during fabrication. In the laminar flow regime, the Hagen-Poiseuille equation is used to correlate the flow pressure drop characteristics as shown in Equation 3-1.

$$Q_F = \frac{n\pi D_i^4 (\Delta P_l)}{128 \mu L} \qquad (3\text{-}1)$$

where:

Q_F = volumetric flow rate through tubes

n = number of fibers

D_i = fiber inside diameter

ΔP_l = pressure drop

μ = viscosity

L = fiber length

The evaluation from Equation 3-1 indicated a relationship between the number of fibers present and their inside diameters. A knowledge of the number of fibers open after repair to seal leakage where the Dynel overwrap extended through the tube sheet (i.e., 1.5 million) indicated the average inside diameter of the fibers to be 47.7 microns.

A second method was developed from spin conditions. The cross-sectional area of the fiber can be determined from the spinning mass extrusion rate:

$$\dot{M} = \frac{\rho\pi\,(D_o^2 - D_i^2)\,\dot{L}}{4} \qquad (3\text{-}2)$$

where

$\dot{M}$ = mass extrusion rate

ρ = density

D_o = fiber outside diameter

$\dot{L}$ = fiber linear velocity

Using the log mean surface area, the fiber permeation rate is:

$$\dot{Q} = \frac{2\pi n\,\mathcal{P}\,L(\Delta P)}{\ln(D_o/D_i)} \qquad (3\text{-}3)$$

substituting D_o from Equation 3-2,

$$\dot{Q} = \frac{2\pi n\,\mathcal{P}\,L(\Delta P)}{\ln\left(\sqrt{\frac{4\dot{M}}{\rho\pi L D_i^2}} + 1\right)} \qquad (3\text{-}4)$$

where

$\dot{Q}$ = permeation rate

$\mathbb{P}$ = permeability coefficient

ΔP = transmembrane pressure differential

Calculating the permeation rate for various tube inside diameters from Equation 3-4 results in a relationship between the permeation rate and tube inside diameter. The measured permeation rate indicated a tube inside diameter of 48.9 microns. Averaging the results of the two independent methods yielded an average tube inside diameter of 48.3 microns. From the mass rate Equation 3-2, the tube wall size is found to be 8.5 microns. Thus average resulting fiber diameters were approximately 48.3 microns ID and 65.3 microns OD. A second small-scale module, designated SN 3-2, was fabricated using a reduced mass extrusion rate in order to obtain a fiber closer to the baseline 50-microns-ID by 64-microns-OD fiber as well as to further improve fabrication procedures.

In attaching the first tube sheet to the SN 3-2 container wall, a modified epoxy bonding procedure was used and some tube sheet face blockage resulted. The more standard method, used on the other end, was satisfactory. Fiber dimensions were verified using the method discussed above. The nominal fiber dimension was found to be 50 microns ID by 64 microns OD. Preliminary data were obtained on the permeability rate, the permeability ratio, and air separation performance. The permeability ratio (4.31) indicated good tube sheet and fiber integrity; however, both the permeability rates and the air separation performance were lower than expected. (This was felt to be due to the tube sheet blockage that occurred during fabrication.)

Initial Breadboard Module

Following release of the design drawings for the breadboard module, a sketch of which is shown as Figure 3-1, the aluminum parts for three modules (the two intended for use in the full-scale system and a spare) were released to fabrication. Following the correction to the fiber dimensions and successful fabrication of module SN 3-2, spinning of the fibers to fabricate the required membrane surface area was also initiated. The first breadboard size unit was designated SN R-1.

1. Fabrication

Following completion of the fabrication of the aluminum module cases, partially shown in Figure 3-2a, the cases were pressure tested to verify weld integrity and seal design. No problems were encountered in the fiber spinning operation for the first full-scale breadboard module. Tests were conducted on fiber samples to ensure that hoop strength and flux characteristics of the fiber were acceptable. These tests included single gas permeability

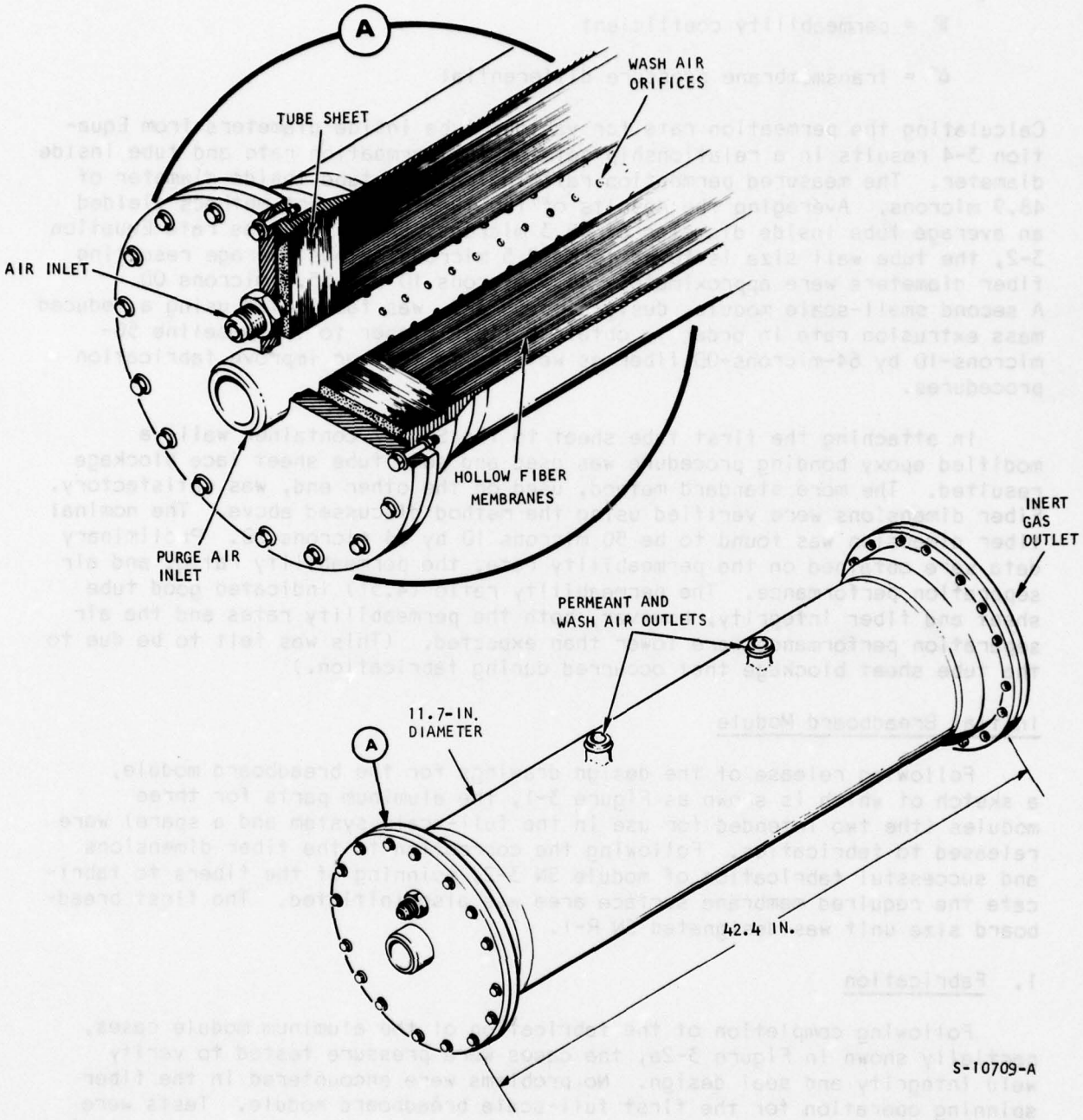
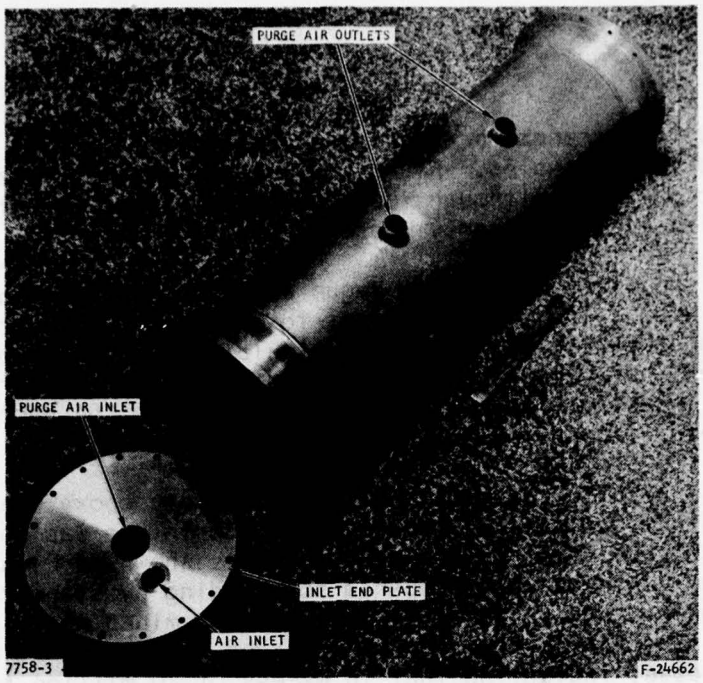
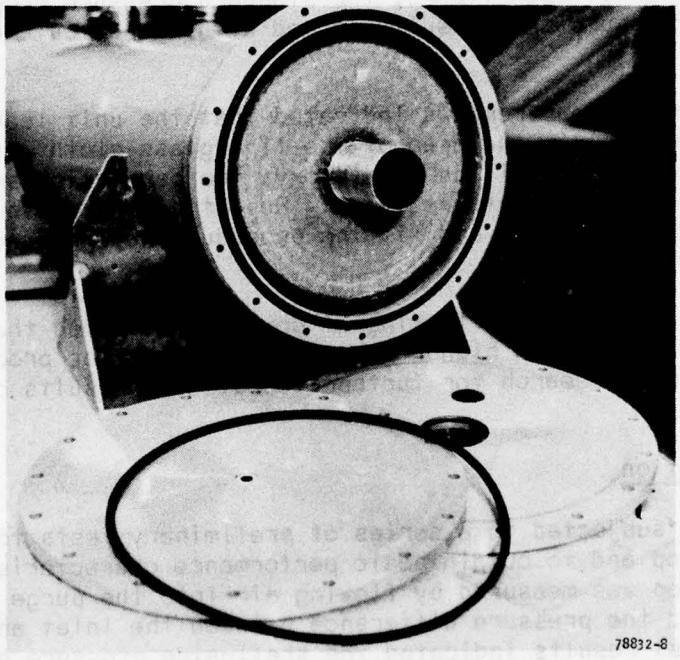


Figure 3-1. Breadboard Module Design



a. MODULE CONTAINER AND END PLATE



b. FIBER BONDED INTO MODULE CASE

F-26057

Figure 3-2. Breadboard Test Module

measurements with 50-psid transmembrane pressure and pressure step experiments on randomly selected fiber samples. Fiber quality was consistent and performance levels were acceptable, although the permeability coefficient was somewhat lower than anticipated from early Phase I results.

Fabrication of the fiber bundle was begun after verification of the fiber properties was completed. The first step was to wind the fibers around the purge tube. The number of fibers wound was calculated to be 9.46 million, based on the denier of the fiber, the length of the module, and the fiber weight. This resulted in an excessive tube bundle packing factor of 64 percent indicating a possible concern with shell-side pressure loss.

The rough bundle was flanged with a fiberglass cloth epoxy wrap and machined to fit into the aluminum case. The machined fiber cartridge was bonded to the aluminum case at each tube sheet end; a photograph is shown as Figure 3-2b. Previously, the aluminum surfaces were prepared for bonding by standard chromic acid etching techniques. During assembly, it was determined that, due to the high packing factor, the tube bundle could be made larger and still fit satisfactorily within the aluminum case, indicating that in excess of 10 million fibers can be placed within the aluminum case (the required baseline design point was 8.33 million fibers).

To verify the number of open fibers, the standard pressure drop measurement technique was used. Pressure drop results agreed with the calculated number of fibers.

Single-gas permeation measurements indicated that the unit leaked. Leaks were found in the tube sheet in the area of the fiberglass cloth wrap. This leakage area was routed out and filled with epoxy; the permeation separation factor increased to 4.04, an acceptable value. Repeating the pressure drop experiment showed that the routing and filling procedure had reduced the number of open fibers to 8.26 million.

During preliminary performance testing at Dow, it was noted that the shell-side pressure drop was much higher than predicted. After proof testing, the unit was shipped to AiResearch for further tests. The results of the tests are discussed below.

2. Performance Evaluation

Module SN R-1 was subjected to a series of preliminary tests to evaluate shell-side pressure drop and to obtain basic performance characteristics. Shell-side pressure drop was measured by flowing air into the purge tube and measuring flow rate and the pressure difference between the inlet and outlet on the shell side. Test results indicated the shell-side pressure drop to be greater than had been expected when extrapolating data developed during the Phase I program.

An analysis of the effect of average packing factor on pressure drop confirmed the sensitivity to the design parameter. It is believed that the additional pressure drop was experienced due to areas within the tube bundle where the packing factor, due to fiber shift or uneven assembly technique, was

much higher than the average value. The net effect of the higher pressure drop on the shell side was to reduce the transmembrane pressure differential for oxygen/nitrogen separation, particularly when the shell-side purge flow was used. This, in turn, reduces the inert gas generation capacity. With updated permeability coefficient data, the increased packing factor, and the increased shell side pressure drop, a review was made of alternates:

- Utilization of the current parallel wrap configuration and high packing factor. There were two system concepts associated with this approach: (1) simplification of the system by eliminating purge flow and increasing the generation rate by increasing the tube-side pressure, and (2) continued use of purge flow and increases in the tube-side pressure. Since a conservative pressure ratio was used for the turbocompressor design point, higher output pressures are achievable although at a greater aircraft penalty.

- Utilization of the current parallel-wrap configuration, with reduced packing factor and wash flows at current tube-side pressures. This would require additional fiber surface area to meet the design point flow rate, which could be provided by additional modules.

- Utilization of a non-parallel wrap configuration to reduce shell-side pressure drop. A bias-wrap configuration may be expected to reduce shell-side pressure drop; however, the effect on packing factor remains unknown.

All three alternates were actively evaluated.

3. Additional Intermediate Modules

Two additional SN 3 scale modules, SN 3-3 and SN 3-4, were manufactured, tested, and evaluated. The hollow fibers for SN 3-3 were wound into a bias configuration. Previous modules (SN 3-1, SN 3-2, and SN R-1) were fabricated using a parallel-fiber configuration. Module SN 3-4 was constructed in a parallel-fiber configuration but with a much lower packing factor than previous parallel units (46 percent). The details of module data for all five units constructed to date are given in Table 3-2, which lists each module, with individual values indicated for various module parameters. The first parameter is the number of fibers present; two numbers are shown. The first value has been arrived at by knowledge of the fiber weight used during manufacture together with the fiber weight per unit length as spun and the length of the device during this fabrication step. The second value was determined from axial flow-pressure drop experiments on the completed module. The cartridge diameter is the fiber bundle diameter including Dynel overwrap. The SN 3 series units were made using a 1.5-in.-dia wash tube; the SN R-1 unit has a 2.5-in.-dia wash tube. Packing factor values given are based on the fiber outer diameter, and the value listed for SN 3-3 is an average value for that unit that has been adjusted to include the added fiber area resulting from the bias-wrap configuration. Fiber dimensions and active area for each module are then presented.

TABLE 3-2

DESIGN EVALUATION MODULE DATA SUMMARY SHEET

	SN 3-1	SN 3-2	SN R-1	SN 3-3 (Bias)	SN 3-4
Number of fibers, millions					
By weight	1.74	1.59	9.46	1.02	1.43
By flow - ΔP_l	1.34	1.25	8.26	0.99	1.15
Cartridge diameter, in.	4.75	4.40	10.0	4.44	4.5
Packing factor, percent	56	59	64	42	46
Fiber dimensions, ID x OD, microns	48 x 65	50 x 64	50 x 64	50 x 64	50 x 64
Active area, sq ft	3100	2863	16,000	2130	2440

Tests on modules SN 3-2 and SN R-1 indicated the presence of significant radial pressure gradients across the fiber bundle on the shell side. Later modules SN 3-3 and SN 3-4 were constructed with lower packing factors to evaluate the effect of decreasing the shell-side pressure buildup. Figure 3-3 shows the observed relationship between shell-side pressure gradient and device packing factor for the last three SN 3 modules with shell-side flows of 0.53 lb/min. Pressure loss begins to rise sharply at packing factors higher than 40 percent. Figure 3-4 presents shell-side radial pressure drop data as a function of radial shell-side flow for modules SN 3-2, SN 3-3, and SN 3-4 at high flow rates.

Breadboard Test Modules

Assembled module shell-side pressure loss characteristics were evaluated and the test data correlated to establish final breadboard module design data. These data provided a means of combining the packing factor-dependent pressure loss and available surface area with permeability and gas concentration analysis to determine the most favorable packing factor for the existing module cases. Test data evaluated the effects of packing factors in the critical 40 to 60 percent range; analysis indicates that the most favorable overall performance can be achieved at a packing factor of about 50 percent.

Test and computer simulations indicated that the wash mode of operation remained more favorable than the non-wash mode for this packing factor using the existing breadboard module cases. The optimum wash rate at the design point remained in question due to the counterbalancing effects of reduced shell-side oxygen partial pressure with the increasing wash flow and the associated increase in shell-side absolute total pressure.

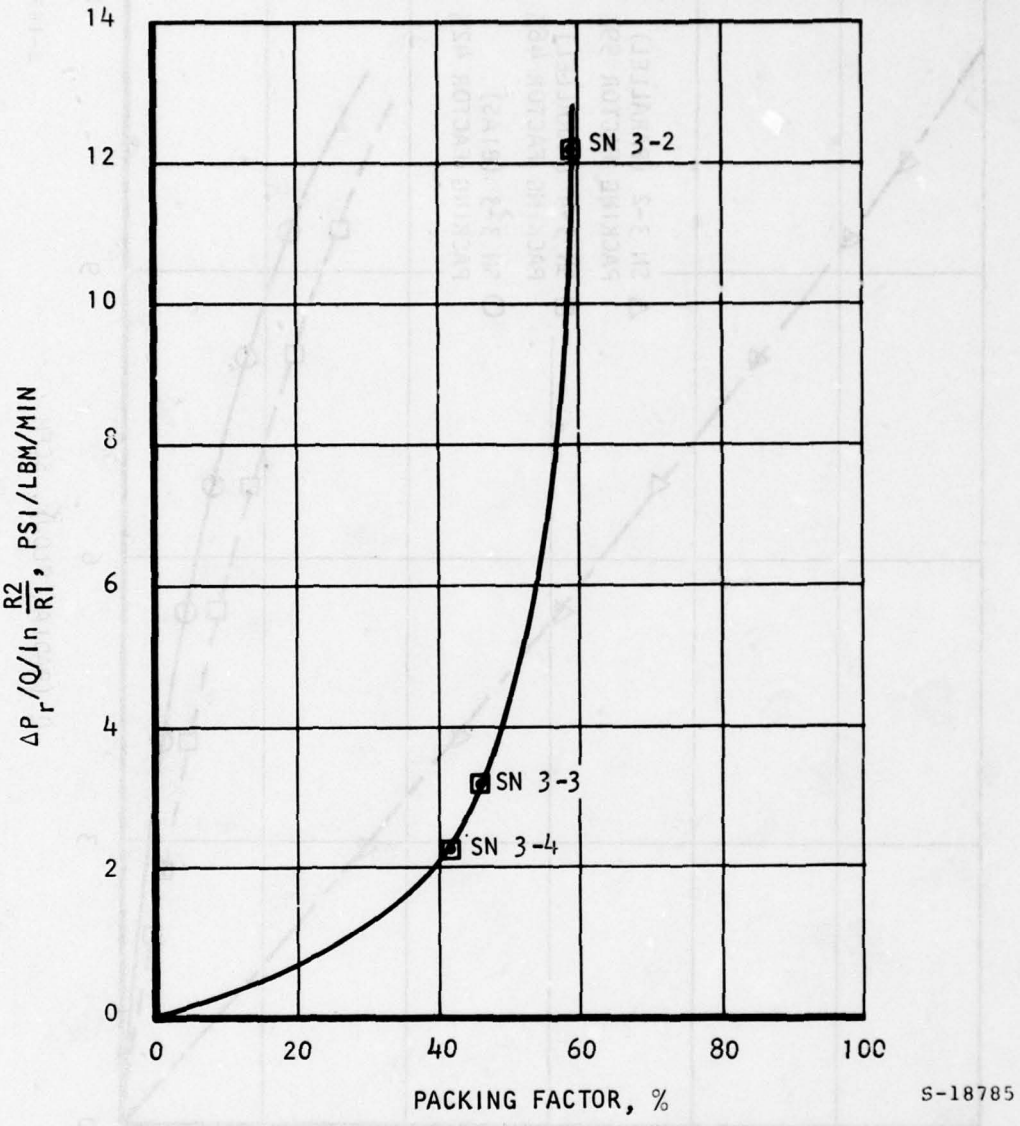


Figure 3-3. Shell-Side Pressure Gradient vs Packing Factor

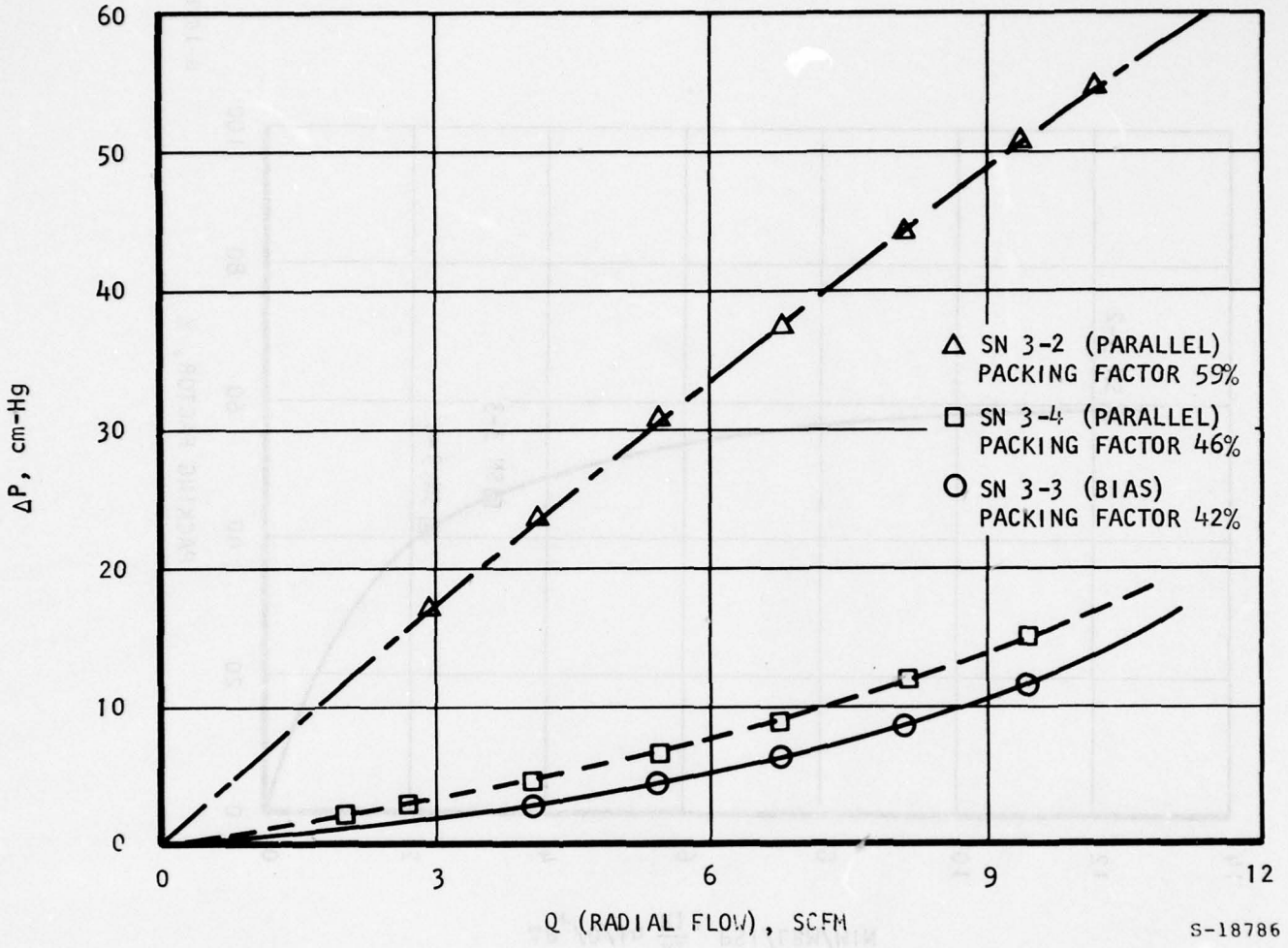


Figure 3-4. Radial Flow-Pressure Drop Results

As a part of the investigation, the bias-wrap module, although characterized by variable local packing factors, indicated no particular deviation from the parallel-wrap modules, although some flow distribution advantages may be expected. As a result of these data, the bias-wrap technique was not pursued at this time, and the decision was made to use three modules in the final system design.

To implement this decision, the destruction of the first breadboard test module (to recover the aluminum case) and the construction of the new breadboard test modules was initiated. All three new modules were to return to a packing factor of 50 percent as a design goal.

The fabrication of the three final breadboard test modules was undertaken. Basic fabrication data for the three modules are shown in Table 3-3.

TABLE 3-3

BREADBOARD TEST MODULE FABRICATION DATA

Fabrication Parameter	Module		
	SN R-2	SN R-3	SN R-4
Fiber size (ID x wall), microns	50 x 7	50 x 7	50 x 7
Number of fibers (by wt), millions	8.08	8.15	9.58
Packing factor, percent	52	52	56
Fiber bundle OD, in.	10.25	10.3	10.75
Surface area, sq ft	14,170	14,290	16,800

1. Module SN R-2

No significant problems were encountered in module SN R-2 fiber bundle fabrication. During fiber bundle manufacture, packing factors were measured at several bundle diameters. Approximately one-half of the fibers were in place at a bundle diameter of 7.5 in., where the packing factor was 52 percent. Since the final overall packing factor remained at 52 percent, this indicates a fairly uniform packing factor for most of the bundle.

A problem was encountered during the bonding of the fiber cartridge into the aluminum case. Some epoxy leakage occurred on bonding the first end into the case. The liquid epoxy flowed down to the lower end of the fiber bundle and closed a small number of tubes (less than 5 percent, some of which were reopened later). Initial tests on SN R-2 indicated only about 5.5 million open tubes; manufacturing data indicated there were 8.08 million fibers present

in SN R-2. Microscopic examination of the tube sheet face indicated that some fibers were not cleanly open. Several techniques were investigated to achieve a clean fiber cut in the tube sheet face before markedly visible improvement under the microscope was achieved. Both ends of SN R-2 were cut by the developed technique and the unit was checked for the number of open tubes present by the gas axial flow-pressure drop experiment. Results indicated substantial improvement in the number of tubes open: 7.74 million tubes (96 percent) open against the previous value of 5.5 million open.

2. Module SN R-3

The second breadboard test module, SN R-3, was fabricated and tested. Tube sheet problems were encountered in the fabrication of this module. One tube sheet end had a circumferential crack present that was repaired with an estimated 6 percent fiber loss. There was also a delamination of the epoxy-aluminum case bond in this same tube sheet, which was repaired with no fiber loss. Tests conducted after repairs showed 7.37 million open fibers (an estimated 96 percent of the fibers remaining open after the crack was repaired). Performance evaluation of the integral packing factor at several bundle diameters shows the trend is similar to that seen in SN R-2; an overall packing factor of 52 percent was achieved.

3. Module SN R-4

Except for the large packing factor, fabrication of module SN R-4 progressed without incident until the fiber bundle was bonded into the aluminum case. The fiber ends were opened using the techniques developed for SN R-2. Cracks in both tube sheet faces similar to those seen in SN R-1 and SN R-3 developed after the tube sheets were formed. The cracks were circumferential about the purge tube at about two-thirds of the fiber bundle radius. Repairs of the crack regions were begun by routing out the area and sealing the groove with epoxy. Several repair attempts were made before the leak regions were eliminated. Successful leak repairs were verified by measuring the oxygen-nitrogen single gas separation factor after the repairs were completed. Axial flow-pressure drop measurements indicated 7.73 million open tubes of 50 micron ID and 40 in. overall length. Figure 3-5 shows the inert gas end of the repaired module SN R-4 tube sheet.

4. Module Acceptance Tests

Upon completion, all three modules were subjected to initial tests to establish their suitability for full-scale test. Shell-side pressure losses were measured, and tube-side flow pressure drop tests were conducted to estimate the number of active fibers. Additional tests conducted on the modules measured the apparent permeability to both oxygen and nitrogen gas. These tests, conducted at 50-psig nominal transmembrane pressures, when combined with fabrication data, provide a means to calculate the apparent permeability coefficients for both test gases. A summary of the test conducted on the first two breadboard modules is given in Table 3-4.

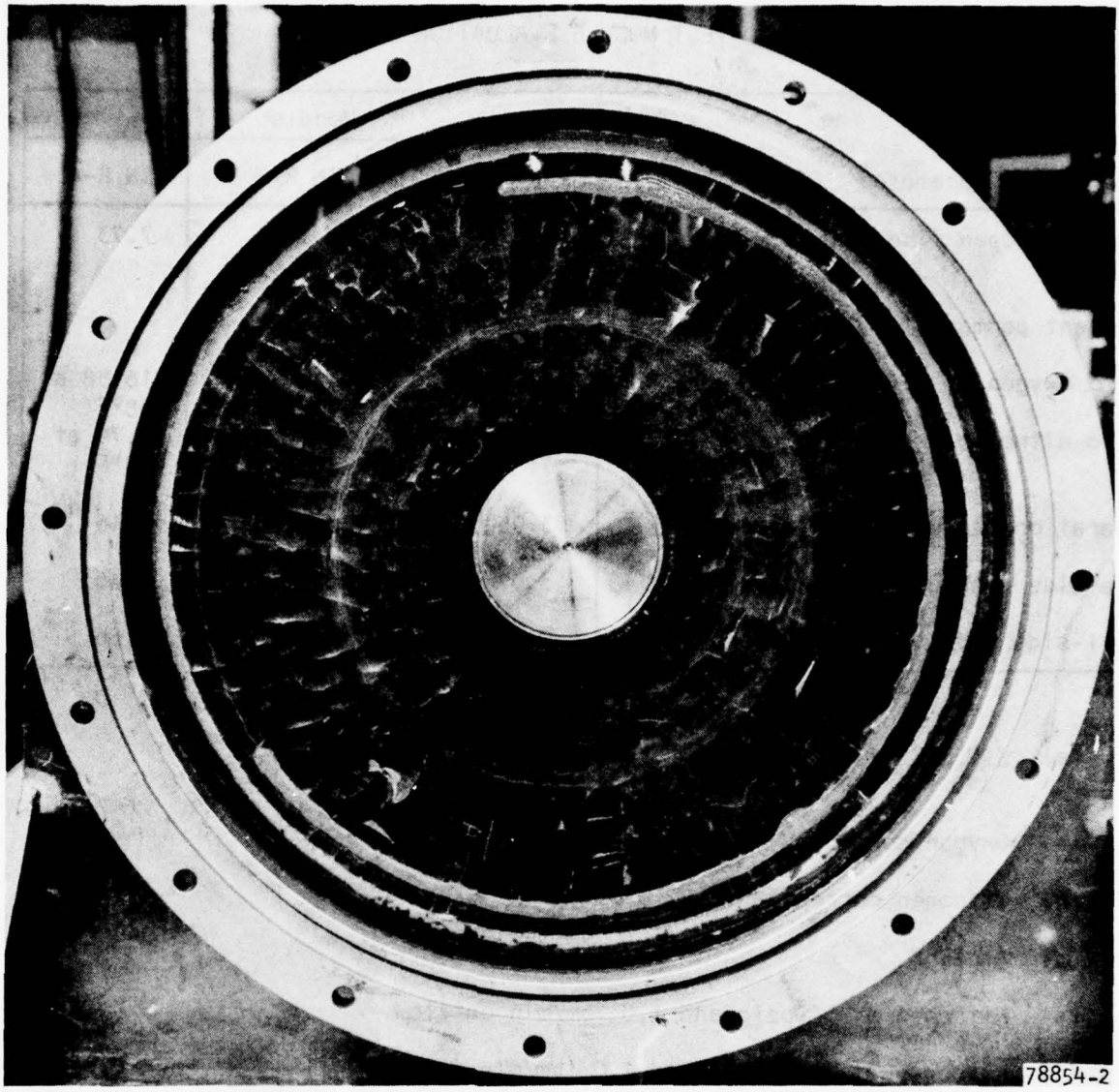


Figure 3-5. Tube Sheet Following Repair

TABLE 3-4

BREADBOARD TEST MODULE EVALUATION DATA

Test Parameter	Module		
	SN R-2	SN R-3	SN R-4
Number of open fibers (by ΔP_1), millions	7.74	7.37	7.73
Apparent permeability coefficient,[a]			
to oxygen	17.27 at 66°F	18.99 at 72.5°F	16.58 at 68°F
to nitrogen	4.64 at 71°F	5.10 at 74°F	4.79 at 68°F
Separation factor	3.95[b]	3.81[c]	3.46[d]
Tube-side pressure loss, psi[e]	3.97	3.95	4.46
Shell-side pressure loss, psi[f]	0.54	0.92	1.86

(a) $\frac{(\text{cu cm/sec at STP})(\text{cm})}{(\text{sq cm})\ (\text{cm Hg})} \times 10^{10}$

(b) Oxygen corrected to 71°F

(c) Nitrogen corrected to 72.5°F

(d) At 68°F

(e) Nitrogen at 50 psig and 1.0 lbm/min outflow

(f) Nitrogen at 14.7 psig and 1.0 lbm/min flow

LABORATORY TEST FACILITY

To provide maximum test flexibility, the laboratory test setup shown in Figure 3-6 was constructed to provide the performance testing of the three breadboard test modules. To simulate actual flight test conditions, the modules are located inside a large vacuum test chamber capable of maintaining the ambient pressures (altitude) and rates of pressure change (ascent or descent) discussed for the airborne system design (Section 4). A separate chamber is used to simulate the design fuel tank ullage volume. Pressure, temperature, and flow rates are controlled so that both steady-state and transient conditions during typical flight profiles can be simulated. The facility represents the first attempt to join the modules with controls and components typical of flight test hardware to establish the entire IGG system. Accordingly, where possible, flight hardware was used for flow and pressure control of the IGG system. The chamber pressure control valve (Item 22) is a modified 707 cabin pressure control valve. Modified aircraft valves are used for the air inlet valve (Item 13), the purge air valve (Item 14), the inert gas flow control valve (Item 16), and the simulated fuel tank outflow valve (Item 19).

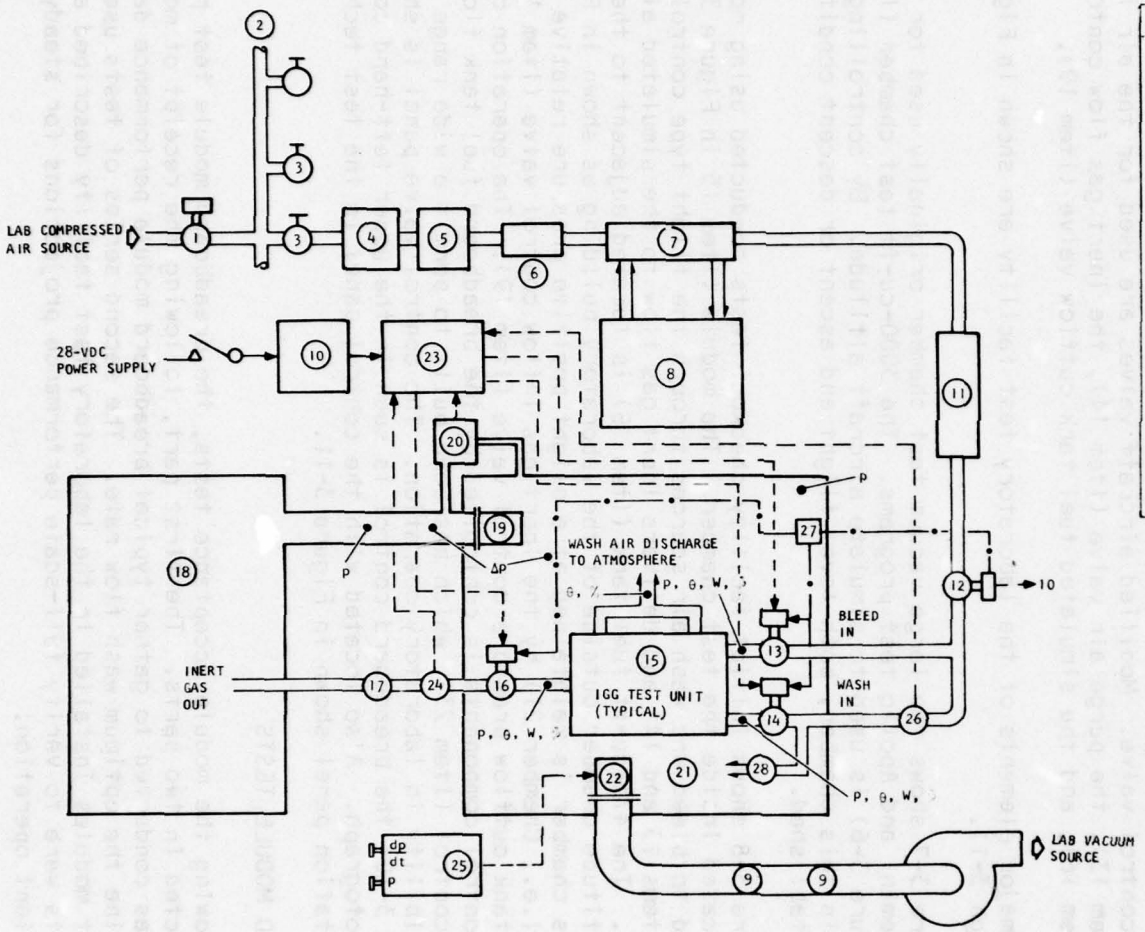
The major elements of the laboratory test facility are shown in Figures 3-7 through 3-11.

Figure 3-7 shows the large vacuum test chamber originally used for NASA project Gemini and Apollo test programs. The 3000-cu-ft test chamber (Item 21 in Figure 3-6) is used to simulate aircraft altitude. By controlling the pressure in this chamber, both level flight and ascent or descent conditions can be established.

Figure 3-8 shows initial facility checkout tests conducted using module SN R-1 located inside the test chamber. The module (Item 15 in Figure 3-6) is plumbed to bleed and wash air sources through the flight type control valves (Items 13 and 14) and delivers inert gas flow to the simulated aircraft fuel tank. The 473-cu-ft fuel tank (Item 18) is located adjacent to the test module altitude chamber outside of the laboratory building as shown in Figure 3-9. This chamber is maintained at a slight positive pressure relative to ambient (i.e., Chamber 21) by the inert gas inflow control valve (Item 16) and the fuel tank outflow pressure control valve (Item 19). The operation of these various control components is controlled by the breadboard fuel tank flow/pressure control (Item 23), which has been built to permit a wide range of test flexibility in laboratory operation. The control valve panel is shown in Figure 3-10; the breadboard control is seen in the upper left-hand corner of the photograph. Also located with the control panel is the test technician instrumentation panel shown in Figure 3-11.

BREADBOARD MODULE TESTS

Following the module acceptance tests, the breadboard module test program was conducted in two parts. The first part, following the receipt of module SN R-2, was conducted to gather typical breadboard module performance data and to determine the optimum wash flow rate. The second series of tests used all three test modules installed in the laboratory test facility described above. These tests were to verify full-scale performance projections for steady-state and transient operation.



ITEM	DESCRIPTION
1	LAB PRESSURE REGULATOR, 300 TO 110 PSIG
2	LAB COMPRESSED AIR DISTRIBUTION SYSTEM
3	ISOLATION VALVES (TYPICAL)
4	ACTIVATED ALUMINA CONTAINER
5	MOLECULAR SIEVE CONTAINER
6	PRE-FILTER; 5 μm NOM, 20 μm ABS
7	LAB HEAT EXCHANGER
8	LAB COOLANT CART
9	LAB SHUTOFF VALVES
10	CONTROL SYSTEM PANEL
11	FINAL FILTER; 0.5 μm NOM, 2 μ ABS
12	MAIN PRESS. REG & SHUTOFF VALVE
13	BLEED PRESSURE REGULATOR, VARIABLE
14	WASH FLOW CONTROL
15	INERT GAS GENERATOR (THREE MODULES)
16	INERT GAS FLOW CONTROL
17	INERT GAS FLOW CONTROL ORIFICE
18	SIMULATED FUEL TANK VOLUME, 473 CU FT
19	OUTFLOW DIFFERENTIAL PRESSURE REGULATOR
20	OUTFLOW DIFFERENTIAL PRESSURE TRANSDUCER
21	ATMOSPHERE TANK, 3000 CU FT
22	ATMOSPHERIC OUTFLOW PRESSURE CONTROL VALVE
23	FUEL TANK FLOW/PRESSURE CONTROL
24	INERT GAS FLOW SENSOR
25	ATMOSPHERIC PRESSURE CONTROLLER
26	WASH AIRFLOW SENSOR
27	PILOT REGULATOR
28	ATMOSPHERIC TANK FEED VALVE ORIFICE

INSTRUMENTATION PARAMETERS
P = PRESSURE θ = TEMPERATURE W = FLOW % = PERCENT OXYGEN

S-18909

Figure 3-6. Inert Gas Generator Laboratory Test Facility Schematic Diagram

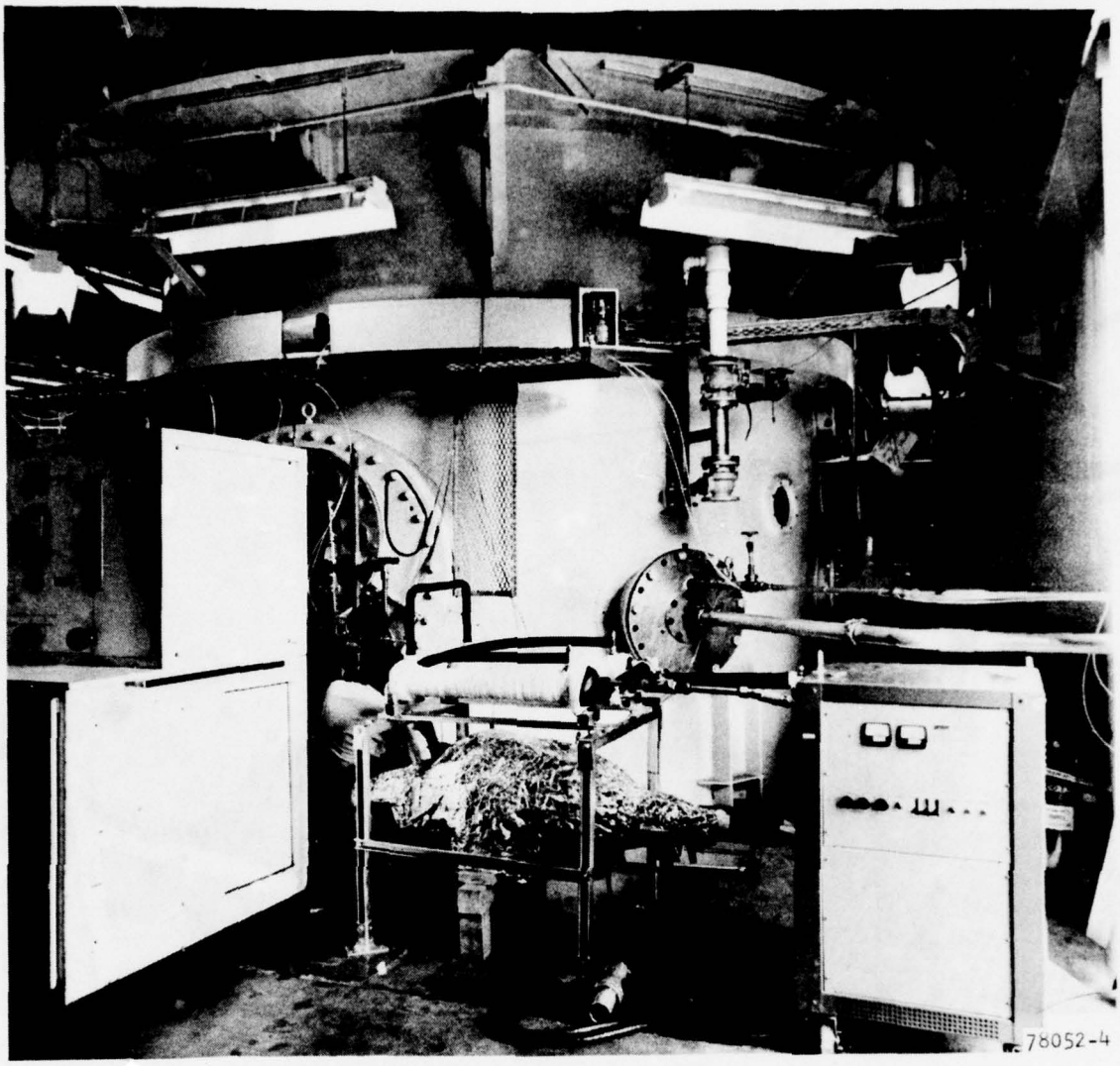


Figure 3-7. 3000-cu ft Altitude Chamber

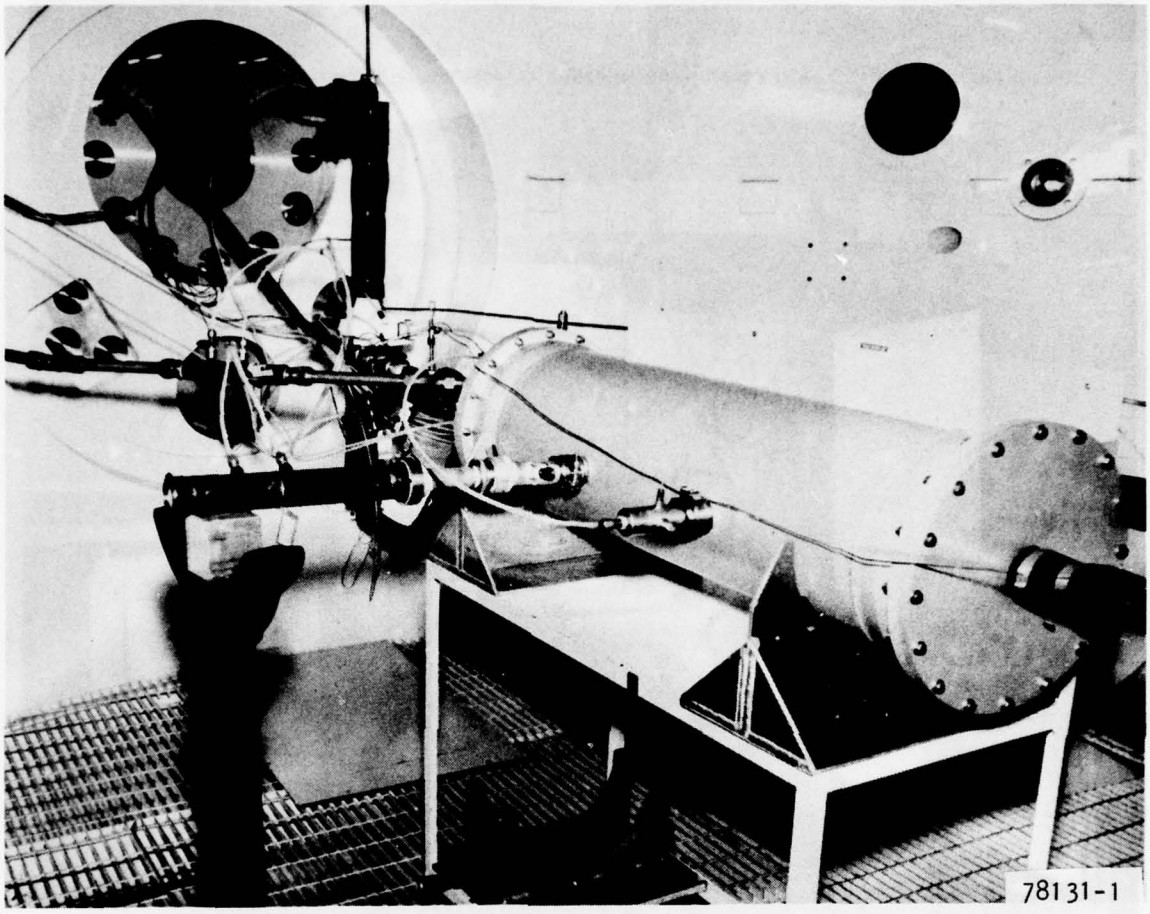


Figure 3-8. Inert Gas Generator Module in Altitude Chamber

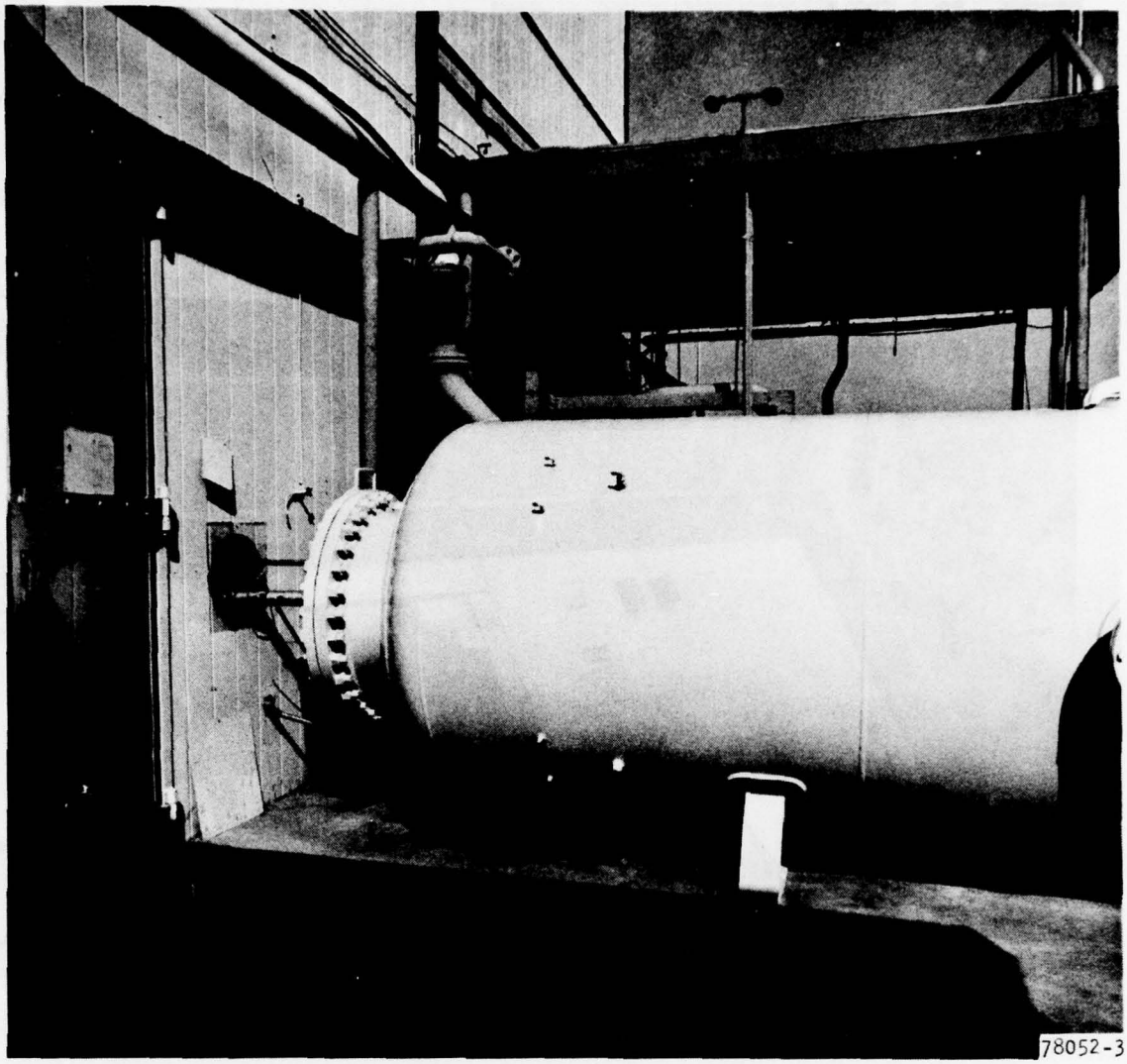


Figure 3-9. Simulated Fuel Tank Volume



Figure 3-10. Facility Control Panel

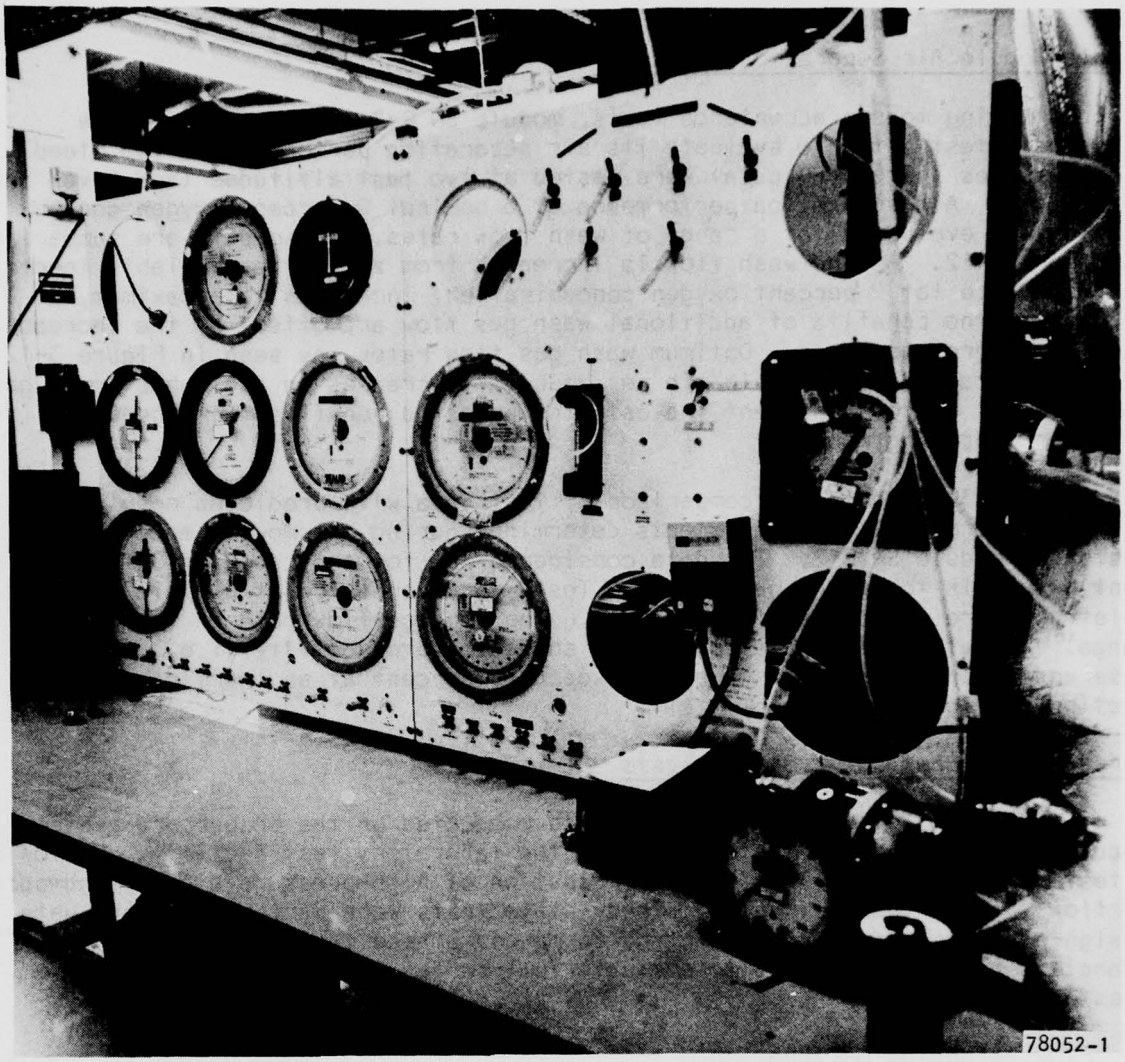


Figure 3-11. Test Instrumentation Panel

Single-Module Air Separation Tests

Following module acceptance tests, module SN R-2 was placed into the breadboard test setup to evaluate its air separation performance. Two bleed air pressures (65 and 80 psia) were tested at two test altitudes (sea level and 15,000 ft). Air separation performance at a nominal 9 percent oxygen concentration was evaluated for a range of wash flow rates. These data are summarized in Figure 3-12. As the wash flow is increased from zero, the available inert gas flow rate (at 9 percent oxygen concentration) increases to a maximum, at which time the benefits of additional wash gas flow are offset by the increased shell-side pressure drop. Optimum wash gas flow rates, as seen in Figure 3-12, are in the range of 1 to 2 lb/min per module. Increases in available inert gas flow rate of 20 to 40 percent indicate the expected benefits from the use of the wash gas operating mode.

Figure 3-13 shows the comparison of test data with predicted results using the permeability coefficients determined during the module acceptance tests for module SN R-2. The data considered are for the range of 8 to 12 percent oxygen in the inert gas output. Tests were conducted at 80-psia tube-side inlet pressure at sea-level conditions using a purge flow rate in the optimum range. An output flow rate comparison shows the productivity (i.e., ratio of observed to predicted flow rate) to exceed 90 percent at an inert gas concentration of 9 percent oxygen.

Three-Module Breadboard System Tests

Three types of full-scale tests were conducted on the breadboard system modules following their installation in the laboratory test facility. Following a test procedure to optimize the distribution of high-pressure airflow and purge airflow through the test units, steady-state tests were performed to evaluate design-point and off-design-point performance. These tests were followed by transient performance tests to evaluate full-scale system operation during mission profiles.

1. Flow Balancing Calibration

Prior to conducting steady-state and mission profile performance testing, the laboratory test facility, with all three test modules installed, was flow balanced for optimum inerting performance. The three air separation modules were connected as shown in Figure 3-14. (The numbers refer to the facility schematic of Figure 3-6.) The system arrangement has the three modules in parallel for both bleed air and wash air pneumatic circuits. Pressure instrumentation is located at the bleed air inlet and outlet, wash air inlet, chamber ambient, and between the bleed air inlet and chamber ambient. Oxygen concentration instrumentation was capable of sampling the outlet of each module or the total output of the combined modules. Flow control valves located at the wash air inlet and inert gas outlet of each module were used to adjust the bleed and wash airflow split to obtain an optimum inert productivity gas from the combined system. The system was flow balanced for the full demand flow rate of 2.33 lb/min at sea level and 15,000-ft altitude conditions. Modules SN R-2 and SN R-3 were about equal in purge flow, whereas module SN R-4 required a rather restricted purge flow due to the higher packing factor created by its

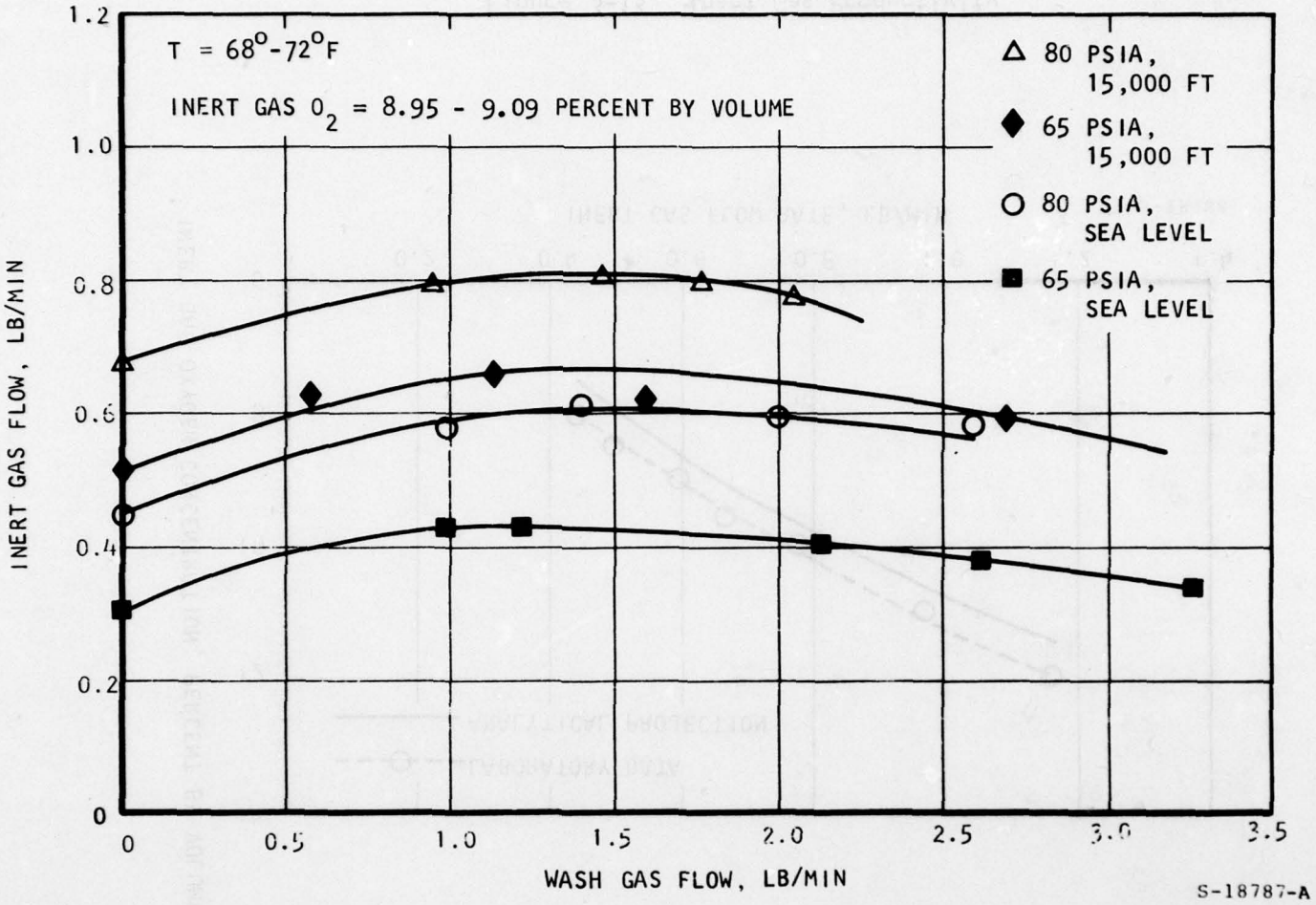


Figure 3-12. Purge Optimization Test Results

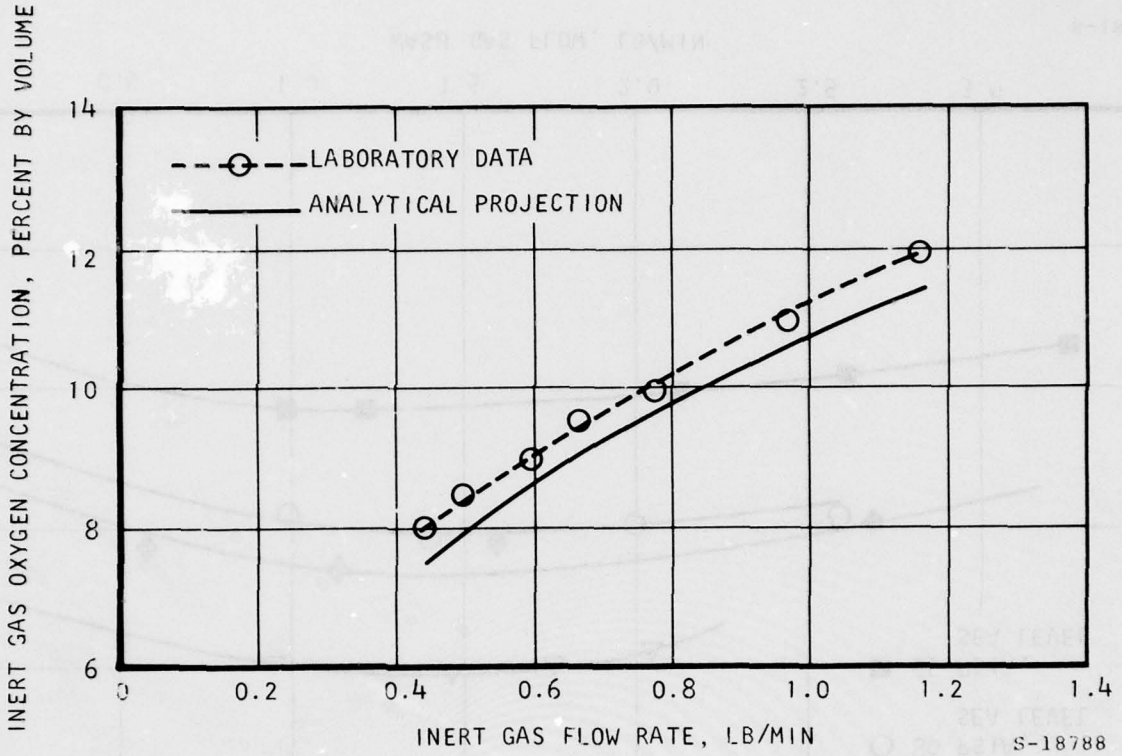


Figure 3-13. Inert Gas Productivity

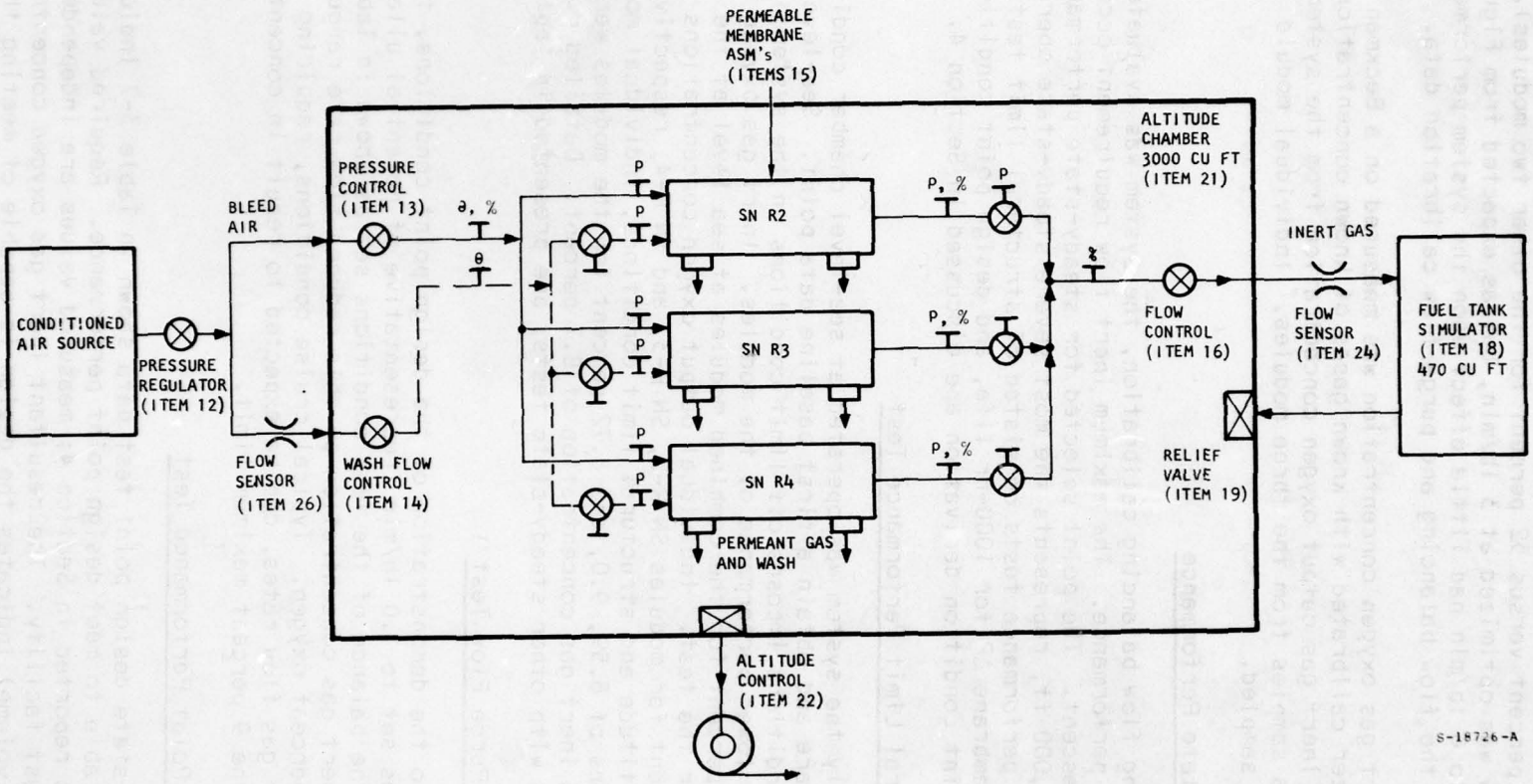


Figure 3-14. Air Separation Module Installation in the Laboratory Test Facility

assembly (56 percent versus 52 percent for the other two modules). The combined purge airflow was optimized at 3 lb/min, but as expected from Figure 3-12, an increase to 6 lb/min had little effect upon the system performance. Table 3-5 presents the flow balancing and purge flow calibration data.

The inert gas oxygen concentration was measured on a Beckman F-3 laboratory oxygen analyzer calibrated with known gases of known concentration just prior to use. The inert gas output oxygen concentration from the system is a result of mixing the samples from the three modules. Individual module inert gas output also was sampled.

2. Steady-State Performance

Following flow balancing calibration, the system was evaluated for steady-state performance. The maximum inert flow requirement occurs during high-speed descent. The point selected for steady-state performance, 2.33 lb/min at 15,000 ft, represents the most severe steady-state operation. The steady-state performance tests consisted of structural limit tests, defined as maximum membrane ΔP for 1000-hr life, and design point conditions; details of design point condition derivation are discussed in Section 4.

a. Structural Limit Performance Test

Initially the system was operated at sea-level chamber conditions to check system hardware and obtain a first baseline data point. Sea-level operation at high flow conditions imposes off-limit conditions on the system hardware, resulting in lower performance of the modules. Inert gas oxygen concentrations reached 9.4 percent for the combined modules at sea level at the increased flow rate used for the test. Individual output oxygen concentrations were 9.2, 9.6, and 9.6 percent for modules SN R-2, SN R-3, and SN R-4, respectively. At 15,000-ft altitude and structural limit conditions, individual module oxygen concentrations of 8.59, 9.0, and 8.72 percent for the modules were obtained with a net system inert gas concentration of 8.7 percent. Detailed results of these tests, along with other steady-state tests, are presented in Table 3-6.

b. Ullage Purge Flow Test

Prior to the demonstration of the design point conditions, the inert gas flow rate was set to 1.0 lb/min (representative of potential ullage purge gas flow) with the balance of the test conditions set as shown in Table 3-7. Resultant inert gas concentration at this reduced flow rate ranged from about 5.0 to 5.4 percent oxygen. Typical cruise conditions, requiring about 0.25 lb/min inert gas flow rates, can be expected to result in concentrations also well below the 9 percent maximum limit.

c. Design Point Performance Test

Steady-state design point test data shown in Table 3-7 indicated that the modules are able to meet design point performance. Required values are from the analysis reported in Section 4; measured values are independently set using the test facility. The resultant inert gas oxygen concentration of 8.9 percent (by volume) indicates the design is capable of meeting the 9 percent maximum requirement established for the modules.

TABLE 3-5

FLOW BALANCING CALIBRATION

Purge Air Control Valve Position			Purge Flow, lb/min	Module ΔP, psi	Bleed Air Inlet Temp, °F	Total Inert Gas Flow, lb/min	Inert Gas Oxygen Content, %				Chamber Temp, °F	Chamber Altitude
SN R-2	SN R-3	SN R-4					SN R-2	SN R-3	SN R-4	3 Modules Combined		
Full open	Full open	Full open	2.0	58.8	72	1.78	9.1	9.6	9.6	9.4	72	Sea level
Full open	Full open	Full open	8.5	58.8	72	2.3	10.6	11.0	11.0	10.8	72	Sea level
Full open	Full open	Full open	3.0	74	71	2.3	8.61	9.02	10.1	9.23	72	15,000 ft
Full open	Full open	Full open	3.0	74	72	2.3	8.56	8.91	8.64	8.69	72	15,000 ft
Full open	Full open	1/2 open	4.0	74	72	2.3	8.56	8.93	8.70	8.74	72	15,000 ft
Full open	Full open	1/2 open	6.0	74	72	2.3	8.78	9.13	10.75	9.60	72	15,000 ft
Full open	Full open	1/2 open	2.0	74	72	2.3	--	--	10.36	9.31	72	15,000 ft

TABLE 3-6

STEADY-STATE TEST RESULTS

Test Condition	Bleed Air Inlet Press, psia	Bleed Air Inlet Temp, °F	Purge Flow, lb/min	Purge Air Temp, °F	Module to Chamber ΔP, psi	Chamber Altitude	Inert Gas Flow, lb/min	Inert Gas Temp, °F	Inert Gas Oxygen Content, % by Volume
Sea level structural limit	88.7	74	3.0	74	74	Sea level	2.3	75	9.4
Altitude structural limit	82.3	75	3.0	74	74	15,000 ft	2.3	75	8.7
Ullage purge flow	74.0	75	3.0	74	65.7	15,000 ft	1.0	75	5.0 to 5.4
Design point	74	75	3.0	74	65.7	15,000 ft	2.3	75	8.9

TABLE 3-7

BREADBOARD INERT GAS GENERATOR
DESIGN POINT PERFORMANCE

Test Condition	Required	Measured
Inlet air pressure, psia	74.0	74
Inlet air temperature, °F	75	75
Ambient pressure altitude, ft	15,000	15,000
Inert gas flow rate, lb/min	2.33	2.3
Purge gas inlet flow rate, lb/min	Optimum	3.0
Inert gas oxygen concentration, percent (by volume)	9 (max.)	8.9

d. Performance Evaluation

An important aspect of the breadboard system performance test is the comparison of full-scale test data with performance projection. Since the airborne system design, discussed in Section 4, is based on the use of the same analytical tools used to project breadboard system performance, it is essential that the breadboard analysis agree with test results within sufficient accuracy to provide confidence in the airborne system design. The most critical point for the comparison is, of course, the module design point. Simulation of the design point, using the test conditions of Table 3-7, resulted in a projected inert gas concentration of 8.7 percent for this condition. The measured value of 8.9 percent is felt to compare favorably with this value.

Under a contract to the Eustis Directorate of the United States Army Air Mobility Research and Development Laboratory (USAAMRDL), a small air separation test module was built and tested. The module, consisting of 3.93 million fibers of 50 microns ID, 7 microns wall thickness, and 36 in. active length, is the first module designed for and tested in the non-wash operating mode. Since the airborne system preliminary design undertaken during this program includes non-wash module operation during the cruise segment of the baseline mission profile, the performance of non-wash mode test modules is of concern to this program.

The non-wash digital computer mathematical model performance evaluation program was used to predict performance of the air separation modules for the airborne system design during the lengthy cruise segment of the mission profile. Figure 3-15 shows the results of an analysis using this program compared with test results for a nominal 55-psig inlet pressure for both nominal 15,000-ft altitude and ambient permeant exhaust gas pressures. As can be seen by the

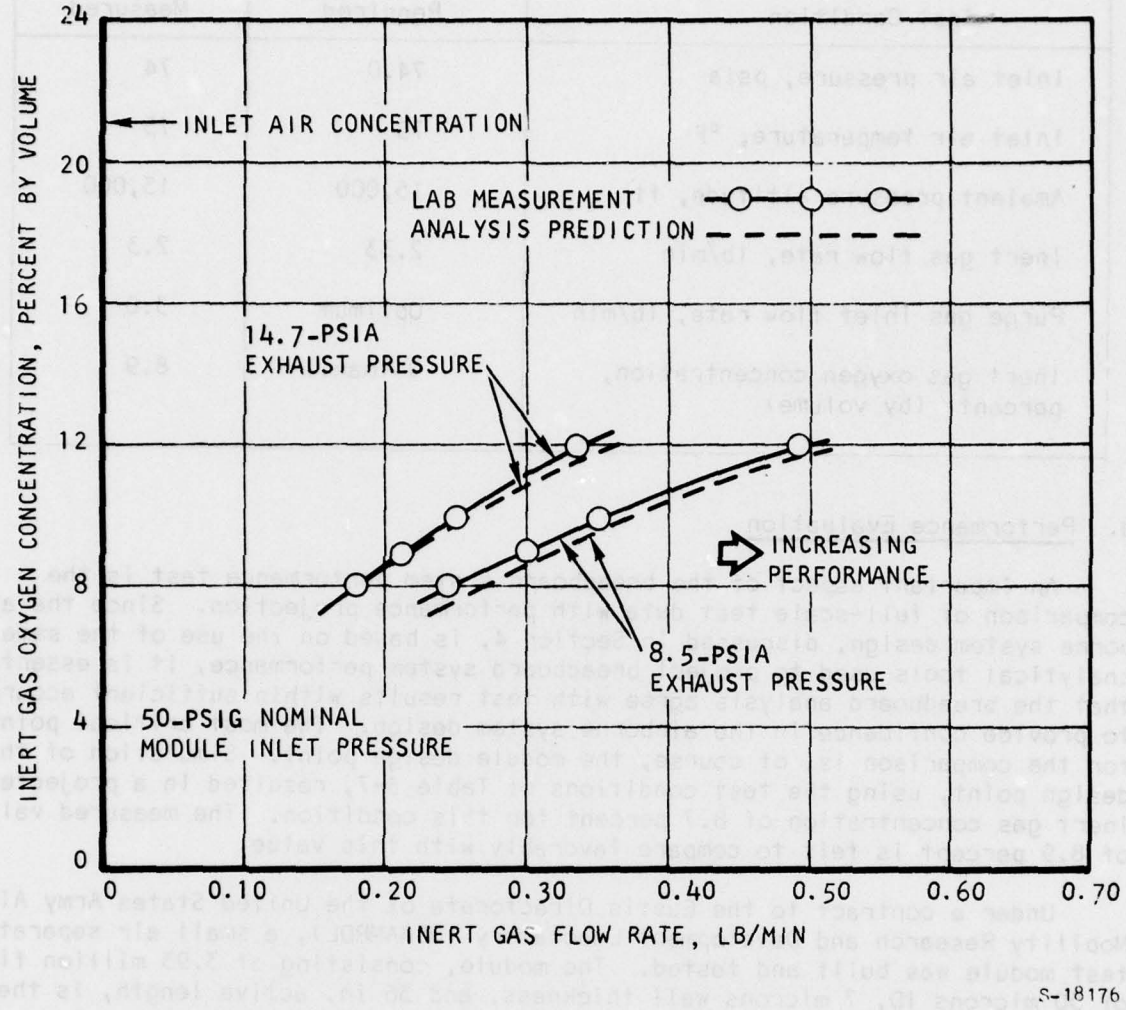


Figure 3-15. Comparison of Analytical Predictions and Laboratory Test Data

similarity of analytical predictions to actual laboratory test data, both absolute values of oxygen concentration and the general trends are in close agreement. At the 9-percent level, the predicted flows are seen to be over 93 percent of the measured flows, when the reduced permeant exhaust gas pressure (8.5 psia) is considered, and about 95 percent of the measured flows at ambient permeant exhaust gas pressure. More importantly, at the measured flows the oxygen concentration is within 0.5 percent of predicted values.

3. Mission Profile Performance Tests

The mission profile simulation utilized for this program is shown in Figure 3-16. The varying altitude ascent and descent rates of the actual mission profile are transformed into constant slopes with sharp transmission points to facilitate testing, and the resultant altitude test curve is shown in Figure 3-16 as chamber altitude.

For the mission profile simulation test, all three breadboard air separation modules remained in the 3000-cu ft altitude chamber as shown in Figure 3-14. The test chamber altitude program is obtained by adjusting an altitude controller located in the system instrumentation and control panel. System bleed air input and inert gas output are controlled by the system master controller located outside the altitude chamber. Pressure feedback signals from transducers located within the test facility are utilized by the master controller to maintain predetermined gas flows during the mission simulation altitude profiles.

A combined inert gas sample from all three breadboard air separation modules was analyzed for oxygen content during the mission profile simulation test. Test results from this sample are plotted in Figure 3-16 as inert gas oxygen concentration. During the test runs, the automatic control features of the system maintained the inert gas concentration between 7 and 9 percent oxygen throughout the critical 25,000- to 10,000-ft descent, at a 3000-fpm descent rate. Although difficulties in the precise setting of the altitude chamber descent rate resulted in short inert gas flow rate excursions above the design rate (momentarily up to 3 lb/min in one case), the facility automatic test system and the module response were able to compensate as required to maintain the inert gas oxygen concentration below the 9 percent limit.

Transient performance tests indicated no unexpected module performance problems during runs simulating the design mission profiles. The tests have, however, shown the need to improve the test facility and test support hardware assembled in support of this test. Specifically, a means to more finely control the altitude chamber ascent/descent rate, and to adjust the electronic controls for a more precise regulation of demand flow rate as a function of fuel tank-to-local ambient pressure, will greatly simplify this test and add to the value of the data on future programs.

BREADBOARD MODULE DESIGN REVIEW

The purpose of the full-scle breadboard ASM design, fabrication, and testing accomplished during program Phases II and III was to provide full-scale ASM design and performance data that would enable realistic projection of

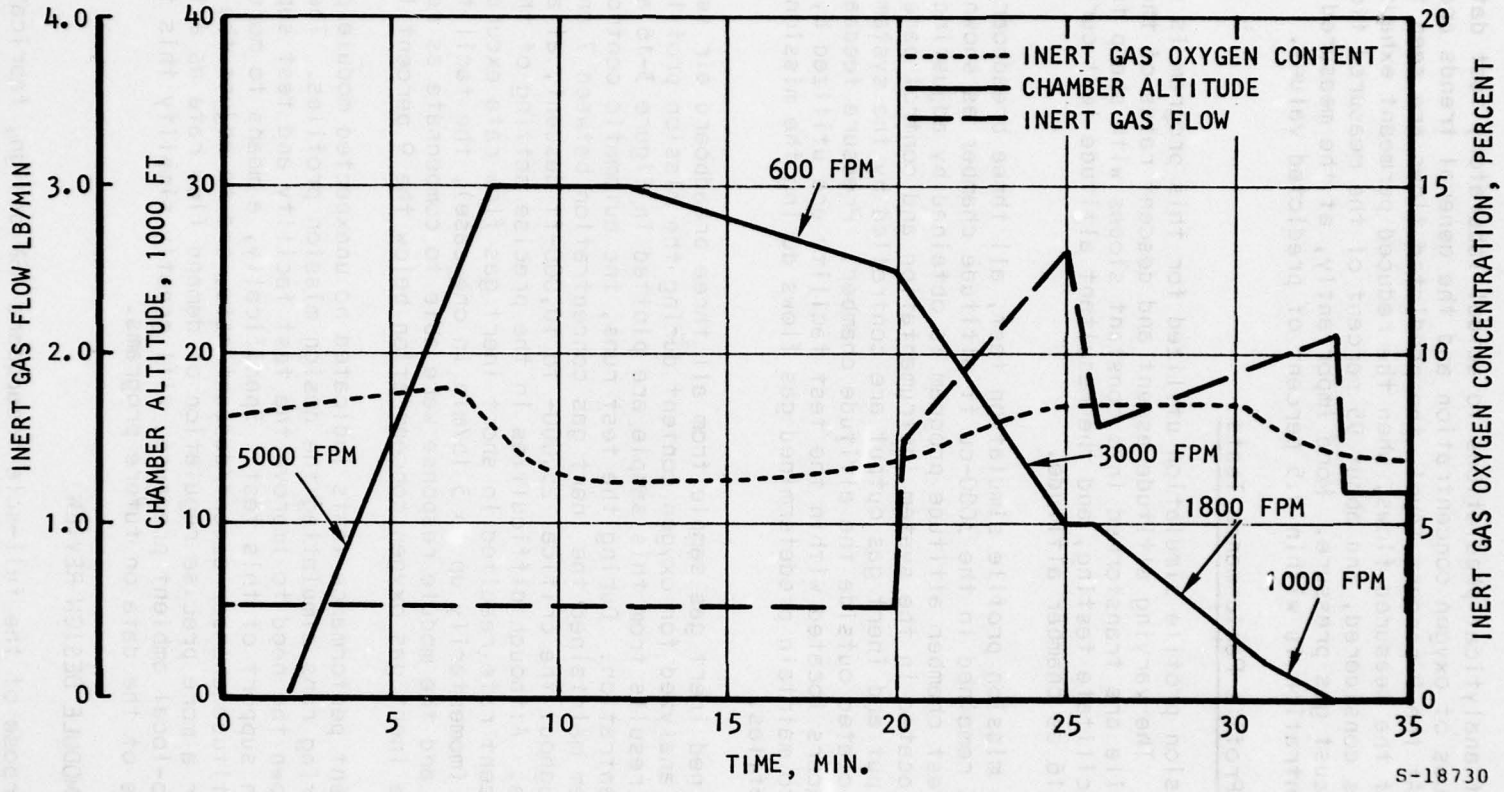


Figure 3-16. Mission Profile Simulation

airborne system designs. While the success achieved in meeting the specified oxygen concentration for both the baseline DC-9 design-point and transient flight profile is in itself a significant accomplishment, the most significant value of the program lies in the acquired experience and knowledge that can be utilized to design and fabricate future systems for flight test and subsequent production.

The design, development, fabrication, and test program described above provided valuable information that will be incorporated into future designs. The breadboard ASM design concept developed for the program proved to be generally suitable for future flight configurations; however, the experience gained as a result of the test program indicates methods to improve the design in the areas of both system sizing and detail ASM design.

With the inclusion of a leakage factor in the digital computer program, the analytical prediction for ASM performance has been adjusted to agree within about 0.2 percent of the measured oxygen concentration based on the number of open fibers; however, the fabrication procedures and post-fabrication tests reveal that only about 92 percent of the fibers assembled into an ASM can be expected to be clearly opened on both ends. Therefore, a 92 percent factor is suggested in the selection of ASM design to account for expected losses in module fabrication.

In addition, testing has revealed the need to consider changes to the detail ASM design. The three breadboard test ASM's were examined and disassembled for inspection. Two design changes (in addition to minimizing weight) are considered desirable for flight hardware. The first of these is the enlargement of the permeant side outlet ports to reduce back pressure. In addition, a means should be provided to prevent the shift of the membrane fibers and protective wrap in a manner that could restrict the flow from the exhaust ports. These changes in design, along with better control of the membrane packing factor, can be expected to allow increased wash flow rates, further improving performance. A second design modification for future ASM's involves a return to the O-ring-sealed, removable cartridge concept used for ASM's fabricated under the previous program. As a result of problems with the tube sheet epoxy adhesion to the aluminum case, differences in thermal expansion coefficients for the assembled tube sheet and the aluminum case, and possible changes required to the formula and cure cycle for the epoxy, forming a leak-free tube sheet was unexpectedly difficult. Post-test inspection of the tube sheet surfaces revealed the continued propagation of cracks first observed and repaired at the time of module fabrication. While changes to tube sheet epoxy preparation and cure cycle alone may prevent the reoccurrence of this problem, the desirability of a removable membrane cartridge and elimination of the bonding of materials of differing thermal expansion coefficients favor the use of an O-ring-sealed assembly.

Preceding Page BLANK - NOT FILMED

SECTION 4

AIRBORNE SYSTEM PRELIMINARY DESIGN

The purpose of the program has been to develop hardware and to test performance in order to confidently project permeable membrane inert gas generator (IGG) fuel tank inerting system designs for eventual adoption in aircraft applications. To perform these evaluations in a meaningful manner, a transport category aircraft was selected as the design baseline for an airborne system preliminary design. For this study, the McDonnell Douglas DC-9 aircraft was selected as typical of small turbine-powered transport category aircraft currently in service with airlines in the United States.

The DC-9, in revenue passenger service since 1967, has a typical cruise operation at 35,000 ft with a capacity of over 100 passengers, with typical durations of up to several hours. For the purposes of the study, a Series 30 airplane, powered by Pratt and Whitney JT8D-7 or -9 twin engines, with a 24,650-lb fuel capacity, was used. Aircraft performance and operation in accordance with the McDonnell Douglas Series 30 performance report (Ref. 4-1) has been assumed.

The preliminary design, initially established at the conclusion of the Phase I laboratory test program, has been updated to reflect data provided by program activities in the second (breadboard module design) and third (breadboard module test) phases. The preliminary design presented in this section therefore provides an airborne permeable membrane IGG fuel tank inerting system design based on the latest data available at the time of this report.

AIRCRAFT REQUIREMENTS

The design of a permeable membrane IGG fuel tank inerting system, which consists of one or more IGG systems containing permeable membrane air separation modules (ASM's), requires the optimization of the IGG ASM's for the fuel tank inerting system requirements and the selection of the required additional components and controls to establish inerting system operation to design requirements. The evaluation of ASM design and complete IGG system design is an iterative process. For ease of explanation, the evaluation of aircraft operation, ASM, IGG, and final aircraft system design will be described as a single process. Since the system design is sensitive to pneumatic air source pressures and the required inert gas flow rate, these parameters will first be evaluated in terms of aircraft operation.

Ref. 4-1: DC-9 Douglas Jet Transport, Series 30, General Performance Report, MDC-J5225, August 1974.

Available Air Pressure

As established in the previous conceptual study (Ref. 4-2), the system design point occurs during aircraft descent. This is true because the inert gas flow rate required by the fuel ullage is large at the same time the air pressure is low (due to low engine throttle settings). Several likely locations of pressurized air may be considered. The DC-9 environmental control system (ECS) packages are located near the engines in the aft part of the fuselage. In this immediate area, a likely area for installation of the IGG system, three possible sources of pressurized engine bleed air are available: (1) the bleed air manifold near the inlet to the ECS packs, (2) the air from the ECS pack following compression by the air cycle turbocompressor, and (3) the high-stage (13th) or low-stage (8th) unregulated bleed air at the engines. Since, as will be seen later, the air requirement of the IGG system is quite small, all are considered viable alternatives. Figure 4-1 shows these three pressures as a function of aircraft altitude for descent. (High-stage bleed air and bleed air manifold data were taken from available ECS design performance data.) The air cycle compressor discharge pressure data is taken from the digital computer program for DC-9 ECS performance profiles; hot-day conditions are shown. The DC-9 bleed air manifold pressure is normally provided by the low-pressure, 8th-stage compressor bleed of the Pratt and Whitney JT8D engines. The bleed air pressure system of the DC-9 is designed to maintain this pressure within a nominal 5-psi control band. If the bleed air manifold pressure begins to fall below a nominal 18.5-psig setting, high-stage compressor bleed air is added by the action of a modulating valve to maintain the nominal bleed air manifold at a minimum of 18.5 psig. The manifold pressure is prevented from exceeding a nominal 23.5 psig by a pressure limiting regulator that acts on the low-stage bleed pressure. Low-stage bleed pressure can be high during certain operational modes such as takeoff when engine throttle settings and ambient pressure are high. Flow from the high to the low stage is prevented by a check valve.

Aircraft Descent Rate

A typical altitude profile, showing general flight segments for the baseline aircraft, is shown in Figure 4-2; the two principal descent profiles are shown in Figure 4-3. The descent profiles of Figure 4-3 indicate the aircraft pressure altitude as a function of time from the initiation of descent for a standard day as taken from the McDonnell-Douglas general performance report previously referenced; a landing weight of 90,000 lb has been assumed. Total time required to descend to sea level from 30,000 ft is about 20 min.

Ref. 4-2: Manatt, S.A., Feasibility Study and Demonstration of Nitrogen Generation for Fuel Tank Inerting, Federal Aviation Administration Report, FAA-RD-74-112, June 1974.

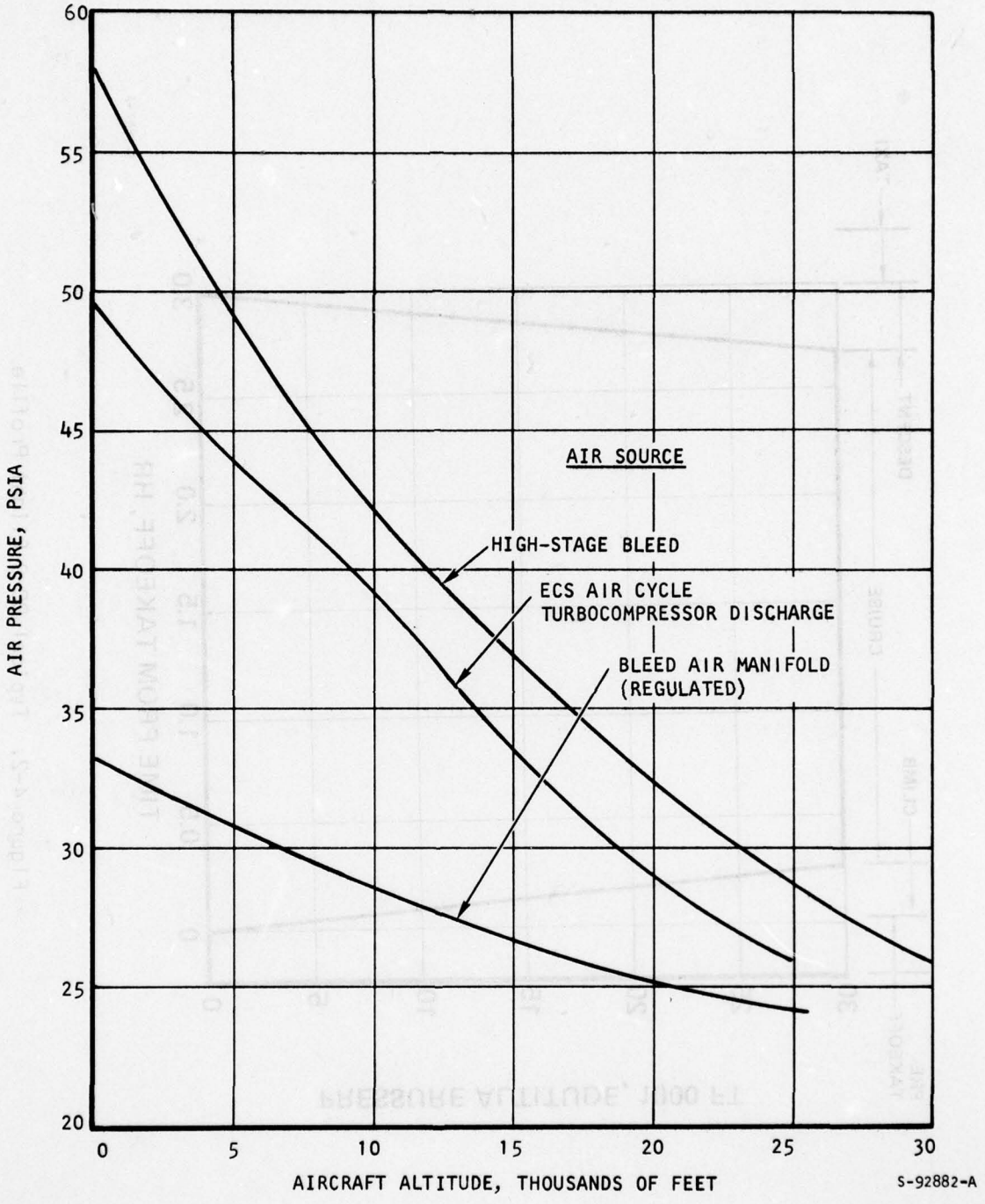


Figure 4-1. Air Pressure at Various Locations During Descent

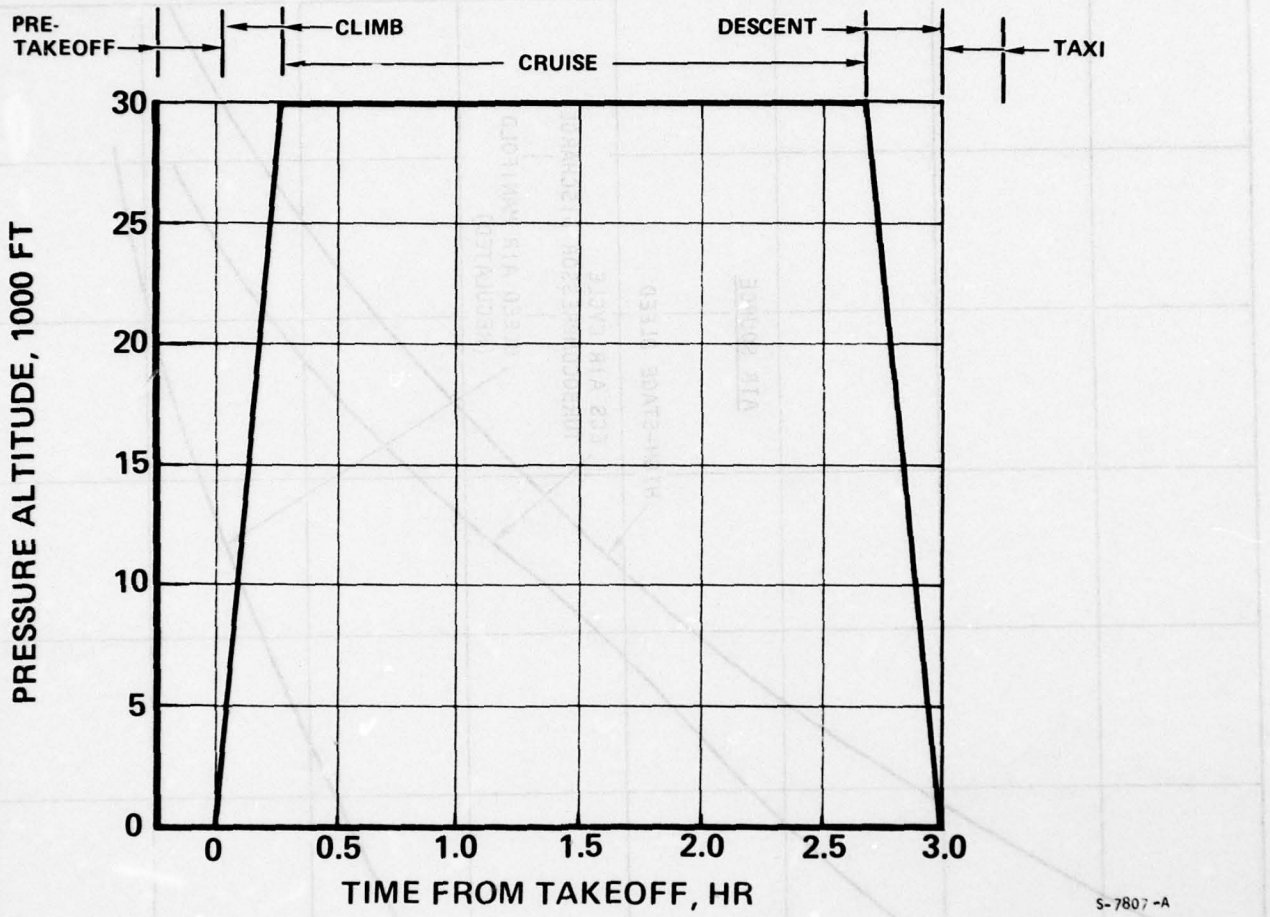
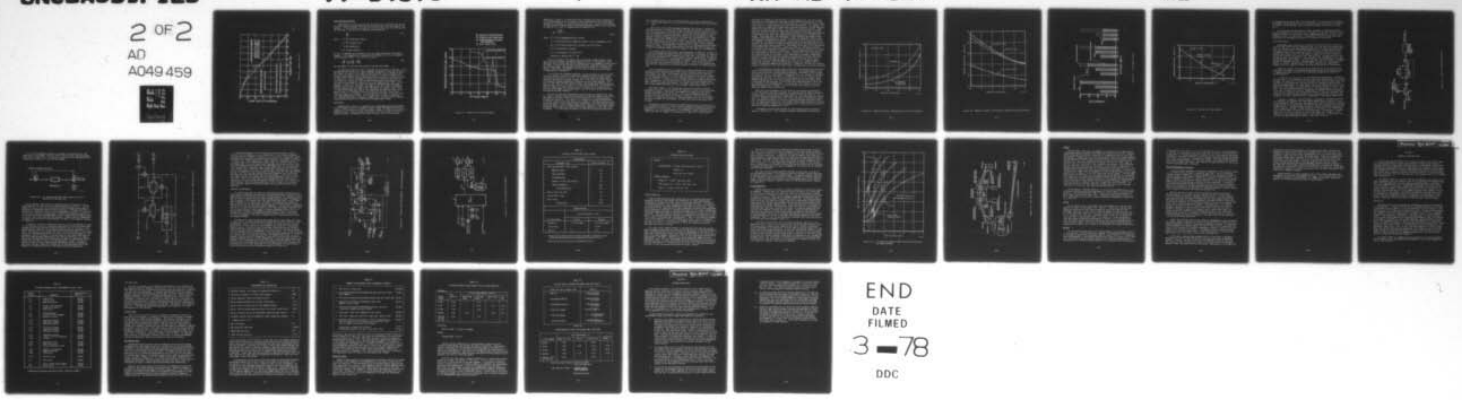


Figure 4-2. Typical DC-9 Flight Profile

AD-A049 459 AIRESEARCH MFG CO OF CALIFORNIA TORRANCE F/G 1/3
DESIGN, FABRICATION, AND TESTING OF A FULL-SCALE BREADBOARD NIT--ETC(U)
SEP 77 S A MANATT DOT-FA75WA-3658
UNCLASSIFIED 77-14376 FAA-RD-77-147 NL

2 OF 2
AD
A049459



END
DATE
FILMED
3-78
DDC

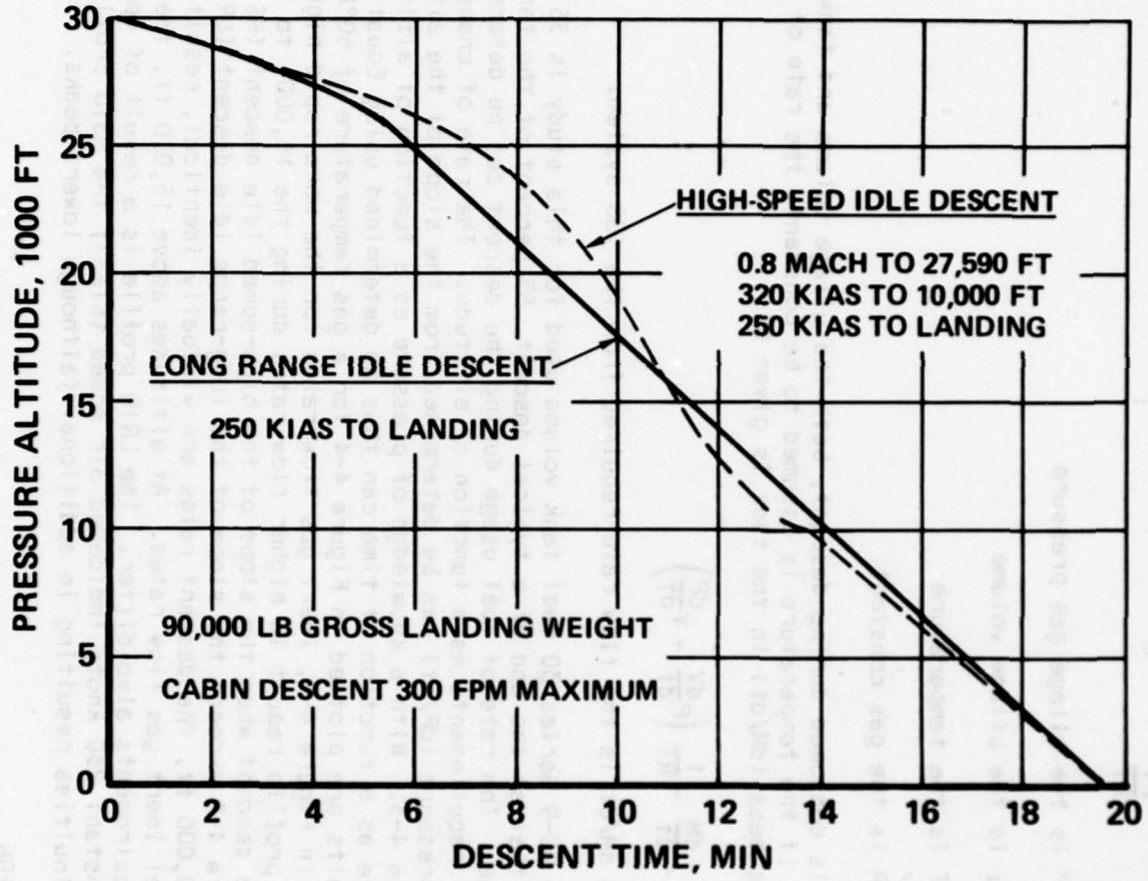


Figure 4-3. Descent Profiles

Inert Gas Delivery Rate

Determination of the required inert gas flow rate to repressurize the fuel tanks for these two descent profiles can be determined from a knowledge of the descent. If the inert gas is assumed to follow the ideal gas law, the mass (M) of inert gas in the fuel tank ullage may be expressed as:

$$\frac{PV}{RT} \qquad (4\text{-}1)$$

where P is the ullage gas pressure

V is the ullage volume

T is the temperature

R is the gas constant

As fuel is consumed during descent, both the ullage volume and tank pressure change. If the temperature is assumed to be constant, the rate of change of inert gas mass (dM/dt) in the tank is given by:

$$\frac{dM}{dt} = \frac{1}{RT}\left(P\frac{dV}{dt} + V\frac{dP}{dt}\right) \qquad (4\text{-}2)$$

The term dM/dt is the flow rate required from the IGG system.

The DC-9 Series 30 fuel tank volume used for this study is 3679 gal. It is assumed that at the end of a typical descent, 85 percent of the tank volume will be ullage. The rate of fuel usage during the descent can be determined from the fuel requirements as a function of altitude. The rate of change of the ullage pressure (dP/dt) can be determined from the slope of the altitude curve of Figure 4-3. With a knowledge of pressure as a function of altitude, the flow rate as a function of time can thus be determined using Equation 4-2. The results are plotted in Figure 4-4 for a gas temperature of 60°F. As can be seen in Figure 4-4, inert gas flow rates for the more rapid high-speed descent profile result in higher flow rates during the 15,000- to 10,000-ft-altitude descent when the slope of the high-speed idle descent (HSID) curve in Figure 4-3 exceeds the slope of the long-range idle descent (LRID) curve. Below 10,000 ft, the descent rates are virtually identical, resulting in identical inert gas flow rates. At altitudes above 15,000 ft, the inert gas flow requirements also differ. The LRID profile is a result of operation at a constant 250 knots indicated air speed (KIAS); the HSID profile contains discontinuities resulting in additional (although lower) peaks.

ASM DESIGN

Membrane mass transfer is assumed to be in accordance with the activated diffusion model; that is, the gases transfer through the membrane walls by a process of first dissolving into the polymer surface, followed by concentration-gradient-driven diffusion through the polymer, and finally evolution at the opposite surface. Although gas diffusion is only a part of the transfer

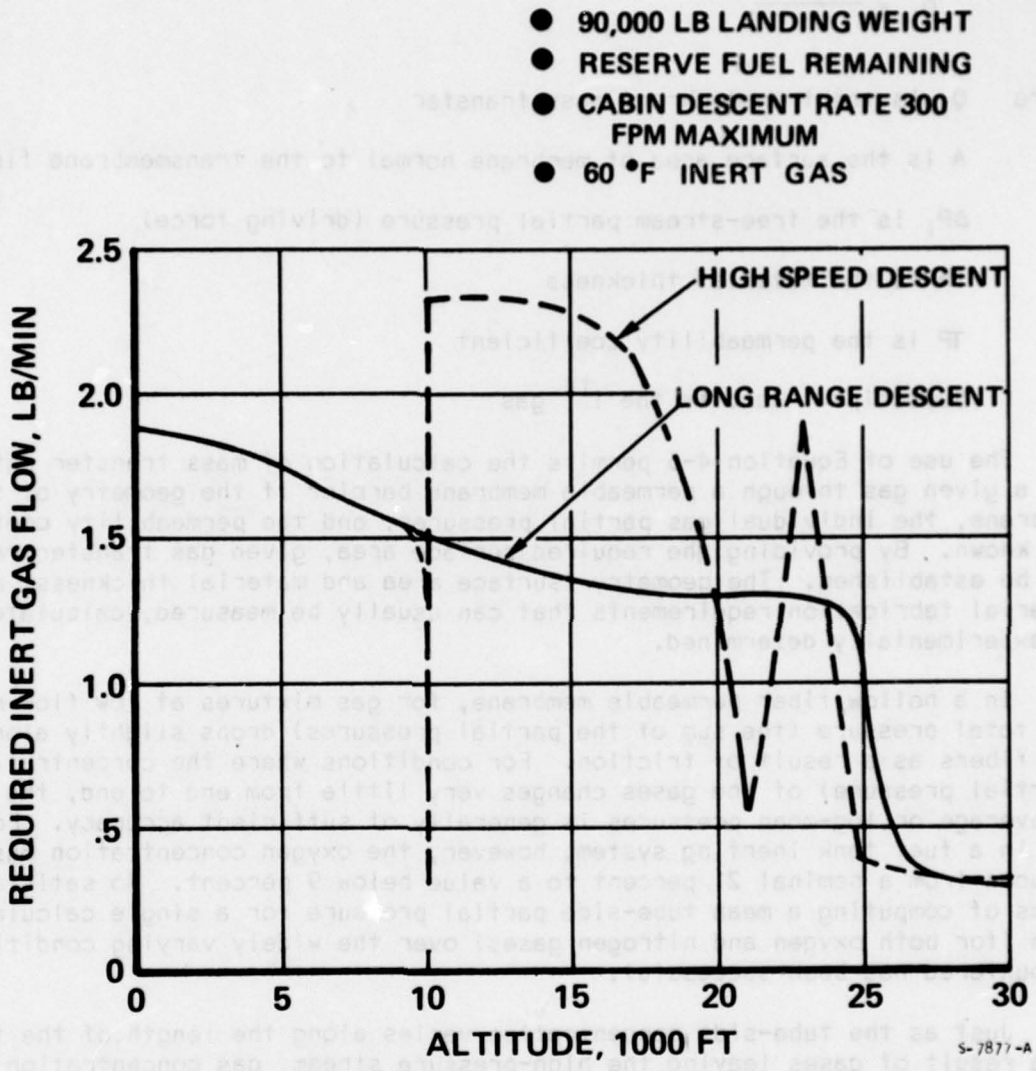


Figure 4-4. Descent Inert Gas Requirements

mechanism, it usually is rate controlling, allowing the surface concentration of dissolved gases to be in near-equilibrium concentration with free-stream gas partial pressures, in accordance with Henry's Law. The basic relationship to describe mass transfer across a permeable membrane boundary may be described by Equation 2-1, which is repeated here as Equation 4-3:

$$\dot{Q}_i = \frac{TP_i A \Delta P_i}{th} \qquad (4\text{-}3)$$

where $\dot{Q}_i$ is the transmembrane mass transfer

A is the surface area of membrane normal to the transmembrane flow

ΔP_i is the free-stream partial pressure (driving force)

th is the material thickness

TP is the permeability coefficient

Subscript i denotes the i^{th} gas

The use of Equation 4-3 permits the calculation of mass transfer rates for a given gas through a permeable membrane barrier if the geometry of the membrane, the individual gas partial pressures, and the permeability coefficients are known. By providing the required surface area, given gas transfer rates can be established. The geometry (surface area and material thickness) are material fabrication requirements that can usually be measured, calculated, or experimentally determined.

In a hollow fiber permeable membrane, for gas mixtures at low flow rates, the total pressure (the sum of the partial pressures) drops slightly along the fibers as a result of friction. For conditions where the concentration (partial pressure) of the gases changes very little from end to end, the use of average or log-mean pressures is generally of sufficient accuracy. For use in a fuel tank inerting system, however, the oxygen concentration must be reduced from a nominal 21 percent to a value below 9 percent. No satisfactory means of computing a mean tube-side partial pressure for a single calculation (for both oxygen and nitrogen gases) over the widely varying conditions encountered has been successful.

Just as the tube-side concentration varies along the length of the tube as a result of gases leaving the high-pressure stream, gas concentration along the length of the shell side varies from the addition of the gas permeated through the tube walls. This results in a reduction of oxygen concentration in the gas flowing inside the tube and an increase in the oxygen concentration around the tubes. The increased oxygen concentration (partial pressure) around the tubes tends to inhibit oxygen concentration reduction in the tubes (oxygen permeation rates tend to be reduced and nitrogen permeation rates tend to be increased). It is desirable to prevent this buildup of oxygen concentration.

For a system using air, this is accomplished by flushing (or washing) the shell side of the tubes with air to drive the oxygen concentration back toward 21 percent.

Thus, for a hollow fiber permeable membrane, the problem in computing the mass transfer of oxygen and nitrogen through the tube walls lies in the fact that this rate is a function of position along the tube based on the local value of concentration along the tube. (An analysis shows the gas diffusion rate to be several orders of magnitude greater than the permeability rate, thereby allowing the assumption that the tube-side gas concentration is homogeneous at any given distance down the tube.) The local mass transfer rates for both gases vary as a function of their local partial pressures (which, in turn, are the cumulative result of mass transfer rates in the preceding length of tube.) The mathematical formulation of a high-pressure-side element of mass or volume is further complicated by the fact that both the mass and volume of the element change along the length of the tube, due to permeation.

To evaluate design requirements and performance of designs at a number of conditions, mathematical models have been constructed to represent the behavior of the hollow fiber permeable membrane just described. The models are used to investigate the behavior of a single typical tube by approximating its performance in the analysis of a large number of segments. By this means, concentration variations within any one element are small. Thus, a profile of the tube-side gas flow rate and concentration, and a profile of the permeant gas flow rate and concentration, are established as a function of length along the tube.

The simultaneous solution of equations is best performed by an iteration process of establishing the conditions at each successive node, solving for the permeant flow rates of both gases, and then calculating the resulting conditions at the node. Due to the iterative nature of the solution applied to this mathematical model, a digital computer program, in several versions, has been devised. In addition to the constant shell-side oxygen concentration model discussed for the ram wash case, a variable shell-side concentration model recently has been established. This model iteratively establishes the shell-side concentrations at the local permeant concentration levels.

The establishment of IGG ASM designs requires that membrane material characteristics and airborne systems requirements be input to the established mathematical models. The Phase I development tests generated heretofore unknown properties needed for design. Since the two descent profiles of Figure 4-3 differ only above the 10,000-ft elevation, the HSID profile was selected for design-point analysis. Possible design points at the 23,000-ft altitude flow peak, at the 15,000-ft altitude rate, and at sea level, were analyzed.

The design of the ASM for each of these three points of the HSID profile was evaluated throughout a range of possible operating temperatures that could be maintained by the systems. As a first approximation of design operation temperature, the flow requirements for the 3000-fpm 15,000-ft HSID were considered for the full 3000-hr life pressures of Figure 2-11, ignoring the

available air pressure on the aircraft. (Since operating at life limit pressures results in surface area requirements approximately proportional to flow, an analysis of the 23,000-ft altitude and sea-level altitude conditions at lower flows results in reduced membrane surface area requirements.) The permeability coefficients of oxygen and nitrogen were considered throughout the ASM operating temperature range from 40° to 90°F. The results of these analyses for a wash case at a 24 percent oxygen average shell-side concentration, and a non-wash case, are shown in Figure 4-5. These data show that the wash ASM design results in membrane surface area requirements below those required for non-wash ASM design. From these data, the advantages of wash ASM design were again shown. A second trend demonstrated by the data of Figure 4-5 apparently favors lower design operating temperatures; however, since the curves of Figure 4-5 are at full 3000-hr life operating pressures irrespective of pressure available on the aircraft, the attainment of these increased pressures at low temperature would require additional system complexity. Fortunately the system is not constrained to available bleed air pressures. Mechanical means of increasing pressures using centrifugal compressors presents a proven, convenient method of increasing air pressures at relatively low penalties. A second membrane sizing curve for all three potential design points is shown in Figure 4-6. Here the pressure has been maintained at a constant value independent of operating temperature. The data of Figure 4-6 have been prepared using boosted (2 times) high-stage bleed air pressure available at each of the potential design points (from Figure 4-4) and ignore membrane operational life limits. As can be seen in Figure 4-6, analysis using these design values shows the 15,000-ft HSID to require the greatest membrane surface area. In addition, the data for constant pressure consideration show the higher operating temperature to be more favorable.

In consideration of system design, both life limit pressures and available aircraft air pressures (boosted) must be observed. High-stage bleed air pressures, before and after a pressure-doubling boost, are shown on the bar graph of Figure 4-7 for all three potential design points (i.e., 23,000-ft, 15,000-ft, and sea-level aircraft altitudes). The 3000-hr life limit at four operating temperatures (55°, 65°, 75°, and 85°F) are compared on the bar graph. Those pressures exceeding the life limit represent additional physical constraints to be placed on the pressures limiting the use of boosted pressure, which can be produced by the turbocompressor. As can be seen from Figure 4-7, as the operating tempratures increase, life limits rather than available (boosted) pressures become design constraining.

When the required membrane surface area for simultaneous consideration of both the maximum available (boosted) air pressure and the 3000-hr operating life are used as limits, the optimization shown in Figure 4-8 results. The 15,000-ft HSID point generates the requirement for the largest membrane surface area. At temperatures below about 77°F, as can be seen by reference to Figure 4-8, the operating pressure is limited by available boosted high-stage bleed air. At temperatures above 77°F, the 15,000-ft HSID design becomes life limited. From the data shown in Figure 4-8, the design point is seen to be the 15,000-ft HSID at an operating temperature of 77°F.

The membrane surface area selected for the airborne system preliminary design is 37,000 sq ft. This surface area meets requirements for operation

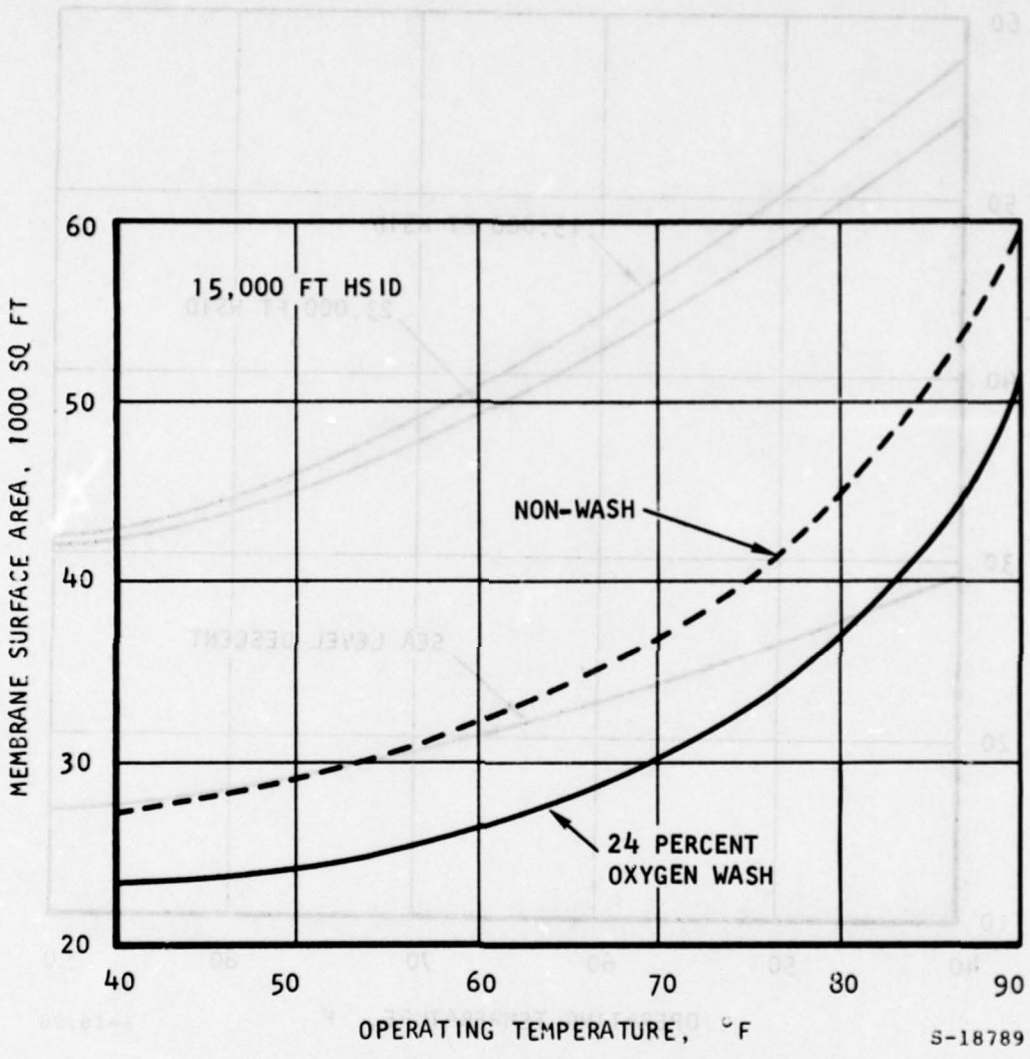


Figure 4-5. Membrane Transfer Area Required, Life Limit Pressures

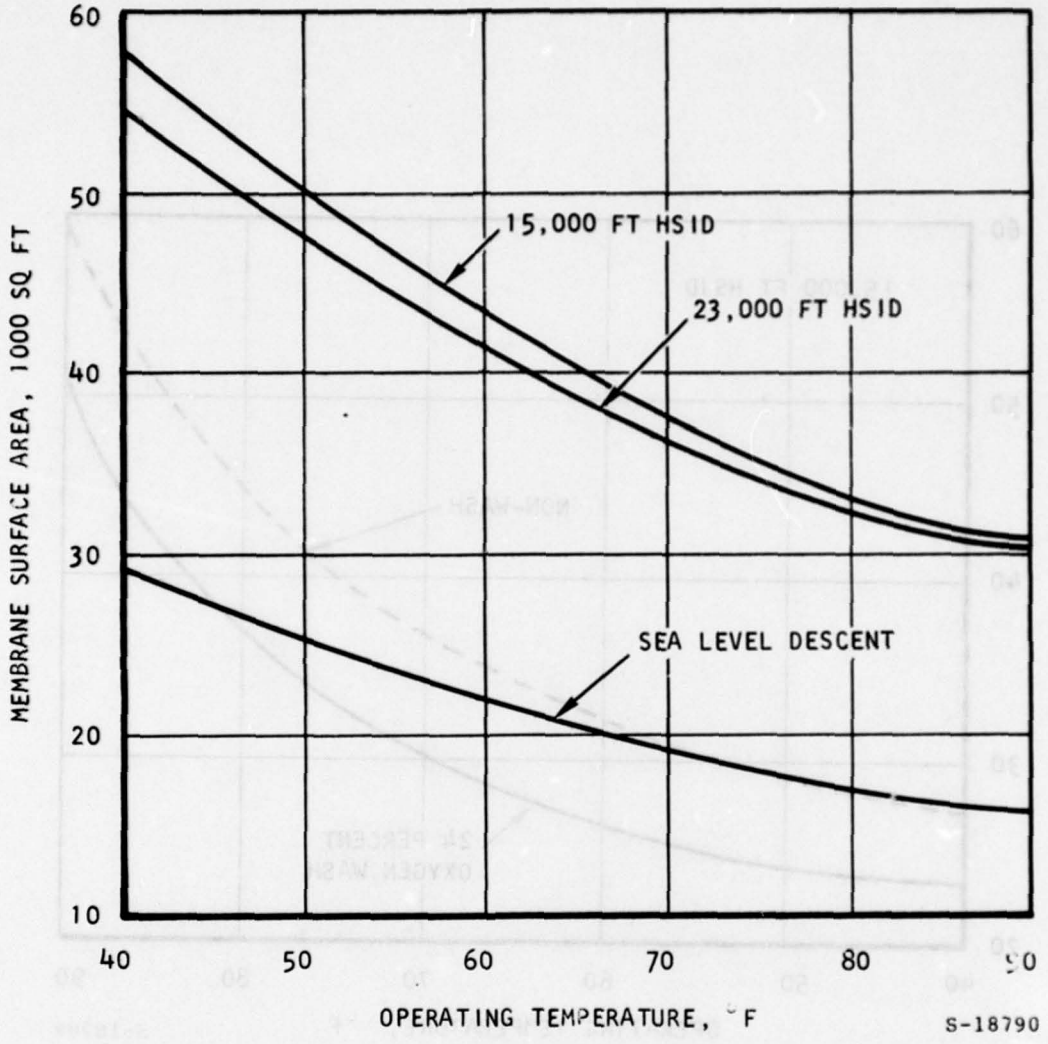


Figure 4-6. Membrane Transfer Area Required, Boosted Available Pressures

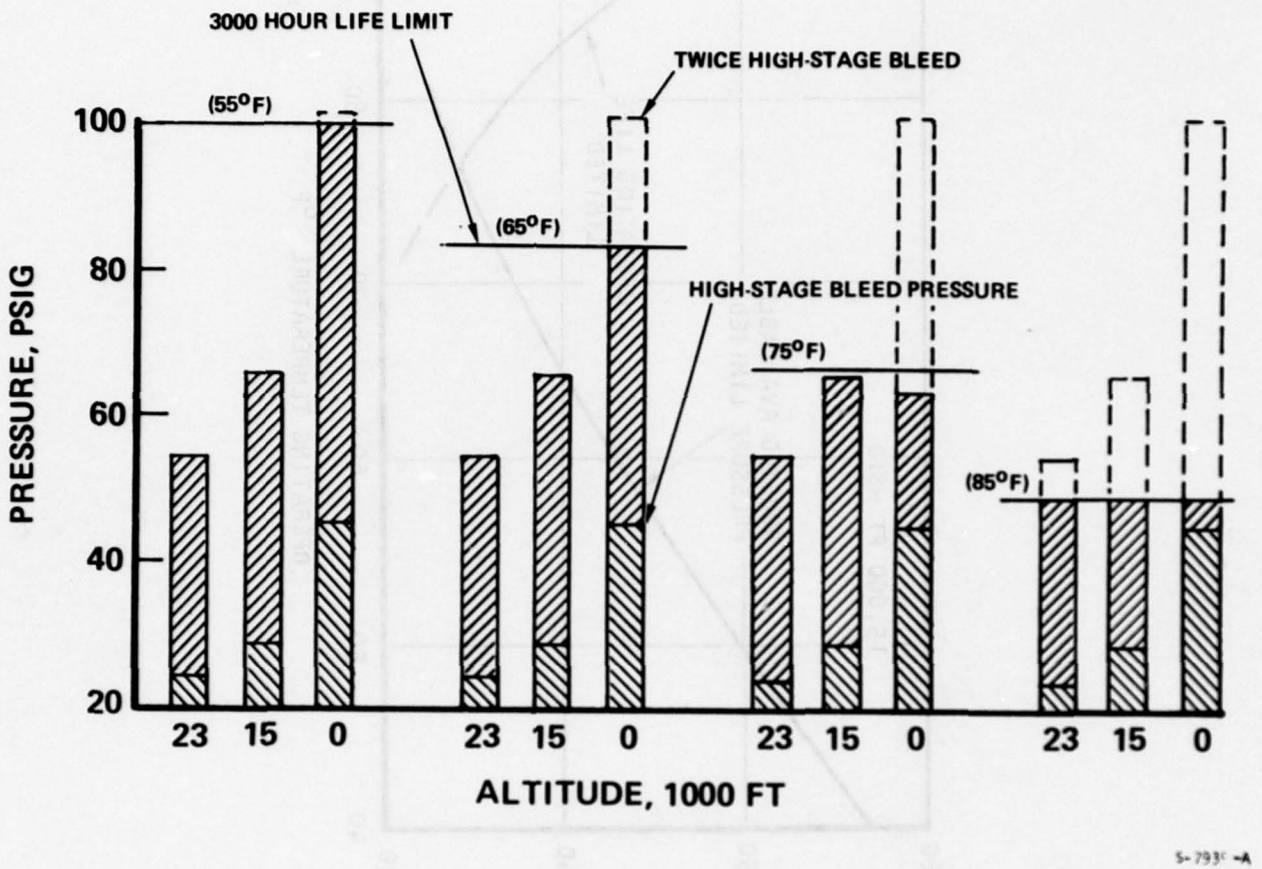


Figure 4-7. Life Pressure Limits

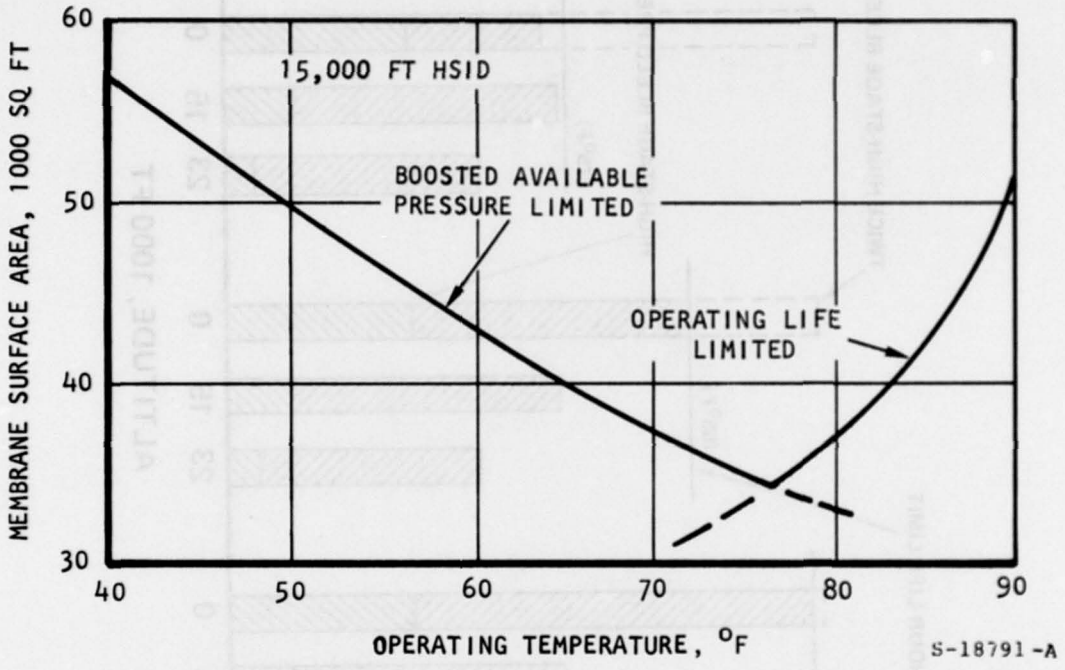


Figure 4-8. Design Point Requirements

at temperatures as low as 70°F or as high as 80°F. To allow for fiber losses in assembly as encountered during the breadboard fabrication phase, a 92-percent utilization factor has been used, bringing the design surface area to 40,000 sq ft.

As can be seen in the discussion above, increases in available pressure due to advanced throttle settings (or, of course, in other applications) can be expected to result in operation at lower temperature-pressure limit/life limit crossover points. This can result in substantial ASM surface area requirement reductions with accompanying reductions in system size and weight.

IGG SYSTEM DESIGN

Development tests conducted by the FAA on the DC-9 and the Air Force on the C-141 and KC-135 aircraft have shown that fuel tank inerting systems compatible with aircraft flight requirements can be built to establish the required inert gas concentration in flight test aircraft using nitrogen gas stored as a cryogenic liquid as the inert gas source. The Air Force Military Airlift Command (MAC) Galaxy C-5A fleet has recently undergone a retrofit program to include the protection offered by fuel tank inerting. The application of the technology under investigation in this program is the replacement of the inert gas storage and supply dewars in current fuel tank inerting systems with onboard systems to generate inert gas. These advanced IGG fuel tank inerting systems consist of properly designed ASM's with their associated air temperature, pressure, and flow controls to meet IGG flow and concentration requirements.

Bleed air, whether delivered from the bleed air manifold, ECS air cycle compressor discharge, or high-stage engine bleed ports, can be expected to be at temperatures above the nominal 75°F ASM design temperature selected for system operation.

In order to cool this air to or near ASM design temperatures, low-penalty ram cooling air in a high-density plate-fin aircraft heat exchanger is utilized as shown in Figure 4-9. At high altitude and at many lower altitude conditions, the ram air sink temperature is below the 75°F air separation module design operating temperatures. For these cases, the ram air modulating valve will be partially driven toward the closed position to prevent cooling of the air below 75°F. For those conditions where the ram air sink temperature or flow is not sufficient to reduce the bleed air temperature to nominal ASM design temperatures, a flow diversion valve directs sufficient air through a tube-shell heat exchanger using ECS turbine discharge air to remove additional heat from the bleed air to further reduce bleed air temperatures to ASM design temperatures.

Although, in general, ASM performance is enhanced by increased tube-side air pressure, the membrane life requirements established in Figure 2-11 must not be exceeded. During ascent, when engine power settings are high, pressures exceeding the limits established for membrane life may be expected from unregulated bleed air. Excessive pressures may be limited by pressure regulation of the air entering the ASM. Further extension of the useful life of membranes beyond limits shown in Figure 2-11 may be achieved if the pressure is reduced below the life limit values for all conditions where full pressure is not required to meet design concentrations. Such conditions, in fact, occur for all but the high-flow descent phases of the mission profile.

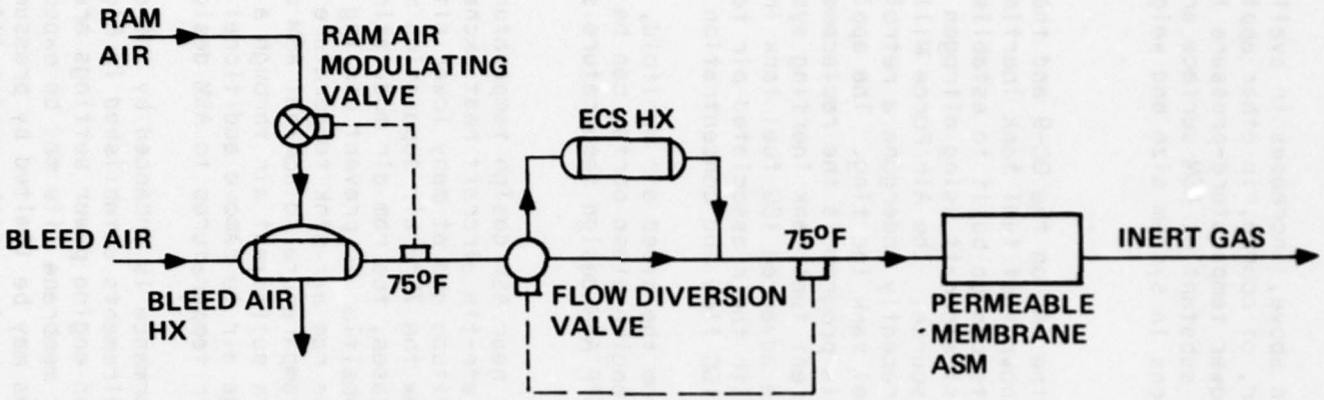


Figure 4-9. Bleed Air Temperature Control

S-793-A

To limit the membrane pressures at reduced (from design point) flow conditions, a flow sensor is shown linked to the fuel tank inert gas demand flow valve in Figure 4-10. This sensor is used to control maximum ASM inlet pressure as a function of inert gas flow demand.

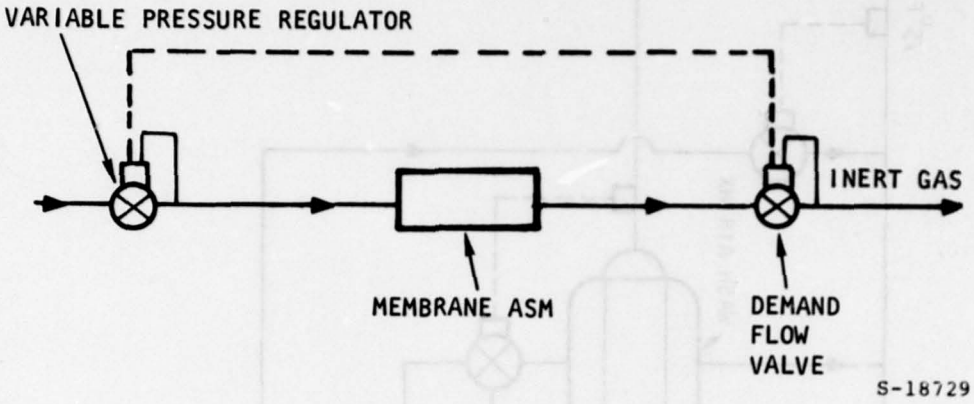


Figure 4-10. Air Separation Module (ASM) Pressure Limit as a Function of Inert Gas Flow

During descent, when source air pressures are low (Figure 4-1), the requirement for the inert gas flow reaches a maximum (Figure 4-4). The ASM design utilizes an inlet of twice the available high-stage engine bleed air pressures at recommended descent throttle settings. To achieve this boost in available air pressure, an air-driven turbocompressor, as shown in Figure 4-11, is utilized. High (13th) stage bleed air enters the compressor stage of the air-driven centrifugal turbocompressor, which increases the discharge pressure of the air to a value twice the inlet pressure. Excess bleed air temperature is reduced by the bleed air heat exchanger, as shown in the schematic diagram of Figure 4-9.

In addition, Figure 4-11 shows the delivery circuit for ASM wash air used (1) to eliminate the loss of efficiency associated with ASM shell-side oxygen concentration buildup that would otherwise develop, and (2) to assist (with the conditioned bleed air) in maintaining design operating temperature in the ASM's. ASM wash air is delivered from the air cycle ECS primary to the turbine side of the turbocompressor where, as a result of providing the power for the compressor, the air is cooled. Since both wash air and conditioned bleed air must be at ASM operating temperatures, the turbine discharge air is used to remove heat from the bleed air, eliminating the need for supplemental ECS air cooling for most modes in which the turbocompressor is used. In order to prevent the wash air from dropping below ASM design operating temperature, additional warm ECS primary air is added to the turbine-heated turbine discharge air as required to maintain the design operating temperatures.

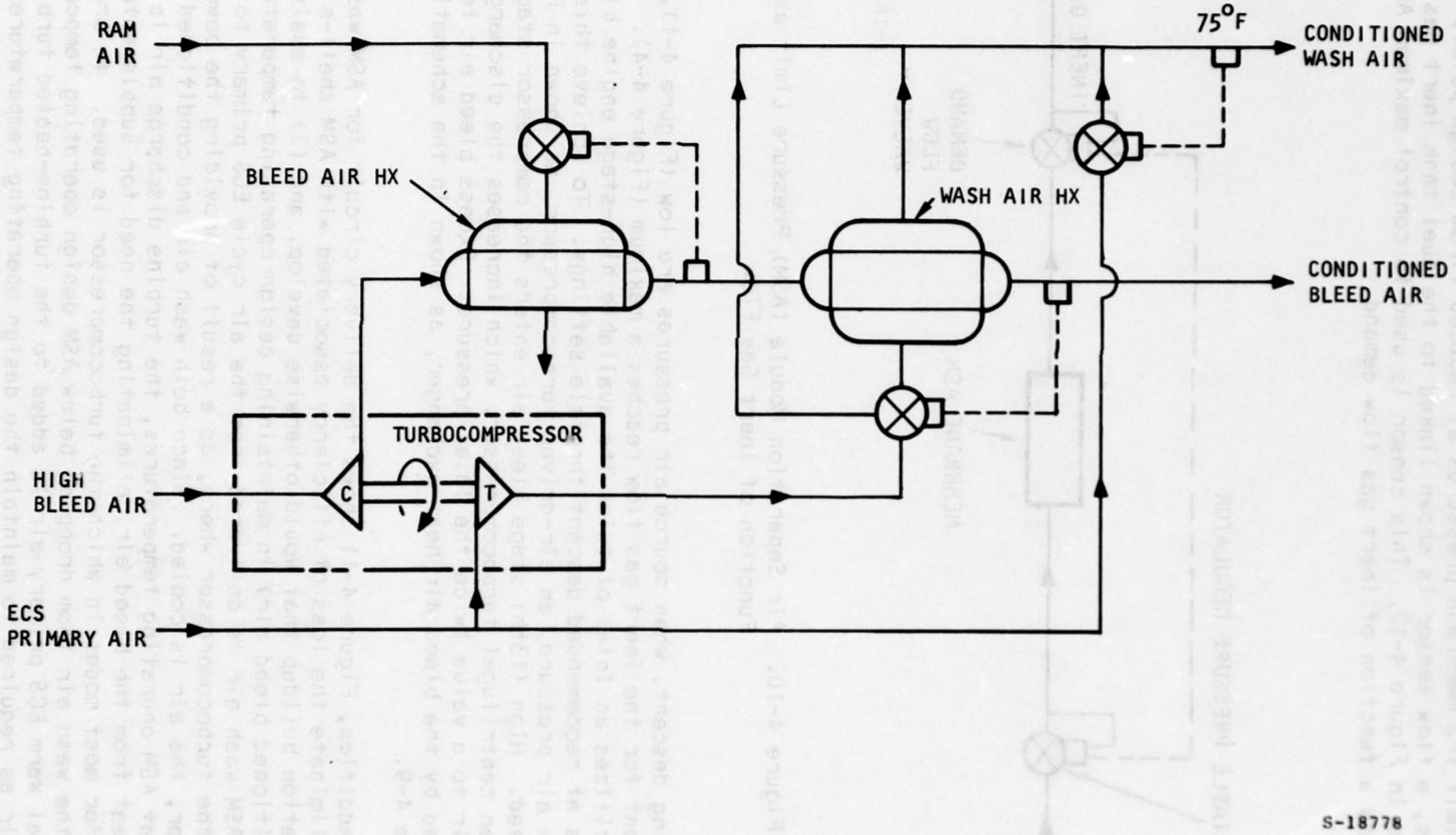


Figure 4-11. Bleed Air Boost and Purge Air Temperature Control

The system schematic of the selected airborne IGG system is shown in Figure 4-12. The system utilizes a combination of the concepts discussed for the schematic diagrams of Figures 4-9, 4-10, and 4-11. Additional system components not previously discussed are also shown in the schematic diagram of Figure 4-12. These components include a low (8th) stage check valve (Item 1-1) and a high (13th) stage shutoff valve (Item 1-2) to permit the use of low-stage bleed air during higher engine settings during most ground, climb, and cruise modes when the penalties for high-stage bleed air are significant. Also included are a compressor bypass check valve (Item 1-6) and a turbine inlet shutoff valve (Item 1-25) to eliminate the turbocompressor from the system for the segments of the mission profile where inert gas flow requirements are small and the low-stage bleed pressures are adequate to eliminate both the bleed air boost and the ASM wash from the system. In addition, Figure 4-12 shows that both the tandem inertial particle separator (Item 1-17) and the filter (Item 1-18) remove particulate contaminants from the bleed air stream prior to entering the ASM and the electronic control unit (Item 1-24), which receives flow and pressure data and in turn is used to set the ASM inlet pressure, select the bleed air source, and activate the boost turbocompressor.

INERTING SYSTEM DESIGN

As previously noted, the fuel tank inerting system for the baseline aircraft basically embodies the operation and protection capabilities historically demonstrated with stored gas fuel tank inerting systems. The important difference is the elimination of the nitrogen storage dewars and their replacement by the IGG system. The complete fuel tank inerting system, shown in block schematic diagram form in Figure 4-13, includes (1) the connecting plumbing to supply services to the IGG system and deliver the inert gas from this system to the fuel tank, and (2) additional system components. The additional components consist of (1) two vent valves (Items 2-1) for fuel tank pressure control, and (2) a unique feature of this system, an ambient-temperature Halon 1301 fire extinguishant (bromotrifluoromethane) storage bottle (Item 3-1) and valve (Item 3-2) to provide an available completely redundant source of explosion and fire suppressant in the event of engine failure, inerting system failure, or emergency descent.

Estimated fuel tank inerting system weight and air requirements are shown in Table 4-1 for the baseline design DC-9 series 30 aircraft. Scaling of the system weight shown in Table 4-1 is of interest for other potential aircraft applications. Direct scaling of system weight, particularly to considerably larger aircraft, is difficult due to nonlinear characteristics and the fact that extrapolated regression analysis often fails to take into account characteristic weights that are independent of scaling factors. This is particularly true for the ASM, which (as can be seen in the previous discussion of its design) is a complex result of pressure, altitude, and temperatures as well as flow; however, based on realistic assumption of availability of similar aircraft air pressures and operation at similar temperatures, first-order approximations can be made. With a knowledge of aircraft fuel tank volume and descent rate, the peak inert gas flow requirements may be established by the use of Equation 4-2. A conservative first-order approximation of system weight for other aircraft can be established using the regression equations of Table 4-2.

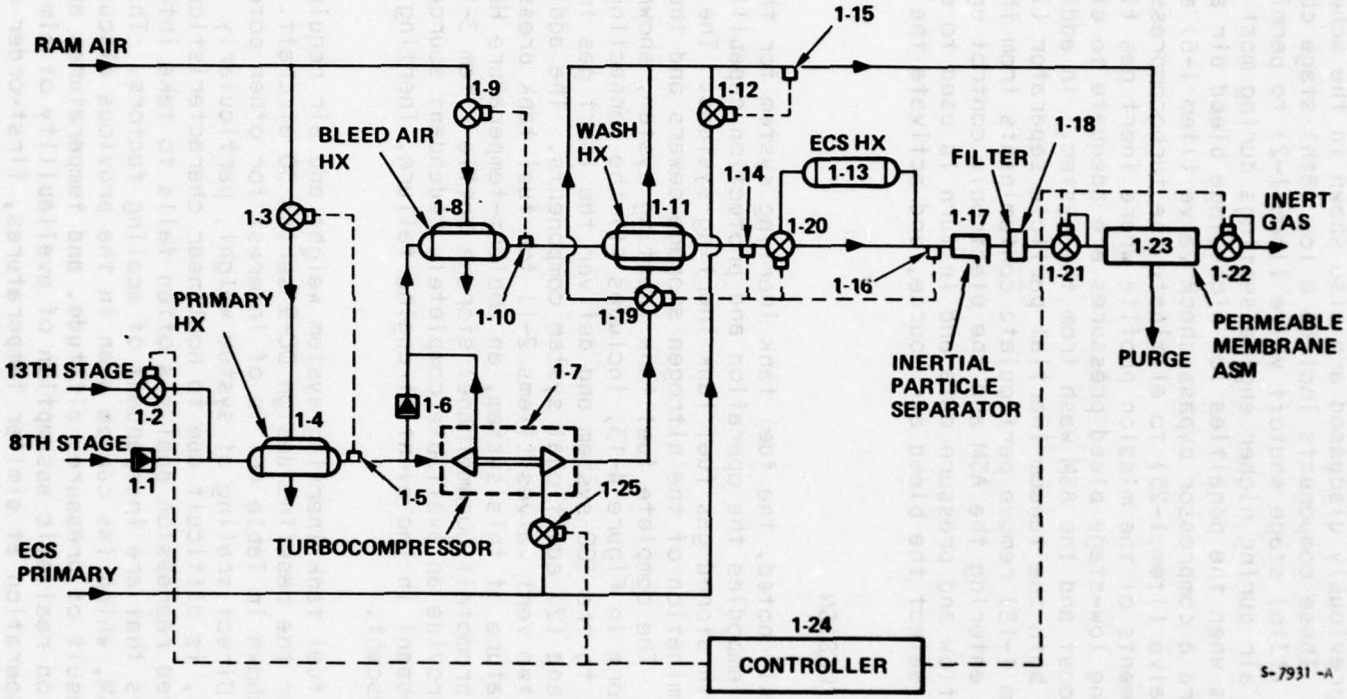


Figure 4-12. Airborne Inert Gas Generator (IGG) System Schematic

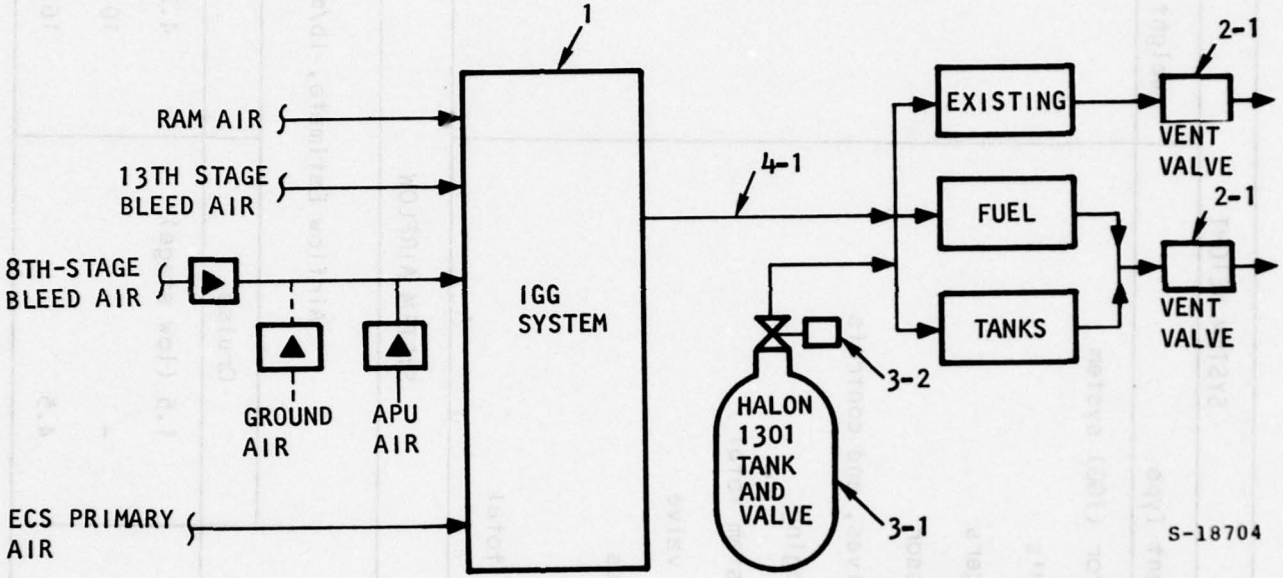


Figure 4-13. Inerting System Block Diagram

TABLE 4-1

ESTIMATED SYSTEM WEIGHTS AND AIRFLOWS

SYSTEM WEIGHT	
Equipment Type	Weight Estimate, lb
Inert gas generator (IGG) system	
Membrane ASM's	120
Heat exchangers	20
Turbocompressor	20
Sensors, valves, and controls	20
System packaging	30
IGG system total	210
Halon, tank, and valve	20
Distribution lines	25
Vent valves	15
System total	270*

SYSTEM AIRFLOW		
	Airflow Estimate, lb/min	
Airflow Source	Cruise	Descent
Bleed air	1.5 (low stage)	4.2 (high stage)
ECS primary	-	10.0**
Ram air	4.5	16.0

*Using the 30 percent penalty factor discussed in Section 5, the installed system weight can be expected to be about 350 lb.

**Aircraft ECS airflow normally exceeds 100 lb/min.

TABLE 4-2

ESTIMATED SCALING FACTORS

WEIGHT

System weight = (75.48) (inert gas flow) + 94.13

Weight, lb

Inert gas flow, lb/min

AIRFLOW (DESCENT)

Bleed air = (1.80) (inert gas flow)

ECS primary air = (4.30) (inert gas flow)

Ram air = (6.85) (inert gas flow)

SYSTEM OPERATION

Once the ASM design has been established for the system design point, available analytical tools enable the evaluation for design performance throughout the mission profiles, and for off-design conditions. For established module designs, inert gas oxygen concentration is mainly a function of air inlet pressure, altitude, temperature, and inert gas flow rates. Actual performance for any combination of these independent variables can be mathematically modeled as a surface in N-dimensional space (in this case 5 dimensions). Resulting oxygen concentration can then be established as a result of the other variables. When the number of dimensions is simplified by elimination of variables (i.e., assuming constant values), the mathematical surface can be simplified to permit two-dimensional representation. Here, if the operating temperature is held constant at 75°F (the design point value), and if a pressure-altitude of 15,000 ft is selected as an example, the effects of variable inert gas flow rates and air inlet pressures on inert gas concentration may be expressed as a family of curves.

It is of further system interest to evaluate both the wash and non-wash operating modes to evaluate the limits of the superiority of the wash operating mode. Although analysis has clearly shown the advantages of the use of the wash mode to reduce module shell-side oxygen concentration at the system design point, this mode imposes a theoretical limit on inert gas oxygen concentration performance of the ASM's. Operation at the non-wash mode imposes no such theoretical limit, and for flows reduced below the design-point values, may be expected to result in oxygen concentrations below those theoretically possible for wash mode operation. (Tests at very low flows in the non-wash mode have resulted in inert gas oxygen concentrations below 1 percent).

The family of curves for both wash and non-wash operating mode relating inert gas flow rate and ASM inlet air pressure to inert gas oxygen concentration is shown in Figure 4-14. Pressures from 75 psia (near the design pressure) down to 30 psia are shown. In addition, the mode crossover flows, where further reduction in inert gas flow begins to favor the non-wash operating mode to reduce inert gas oxygen concentration, are indicated for each pressure shown in Figure 4-14. The loci of these points establish a crossover threshold; to the left of the loci, it is more desirable to operate the system in the non-wash mode. Accordingly, for aircraft cruise and ground conditions when air pressure is readily available and inert gas flow demand is low, the use of the non-wash mode has been considered.

Fuel tank inerting system operation can best be explained in terms of various operating modes. The following discussion considers typical operation for ground, ascent, cruise, and descent modes. The special protection offered by the redundant chemical suppressant is then discussed for abnormal operating modes. The discussion below refers to the item numbers shown in the inerting system schematic diagram of Figure 4-13 and the IGG system schematic diagram of Figure 4-12.

Ground Operation

System operation on the ground is possible whenever the propulsion engines are powered. Alternatively, air pressure can be provided by utilizing bleed air from the airborne auxiliary power unit (APU), or from ground air sources if the aircraft is to remain on the ground for long periods of time (sufficient to require a supply of inert gas for leakage, temperature "breathing", maintenance, etc.) without either the engines or APU in use. During ground operation, inert gas flow rates are a small fraction of peak descent rates and are required only to replace fuel consumed from the fuel tanks and maintain pressures against any slight leakage flows. Following refueling, or whenever fuel tank purging is required, the controller (Item 1-25) can be set to establish a minimum inert gas flow (a nominal 0.5 lb/min) to purge any oxygen evolving from the fuel overboard through the fuel tanks. Low-flow ground operation inert gas flow rates will be delivered without the need for wash airflow through the ASM's, resulting in inert gas concentration below 5 percent oxygen. If the temperature of the air at the ASM inlet becomes excessive, the turbocompressor (Item 1-7) will be switched on by the controller to provide cooling air to the wash heat exchanger (Item 1-11).

Inert gas is delivered to the distribution plumbing (Item 4-1) by the demand flow valve (Item 1-22) as required when the ullage gas-to-ambient pressure drops below a pre-set value (nominally 0.3 psid), unless ullage purge flow is requested by the controller, in which case ullage gas pressure will be controlled to the crack pressure of the fuel tank vent valves (Items 2-1) operating at a relief pressure (nominally 0.6 psid). The vent valves are mounted in each of the existing wing vent boxes shown in Figure 4-15. The vent valves, which also will contain secondary pressure relief features as well as negative pressure relief, will be mounted in the area occupied by the standpipes shown in Figure 4-15. The vent valves will be installed in a manner to retain the fuel retention function of the current standpipe.

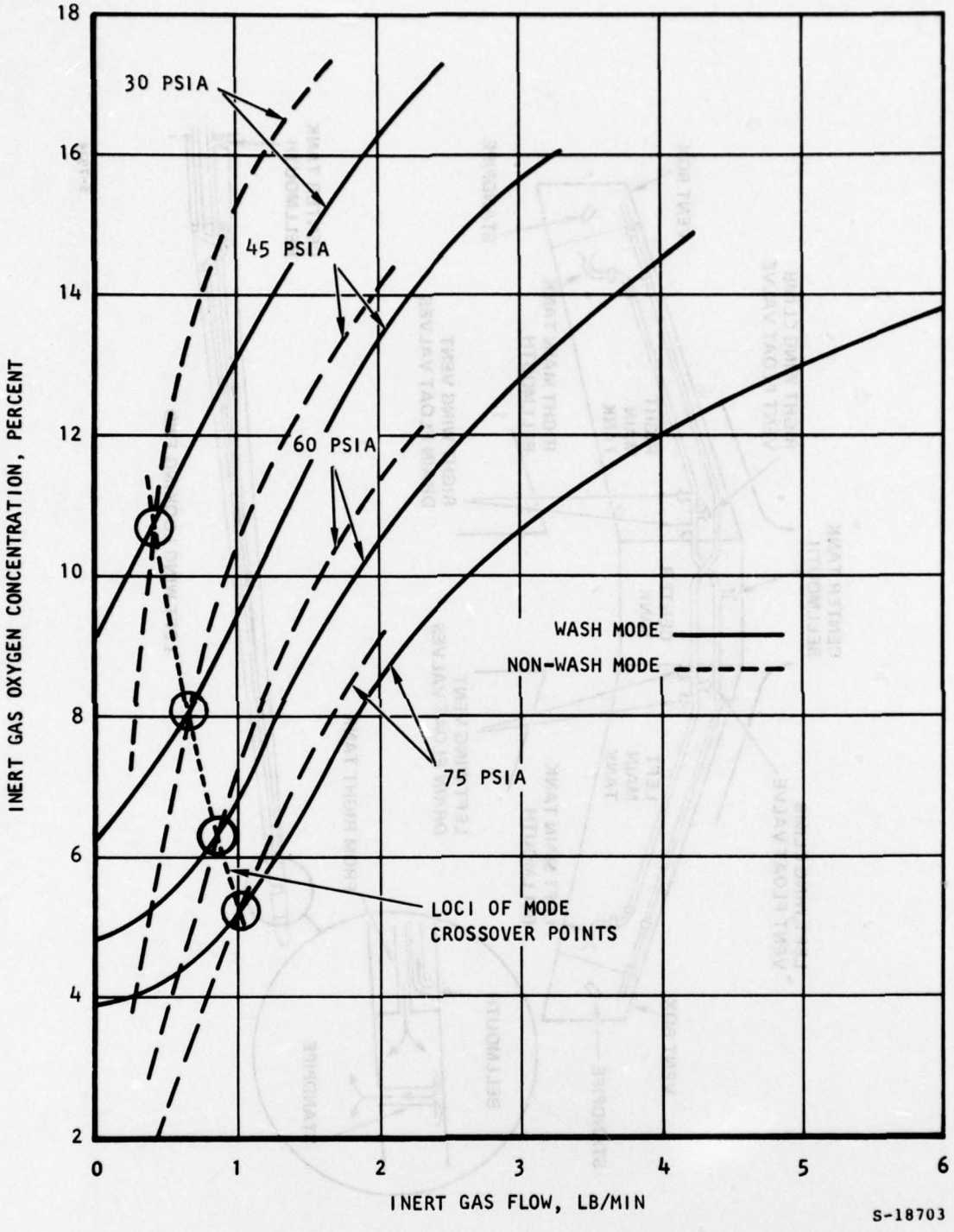


Figure 4-14. Air Separation Module (ASM) Performance Projection and Mode Crossover

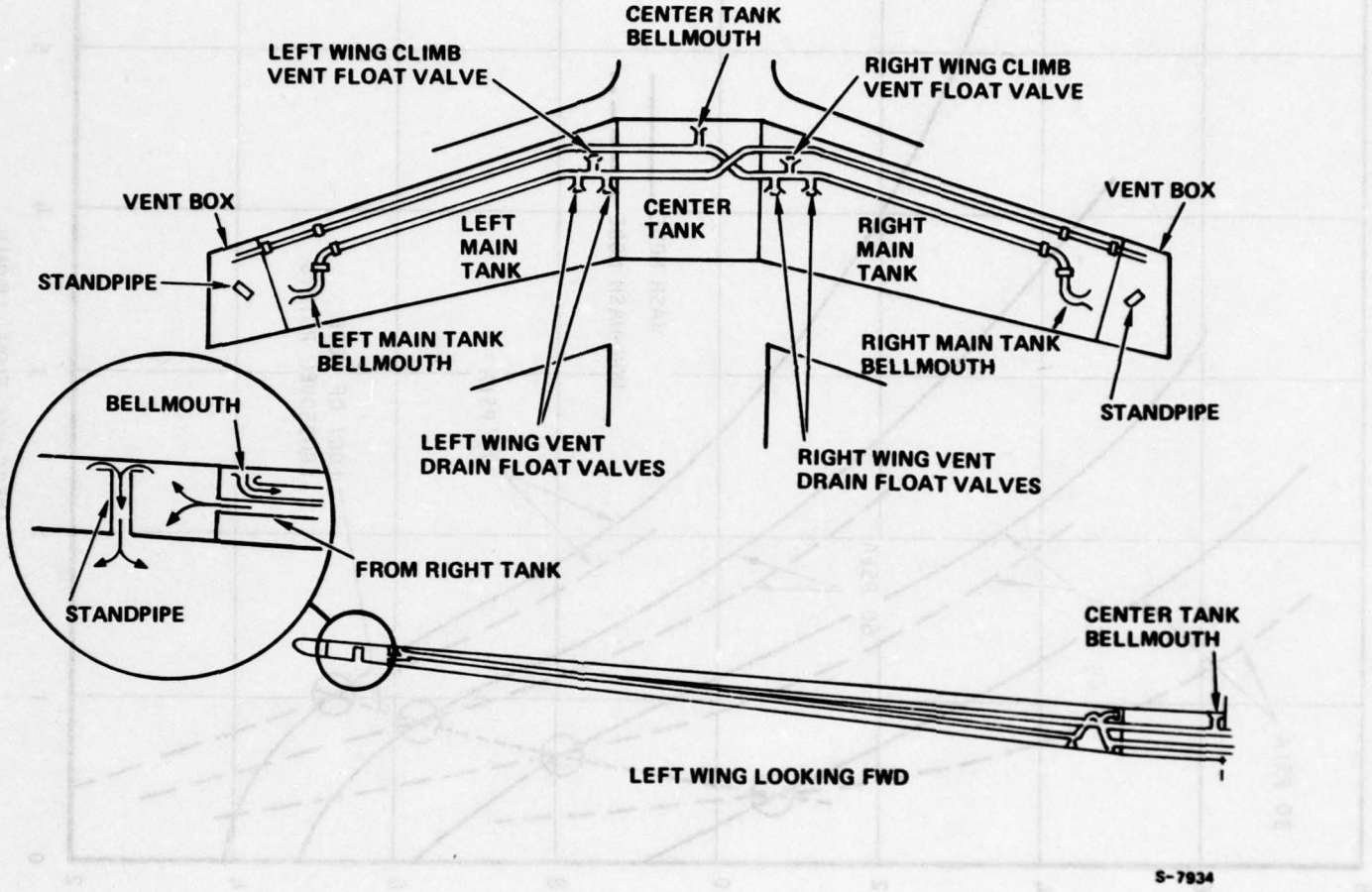


Figure 4-15. Fuel Tank Vent System

Ascent

During ascent, inert gas flow demand will generally not be required due to decreasing ambient pressures and associated increasing fuel tank ullage-to-ambient pressure differentials, resulting in ullage gas outflow to fuel tank vent valves. However, during this period of ascent, when fuel ullage pressures are decreasing, experiments done for the design of current stored-gas inerting systems have shown that the gases dissolved in the fuel tank tend to evolve from the fuel. Evolving oxygen must be purged from the fuel tank ullage to maintain the inert condition of the ullage and vent system. Since the system has the capability of producing inert gas up to design-point flows during descent, a unique characteristic of the IGG system is the availability of low-concentration (Figure 4-14) inert gas for purging ullage space. A function of the controller (Item 1-25) during ascent will be the establishment of an ullage purge flow of a nominal 1.0 to 1.25 lb/min from the IGG system. With the ready availability of inert gas flow for ullage purge during ascent, it is estimated that location of the purge flow distribution system at the opposite end of the fuel tanks from the vent system bellmouths will be adequate for oxygen removal without the need for more complex fuel scrub systems previously required to minimize the use of (stored) inert gas for past fuel inerting systems. All inert gas airflow to the fuel tanks for repressurization, as well as purge flows, will utilize this inert gas distribution manifold.

During ascent, low-stage bleed air is of sufficient pressure and will be selected by retaining the high-stage bleed air valve (Item 1-2) in the closed position. The turbocompressor (Item 1-7) will be activated by opening the ECS primary turbine valve (Item 1-26). Temperature and pressure control will be in accordance with the control system discussions accompanying Figures 4-9, 4-10, and 4-11.

Cruise

During normal level cruise modes, inert gas demand inflow for fuel consumption is small (on the order of 0.1 lb/min). In addition, high-altitude operation provides sufficient cooling capacity using the bleed air heat exchanger (Item 1-8) to cool several times the demand of bleed airflow. For this mode, 8th-stage bleed air is selected (Item 1-8) and the turbocompressor is not selected (via Item 1-29), allowing the ASM (Item 1-23) to operate at low flow rates in the non-wash mode. This results in further decreases in inert gas oxygen concentration approaching 3 percent. An ullage gas purge (at 0.25 lb/min) may be continued, resulting in an inert gas concentration of under 5 percent oxygen. During the cruise operating mode, ASM pressure and temperature are controlled as noted in the discussion of Figures 4-9 and 4-10.

Descent

The IGG system design point occurs during descent, as discussed previously in this section. At the initiation of descent, the high-stage bleed source air is selected by opening the high-stage bleed air valve (Item 1-2). In addition, the turbocompressor is activated by opening the turbine air shutoff valve (Item 1-29) to provide bleed air pressure boost and air conditioned ASM purge air. The operation of the system during descent is in accordance with the discussion

of Figures 4-9, 4-10, and 4-11. For the design HSID mission, the ASM pressure is adjusted as a function of inert gas flow rate, as noted in the discussion of Figure 4-10. At the peak design-point condition, ASM inlet pressure approaches the 3000-hr life curve (Figure 2-11) and inert gas flow rate reaches the design-point flow of 2.33 lb/min. Throughout the descent, inert gas oxygen concentration is maintained between 7 and 9 percent oxygen; the 9 percent peak condition occurs at a 15,000-ft altitude. Upon landing, the system returns to the ground operating mode previously discussed.

Redundant/Emergency Provisions

Inerting system redundancy is desirable independent of the inertant source (i.e., stored liquid nitrogen or generated inert gas). While a stored gas (liquid nitrogen) system is, of course, dependent on an exhaustible supply of the stored gas, an IGG system is dependent on a source of pressurized air. To provide redundant protection in case of the exhaustion of the liquid nitrogen supply, failure of the source of pressurized air, or the failure of either of these primary inerting systems, a backup is highly desirable. In addition, since IGG system penalties depend upon design flow rates, auxiliary means to reduce the flow rate for unusual emergency conditions for which the aircraft would not be expected to be available for immediate dispatch following landing offers a means of reducing IGG system design penalties.

Certain failures of other airborne systems can cause a rapid cabin depressurization, as a result of which the aircraft will be flown rapidly to low altitudes following an emergency descent profile. The rapid descent rates require large inert gas flow rates, so that tank repressurization can keep pace with rapidly increasing atmospheric pressure outside of the tanks. An IGG system designed for the emergency descent profile would be heavier and larger than a system designed for normal flight operations. For example, design of the baseline DC-9 IGG system to include protection for a typical emergency descent at a rate of about 13,000 ft/min from high altitude to 25,000 ft followed by reduction of descent rate to about 6500 ft/min to a "safe" altitude of 15,000 ft could be expected to result in an additional system weight of 290 lb if designed for the 25,000-ft altitude or 170 lb for a system designed to produce a 9-percent inert gas product at the 15,000-ft altitude during these high rates.

Rather than penalize the aircraft design to accommodate a rare occurrence, the primary system is designed for normal flight profiles only and the use of a secondary emergency system is considered for emergency descent. The resultant total redundancy will enhance overall reliability and is not inconsistent with logistics-free operation following an emergency situation in which rapid turnaround is not a normal requirement. The emergency descent secondary system selected for this preliminary design is the fluorocarbon fire extinguishing agent (Halon 1301), delivered from an onboard storage tank.

In the past, system design concepts called for the use of a detonator-actuated burst disc to admit the Halon to the fuel tanks when an emergency descent is sensed. The Halon supply must be adequately sized to inert the fuel tanks (at least 6 percent by volume) for the duration of the emergency descent without assistance from the IGG system. More recently, as a result of

discussions with military operators, it has been noted that it may be more desirable to retain the ultimate inerting capability of the Halon until the situation is most critical (such as immediately prior to an anticipated hard landing or crash) and utilize the IGG system output, albeit at an oxygen concentration greater than 9 percent, until that time. This would retain the redundancy of the system until the critical time determined by the aircraft pilot, who could then command its manual injection into the fuel tanks. Primary system operation during this emergency descent mode would result in the inert gas inflow oxygen concentration peaking at 16 percent at 25,000 ft and again at 13 percent at 15,000 ft, with a return to fully inert ullage gases (less than 9 percent) following leveling-off at the 15,000-ft altitude at the conclusion of emergency descent.

System operation is herein assumed to be in this latter mode where the redundancy could be most advantageously utilized. Should the previous operating mode be selected as more desirable for commercial transport operations, there is, of course, negligible effect on system weight.

Preceding Page BLANK - NOT FILMED

SECTION 5

OWNERSHIP CONSIDERATIONS

To fully evaluate the feasibility of various methods of fuel tank ullage fire and explosion hazard reduction for commercial transport application, technical feasibility and system penalties must be investigated. Additionally, information to allow comparisons of system logistical considerations and (for some systems) dependence on supply of expendables from numerous outside commercial suppliers at airports from which the aircraft operate, would be desirable. Quantifiable data, including projected reliability and cost of ownership data, also would provide a basis for decisions as to the economic viability of systems under consideration.

This section presents a study of the cost of ownership, including initial cost, maintenance cost, and operating cost for the baseline DC-9 permeable membrane inert gas generator fuel tank inerting system discussed in Section 4. The study presents the data for the membrane IGG system; the format, however, is also suitable for an economic comparison of alternate fire and explosion hazard reduction systems. Extension of evaluation of other systems will, of course, eliminate some specific cost elements and add other elements that are not pertinent to IGG systems. Non-quantified ownership considerations, such as the need for a dependable network for the supply of expendable perishable fluids (required by some other types of systems) are not discussed in this section, since they are not applicable to IGG fuel tank inerting systems.

RELIABILITY

Reliability analysis is becoming an increasingly important consideration in system design. In addition to providing a comparative measure of the mean time between failures (MTBF) for various systems, reliability analysis is the starting point for estimating maintainability costs. The baseline DC-9 permeable membrane IGG system design, shown in Figures 4-13 and 4-14, is composed of a number of individual components of the type in use in aircraft pneumatic systems. The membrane air separator, a new technology, has been integrated into a system using components of established performance. Table 5-1 presents an estimate of the MTBF for each system component. Estimated MTBF values for each of the components shown in Table 5-1 are representative of established values for generic components of the same type for similar applications. Where available, data shown in Table 5-1 have been taken from field experience for components used on DC-9, DC-10, B-747, and other commercial aircraft. These data from aircraft operators are summarized in an AiResearch report entitled GUARD (Garrett Unified Automated Reliability Data), and in other field data sources. MTBF estimates for the membrane modules and filter consider the effect of scheduled replacement frequency.

The data of Table 5-1 compare well with data for air cycle environmental control systems (ECS), a pneumatic system adopted for use in most commercial and military aircraft.

TABLE 5-1

ESTIMATED COMPONENT MEAN TIME BETWEEN FAILURES (MTBF)

System Item No.	Component	Representative MTBF, hr
1-1	Check valve	80,000
1-2	Shutoff valve	40,000
1-3	Modulating valve	25,000
1-4	Primary heat exchanger	50,000
1-5	Temperature sensor	50,000
1-6	Check valve	80,000
1-7	Turbocompressor	30,000
1-8	Bleed air heat exchanger	100,000
1-9	Modulating valve	25,000
1-10	Temperature sensor	50,000
1-11	Wash heat exchanger	100,000
1-12	Modulating valve	25,000
1-13	ECS heat exchanger	100,000
1-14	Temperature sensor	50,000
1-15	Temperature sensor	50,000
1-16	Temperature sensor	50,000
1-17	Inertial particle separator	100,000
1-18	Filter*	100,000
1-19	Modulating valve	25,000
1-20	Modulating valve	25,000
1-21	Pressure regulator valve	40,000
1-22	Demand flow regulator	40,000
1-23	Membrane module*	100,000
1-24	Controller	25,000
1-25	Shutoff valve	40,000
2-1	Vent valve	100,000
3-1	Halon storage tank assembly	40,000
3-2	Halon valve	80,000

*Scheduled maintenance required at small fraction of MTBF.

LIFE CYCLE COST

The cost of ownership is an important consideration in the selection of any airborne system for commercial application. Not only the initial acquisition costs but the cost of operating and maintaining the system over its entire life cycle must be considered. In the more sophisticated forms of financial analysis, the relationship between capital expenditure and calendar time has become increasingly important in making business decisions. The selection of discounting rates (if any) for evaluation of expenditure following initial investment is, however, best left until the time of decision. If system life cycle costs are evaluated in terms of absolute cost and the data relating the period of expenditure are available, more sophisticated use of the data may be feasible and applied, as appropriate, by the user. Accordingly, only absolute cost (i.e., undiscounted) values are presented in this section. All costs estimated are in 1977 dollars.

Initial Costs

The initial cost is the price of a shipset of hardware at the time of acquisition of the system. An analysis of the cost of a shipset of hardware for the baseline system has been prepared. The analysis is based on a preliminary design of the hardware components shown and has been verified by cost comparisons made against historical data for other airborne pneumatic systems, with appropriate substitution in hardware content. Based on a lot release of 50 shipsets, production costs are estimated to be $45,000 to $60,000 per aircraft (1977 dollars). This cost figure is exclusive of ground service equipment, integrated logistics support, or other specific data items, as well as aircraft installation. The initial cost (a small component of total aircraft cost) is therefore realistically based on current data. The membrane fiber spinning, a significant fraction of this cost, is subject to downward revision as production capacity and production rates are increased.

Maintenance Costs

Maintenance costs are those costs of ownership that are due to system replacement and repair needs, as well as the amortized cost of new equipment to perform unique maintenance functions, and spare or replacement part costs. The costs of unique ground service maintenance equipment are realized shortly after the initial shipset acquisition costs. The remaining costs for preventive as well as corrective maintenance occur over the life of the system. To evaluate these costs, a maintenance support policy based on approved plans typical of today's commercial jet air transports was used. Numerous cost-related assumptions, summarized in Table 5-2, were required to establish maintenance cost estimates. Where background data were available, historical information was used in determining the maintenance cost assumptions.

Based on the flight system of Figure 4-14, the component reliabilities of Table 5-1, and the maintenance cost assumptions of Table 5-2, elements pertinent to the maintenance support costs are summarized in Table 5-3; cost elements attributable to performance of maintenance are comparable to those presently being demonstrated on similar pneumatic systems in commercial transport service. The estimated maintenance cost per flight hour over the

TABLE 5-2

MAINTENANCE COST ASSUMPTIONS

Equipment design life (except air separation module), yr	20
Aircraft utilization in flight hours (annual)	3000
Typical operator fleet size (DC-9 aircraft)	25
Ratio, engine operation to aircraft flight hours	1.3:1
Ratio, aircraft flight hours to APU operating hours	1:0.75
Ratio, inerting system operating hours to aircraft flight hours	2.05:1
Annual inventory tax on non-consumable spares and AGE, percent	2.5
Inventory control and tax charges for repair materials, percent (Spares cost X 1.15)	15
AGE life, years	20
New (peculiar) AGE costs	78,800
Common AGE and tools	N/A
Labor rate dollars hour	12.75

life of the system (in 1977 dollars) is the result of a preliminary quantitive maintainability analysis to evaluate scheduled on-aircraft preventive maintenance, on-aircraft corrective maintenance, and shop-level maintenance actions. The cost estimate is the result of a study in which each system component has been evaluated in terms of the task frequency (resulting from the reliability analysis of Table 5-1), task definition, maintenance crew size requirements, maintenance man hours per task, and (ultimately) maintenance man hours per flight hour. Labor costs are then evaluated by applying the proper labor rate. Total material and labor costs are expected to be $2.85 per flight hour over the 20-year life of the system.

An examination of the costs of Table 5-3 shows the on-aircraft scheduled maintenance spares costs to be of major significance in maintenance cost evaluations. This cost in turn is largely a result of the replacement life of the hollow fiber permeable membranes, based on the design operating life of 3000 hr at maximum stress conditions (Figure 2-11). The system operation, as described in Section 4, will result in peak design pressures only during (1) the descent segment and (2) the ascent segment when high fuel ullage gas purge rates are required. Calculation based on the mission profile of Figure 4-2 represents less than one hour out of a typical three-hour flight profile.

TABLE 5-3

SUMMARY OF MAINTENANCE COST OF OWNERSHIP ELEMENTS

1.	AGE cost per flight hour	$0.060
2.	On-aircraft scheduled maintenance man hour cost per flight hour (MMH/FH)	$0.047
3.	On-aircraft scheduled maintenance spares cost per flight hour	$2.212
4.	On-aircraft corrective maintenance labor costs (MMH/OH X 2.05 X Rate)	$0.011
5.	On-aircraft corrective maintenance material costs per flight hour (operating costs X 2.05)	$0.084
6.	Shop repair labor costs (MMH/OH X 2.05 X Rate)	$0.049
7.	Shop repair materials costs per flight hour ($/OH X 2.05)	$0.341
8.	Rotatable spares cycle (price of 1 set of repairables for the life cycle plus 2-1/2 percent per annum) per flight hour to support 25 aircraft for 20 years	$0.043
	Listed cost to support 25 aircraft, maintenance logistics cost per flight hour, total	$2.847

Accordingly, applying this one-third ratio to the annual aircraft flight utilization assumption of Table 5-2, the fibers can be expected to be pressurized to stress limits for only about 1000 hours per year, yielding a three-year expected membrane useful life. The significance of membrane replacement cost in the overall maintenance costs then provides inducement to find ways of reducing membrane replacement cost. In addition to the strong possibility of reduced membrane production costs noted in the initial cost discussion above, the encouraging methylpentene polymer crosslinking accomplishments and the possibility of producing cross-linked fiber (as discussed in Section 2) represent potential increases in the life of existing fibers as an alternate and supplemental means to reduce this maintenance cost element.

Operating Costs

Based on design analysis, the average aircraft energies used by the system for various flight segments can be determined for the typical flight profile shown in Figure 4-2. Since the operation of the system requires energies that vary significantly for various flight segments, Table 5-4 shows separate energy requirements for pre- and post-flight ground operation, and for the climb, cruise, and descent flight segments. These energy requirements represent relatively small increases in airflow and electrical power requirements for the baseline design aircraft, and are not expected to increase the requirement beyond aircraft capacities.

TABLE 5-4

ESTIMATED ENERGIES USED DURING TYPICAL SYSTEM OPERATION

PNEUMATIC

Flight Segment	Time Duration, hr	Airflow Requirements (lb/min)			
		High-Stage Bleed	Low-Stage Bleed	ECS Primary Air	Ram Air
Ground	0.20	-	1.70	-	-
Climb	0.30	-	2.75	7.0	12.0
Cruise	2.40	-	1.50	-	4.5
Descent	0.30	4.50	-	10.0	16.0
Landing, rollout and taxi	0.20	-	1.70	-	-

ELECTRICAL

Control power = 20 watts (average)

WEIGHT

System weight = 270 lb

Typical aircraft penalties for turbine-powered transport aircraft installed system energy (and weight) are shown in Table 5-5. These penalty factors, considered for the estimated system requirements from Table 5-4, result in an estimate of the aircraft fuel consumption rate associated with the use of these energies. Application of the appropriate aircraft fuel costs then provides a measure of operating cost associated with the system's use of energies, and with its installed weight.

Aircraft fuel costs have increased substantially in recent years and are subject to further fluctuations in the future. For this study, a cost for Jet-A fuel of $0.40 per gallon has been assumed. To evaluate the operating cost at a future time or in a foreign location, a different fuel cost assumption may be more appropriate. Fuel use and associated costs are shown in Table 5-6. As can be seen, the costs are predominately (approx. 88 percent) due to system weight. The estimated operating cost of $2.00 per flight hour is based on the cost of fuel at $0.40 per gallon. If fuel costs as a function of time were assumed, this value could be adjusted (and its costs discounted) for a time-dependent operating cost analysis.

TABLE 5-5

TYPICAL PENALTY FACTORS FOR POWER USAGE AND WEIGHT

Power Service or Weight Item	Penalty
Ram air	0.264 $\frac{\text{lb fuel/hr}}{\text{lb air/min}}$
Low-stage bleed air	0.958 $\frac{\text{lb fuel/hr}}{\text{lb air/min}}$
High-stage bleed air	1.531 $\frac{\text{lb fuel/hr}}{\text{lb air/min}}$
Electrical power	0.318 $\frac{\text{lb fuel/hr}}{\text{kw}}$
Installed weight	1.3 $\frac{\text{lb installed wt}}{\text{lb equip wt}}$
Installed weight	0.094 $\frac{\text{lb fuel/hr}}{\text{lb installed wt}}$

TABLE 5-6

SYSTEM OPERATING COSTS IN DOLLARS PER FLIGHT HOUR

Flight Segment	Fuel Requirement, lb			Installed Weight
	Bleed air (all)	Ram air	Electrical	
Ground	0.33	-	<0.01	--
Climb	2.80	0.63	<0.01	9.90
Cruise	3.45	-	0.02	79.19
Descent	4.94	0.79	<0.01	9.90
Landing, roll-out and taxi	0.33	-	<0.01	--

Total fuel per mission = 112.29 lb/flight
= 33.0 lb/flight hour

Fuel cost per flight = $\frac{(\$0.40)\ (33.0)}{(6.6)\ \text{lb/gallon}}$

= $2.00/flight-hour

Preceding Page BLANK - NOT FILMED

SECTION 6

PROGRAM CONCLUSIONS

The program reported in the previous sections of this report was an ambitious effort to advance the state of the art in hollow fiber permeable membrane IGG fuel tank inerting systems to the point where hardware can be designed for flight test and subsequent production programs. This effort was successfully accomplished by: investigating and optimizing membrane fiber and module designs; the design, fabrication, and test of full-scale ASM's using the optimized hollow fiber; and the preliminary design of an airborne system based on the data and experience obtained from the breadboard program. The technical tasks completed during the program reinforced, refined, and updated an earlier study that established the feasibility of using this approach to provide fuel tank inerting systems to reduce fuel tank fire and explosion hazards. As a result of the preceding, it is concluded that system design for flight test is the reasonable next step that should be undertaken.

Accomplishments and general conclusions regarding the program are presented below along with briefly summarized supporting rationale.

- Laboratory development has established a reproducible methylpentene membrane fiber possessing properties that make it suitable for airborne system design. The fiber, of 50 microns ID and 7 microns wall thickness, was developed by optimizing the principal manufacturing parameters that affect fiber geometry, repeatability, and material properties. Both permeability and structural life characteristics of the fiber have been established. Internal pressurization with an external wash flow has been confirmed as the most favorable operating mode. The program demonstrated the ability of the material to withstand extremes in the expected operational environment. In addition, a preliminary investigation has indicated that crosslinking adjacent molecular chains could substantially improve the already acceptable fiber structural characteristics to provide increased life and reduced weight.

- Full-scale ASM's for an IGG system sized to meet baseline aircraft requirements have been designed, fabricated, and successfully tested. The three full-scale breadboard test units used the fibers developed in the first program phase. Additional data to further define optimum packing factor and construction techniques were obtained, and wash flow was optimized. Successful system operation was demonstrated in the laboratory at the design-point and transient conditions. The data were used to refine system design tools. Finally, post-test inspection of the breadboard test units provided additional data to improve future ASM design features.

- A test facility was developed that permitted flexible operation and testing of the breadboard modules and utilized an automatic control scheme similar to those suggested for future flight system designs. The test facility permitted the simulation of both steady-state and

transient mission profile operation throughout the aircraft operational envelope. In the automatic mode used to simulate mission profiles, the ASM pressure was regulated as a function of inert gas flow rate. This feature provides a means to extend module life by limiting exposure to maximum stress conditions.

- An airborne system preliminary design completed for the baseline aircraft shows that the system is technically feasible. The airborne fuel tank inerting system design utilizes the hollow fiber developed in the first program phase and incorporates the design, fabrication, and test experience with full-scale ASM's obtained during subsequent phases, thereby providing a design that takes into account all data and experience gained during the program.

- Ownership considerations for the hollow fiber permeable membrane IGG fuel tank inerting system indicate the advantages of a self-contained IGG system and provide an estimate of life cycle costs. The analysis presents estimates for initial cost as well as for maintenance and operation of the system. Based on accepted criteria, the data for the airborne system preliminary design are presented in a format that allows financial escalation and discounted cost flow analysis. The format presented is suitable for comparative system analysis.